A STUDY ON THE SEAKEEPING QUALITIES OF FULL SHIPS

TASAI, Fukuzo
Research Institute for Applied Mechanics, Kyushu University : Professor

https://doi.org/10.5109/7169368

出版情報：Reports of Research Institute for Applied Mechanics. 16 (55), pp.371-458, 1968. 九州大学応用力学研究所
バージョン：
権利関係：

Reports of Research Institute for Applied Mechanics
Vol. XVI, No. 55, 1968

A STUDY ON THE SEAKEEPING QUALITIES OF FULL SHIPS

By

Fukuzō TASAI*

This paper presents experimental and theoretical investigations on the problems associated with seakeeping qualities of two full-ship forms in longitudinal head waves, especially longitudinal ship motions, vertical acceleration, thrust increase, wetness of deck, probability of occurrence of slamming, slamming impact pressure.

The after parts of these two hull forms are the same but the fore parts are different.

The effect of bow forms on the seakeeping qualities is discussed on the basis of the experimental results conducted on 3.0 m models and theoretical considerations.

As for slamming in the ballast condition, it is found that the difference in the bow forms has a great influence upon the impact pressure distribution along the ship length.

1. Introduction

Sea conditions which a ship encounters in her service depend on the sea area, route of the ship and season. Furthermore, even if under the same condition, ships show the various response characteristics or seakeeping qualities according to their dimensions, forms and speed.

The fundamental factors which determine the seakeeping quality of a ship under a sea condition are the ship motions. The motions will be grouped into two kinds of motions, symmetric motions and asymmetric ones (Fig. 1).

The ship motions generally cause an increase of resistance and the loss of propulsive efficiency, and therefore a decrease of ship speed if an available engine power is constant. The author will call this speed decrease "Nominal Loss of Speed". In case of moderate sea state, it is desirable for a ship to be able to run at small N. L. S.

* Professor, Member of Research Institute for Applied Mechanics, Kyushu University, Fukuoka, Japan

When sea state becomes severe, it leads to various troubles such as structural damage or collapse, for example the depression of a deck and damage of super structure caused by shipping green water, the bottom damage due to slamming impact pressure, and other troubles in the engine and propeller shaft due to propeller racing.

Moreover, the comfortability and manoeuvrability of the ship will deteriorate and the transverse stability will sometimes be lost. In the worst case, the ship might be destroyed by being capsized or stranded.

In order to avoid these troubles the captain will be forced to change the course of his ship or drop her speed. The author will call such speed loss "Deliberate Loss of Speed".

We now consider a case when the two ships have the same engin power and dead weight, and navigate on the same route.

Even when these two ships have the same speed in a calm water, it is proper that one of them with a smaller N. L. of Speed and fewer chance of D. L. of Speed is superior to the other.

In order to design ship forms reasonably, we should investigate not only the propulsive performance in still water but also many phenomena in waves as the cause for N. L. of Speed and D. L. of Speed, and the relation between these phenomena and the ship form.

The research to improve ship forms from this point of view may be called the research for "optimum ship form in waves".

For instance, a research, "Which is better *U* form or *V* form?" by E. V. Lewis [1] and M. K. Ochi [2], and another research, "Large bulbous bow ship is more advantageous in still water than ordinary ship, but is it true in waves as well?" by S. Takezawa [3] will be classified as the research for "optimum ship form in waves".

The most important motion and seakeeping problems of a ship depend on the dimension and kind of the ship. For example, in case of a small passenger boat, we should primarily consider the countermeasures against seasickness, comfortability and the safety in the term of transverse stability.

N-ship and *R*-ship (Fig. 2) used for the research in this paper are full ships like a huge tanker, with length-breadth ratio 6. 0, breadth-draft ratio 3. 0, block coefficient 0. 815 and protruding bulbous bow.

The after parts of their hull forms are the same but the fore parts are different, particularly in their stem forms. *R*-ship has a bulbous bow, the bottom of which is raised-up, but the bulbous bow of *N*-ship is of an ordinary type.

We consider the case that *N*-ship and *R*-ship are so large ships that their dimensions are more than 200 m in length. The study on the longitudinal motions and the seakeeping problems related to these motions is, therefore, a matter of primary importance, and the second is that of asymmetric motions.

From this point of view the author investigated the behaviour of these two hull forms in head waves, both for full load and ballast load conditions. In addition, the author studied on the following items, especially the effect of stem forms upon these quantities,

a) vertical acceleration at ship bow and stern
b) thrust increase in waves
c) the probability of shipping green water and impact pressure on the deck
d) the probability of slamming and impact pressure upon the bottom.

Various types of bow forms or bulbous bows have been studied with respect to the performance in still water. The purpose of the study reported in this paper is, however, to pursue how the differences in fore hull forms affect the seakeeping quality of the ship as well as what kind of difference in hull forms has the largest influence upon the seakeeping quality.

The Structure Committee of the Society of Naval Architects of West Japan carried out the analysis of structural damages caused by slamming [4]. The slamming impact pressure of ships with dimension of more than 300 m in length was calculated according to the standard calculation method given by the Committee report[4], and we obtained some representative values of the impact pressure, which were thought to be the cause of bottom damage.

In reality, however, there are few examples of the bottom damage of such large ships.

The committee is now investigating the cause of this discrepancy, and the author hopes this paper will be of some help in filling the discrepancy in question.

This research project was carried out by the close cooperation between the author and Mr. M. Kurihara,* H. Arakawa,* K. Kawasumi** and T. Kita***.

2. Measuring apparatus and experimental method

The bow forms and their profiles of R-ship and *N*-ship are shown in Fig. 2 and Photo. 1. These model ships are 3.0 m long between their perpendiculars. The model experiments were carried out for two conditions of displacement, full load and ballast conditions with 55% displacement of full load condition. The particulars of these models at the two conditions are presented in the following chapters.

2-1 Measuring instruments

Measurements and the instruments are as follows:

a) number of revolutions of propeller
b) propeller torque
c) propeller thrust

} (1)*

---

* Research Associate, Research Institute for Applied Mechanics, Kyushu University.

** Engineer, Initial Design Office, Sasebo Heavy Industries Co., Ltd.

*** Research Engineer of Experimental Tank, an annex to Research Institute for Applied Mechanics, Kyushu University,

d) wave height meter A (2)*
e) 〃 〃 〃 B
f) pitching angle θ
g) heaving displacement Z (3)*
h) surging displacement ξ
i) bow emergence .... (4)*
j) wetness of deck .... (5)*
k) vertical acceleration at 0.1L aft of the forward perpendicular (A_F) (6)*
l) 〃 〃 at 0.1L forward of the aft perpendicular (A_S)
m) water pressure on the deck $P'_{F.P.}$, $P'_{9\frac{3}{4}}$, $P'_{9\frac{1}{2}}$, P'_{9}, $P'_{8\frac{3}{4}}$ (7)*
n) 〃 〃 on the bottom $P_{F.P.}$, $P_{9\frac{3}{4}}$, $P_{9\frac{1}{2}}$, P_{9}, $P_{8\frac{1}{2}}$

(1)* D. C. motor was used for driving the propeller and it was controlled so that number of revolutions might be stationary. Ono Sokki selfpropulsion dynamometer was used. Thrust, torque and revolutions of propeller were digitally recorded.

(2)* "A", which is Kaijō Denki wave height meter of ultrasonic-type, was installed at the fore end of the towing carriage.
"B" of resistance type was set at the side of the towing carriage.

(3)* The instruments described in the reference (5) was used.

(4)* This plobe was set on the bottom at Station $9\frac{1}{2}$ which is located at 0.05L aft of the forward perpendicular. The time from emergence to immersion of the bottom and the numbers of bottom emergence per unit time were measured.

(5)* A pair of electrodes, between which the distance was 10 mm, was put on the forecastle deck at the forward perpendicular F.P., and when shipping water with more than 10mm width was made to flow between these electrodes, electric circuit was closed.

(6)* They were measured by the Shinkō Tsūshinki BA. 2G-120 accelerometer.

(7)* Pressure gauges were Toyota Kōki PMS-5, 0.5H, 5mm in diameter.
We investigated dynamic properties of the pressure gauge by oscillating them in the air. The experimental results are shown in Fig. 80. As seen from the results, the error of measurement due to acceleration of 1.0g was smaller than 0.4cm water head. The gauge on the deck was set on the center line of the ship and the bottom gauge at the position 20mm detached from the center line. (Fig. 72)

The arrangement of these instruments is shown in Fig. 3. Photo. 2 shows the pressure gauge. As stated above the error of measurement by this gauge due to its inertia is negligibly small and its natural frequency is about 10K. C./sec in the air. Therefore we can measure the impact pressure with high accuracy. The gauge was installed on the deck for full load condition and the bottom for ballast condition. $P_{F.P.}$, $P_{9\frac{3}{4}}$, P_9 etc. indicate the water pressures on the bottom at the forward perpendicular F.P., Station $9\frac{3}{4}$, Station 9 etc.

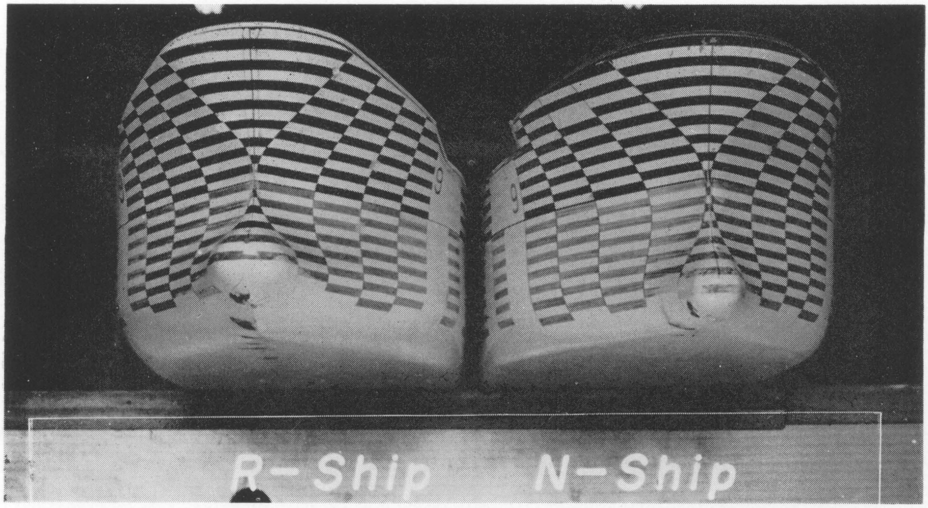

Photo. 1 Front view of full ship models with different types of bulbous bow; R-ship and N-ship

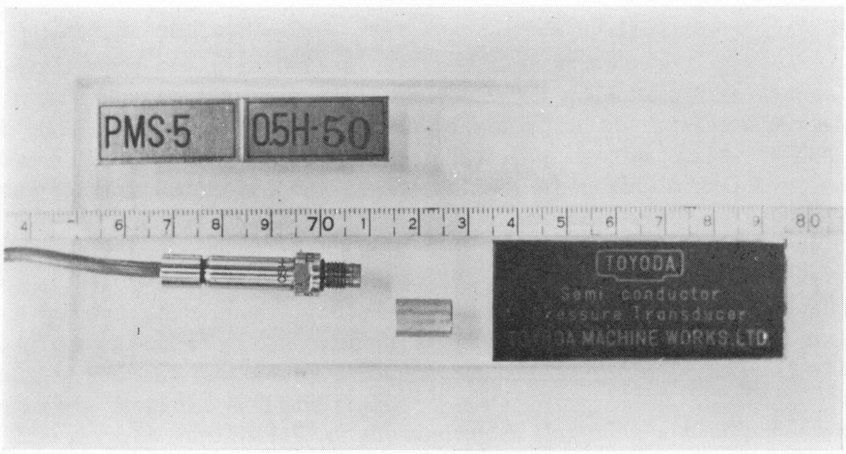

Photo. 2 Pressure transducer

(*Facing p.* 374)

2-2 Waves and model speed

Test conditions in regular waves were as follows:

$$\lambda/L = 0.5 \sim 2.0$$

$$H/\lambda = 1/50, \ 1/40, \ 1/30$$

where λ = wave length and $H = 2\,\zeta_a$ = wave height.

As for irregular waves a detailed account will be given in the section 5-1-2.

Before the experiments of ship motions waves were generated and their heights were measured at the longitudinal center of the tank by means of wave height meter A.

In analyzing the experimental results concerning ship motions these records of wave heights were used.

During the experiments of ship motions both meter A and meter B recorded the wave height, but the information obtained from the records of the meter B was used only for the examination of the relation between wave forms and slamming pressure.

Actual ships corresponding to the model ships used for the experiments can not run at the speed of Froude number $Fn = 0.16 \sim 0.20$ under the severe wave condition, and therefore we did not conduct the experiments at such a high speed in waves, especially in irregular waves.

2-3 Experimental method

The outline of our method of experiments is as follows.

Before starting the towing carriage waves are generated. As soon as the tank is filled with generated waves, we start the towing carriage, which restrains the surging motion of the model ship at this stage. When the towing carriage attains a given constant speed, then the restraint of surge are released and the number of revolutions of propeller is adjusted so that the mean longitudinal position of the model ship is almost kept constant with respect to the towing carriage.

After that, recording is started with all instruments. The self-propulsion test in waves was conducted without a skin-friction correction. We took a picture of the ship motions by a 35mm camera from the side and by two 8mm cinecameras from the side and front.

The pictures were usefull for the analysis of slamming and shipping water phenomena.

The experiments were performed in the interval between March, 1967 and July, 1968, at the large tank, an annex to the Research Institute for Applied Mechanics of Kyushu University.

3. Theoretical calculation of ship motions in regular waves

3-1 Longitudinal motions in head waves

In Fig. 4 a ship advances with constant velocity V in longitudinal regular head waves. Let us introduce the coordinate system O_o-$x_oy_oz_o$ fixed in space and the coordinate system G-$x_by_bz_b$ fixed in the ship, as shown in Fig. 4, where G is the center of gravity of the ship.

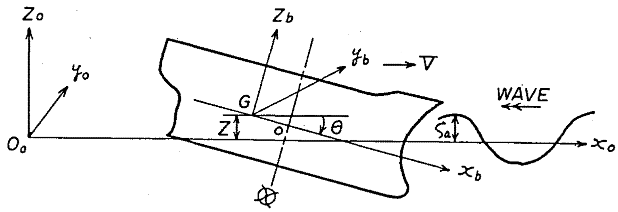

Fig. 4

For the case of head waves, surging motion can usually be neglected. The motion of the ship is then defined by the pitch angle θ (bow down is taken to be positive) and heaving displacement Z (upward displacement is taken to be positive).

The subsurface equation of regular waves progressing in the direction of $-x_o$ is given by

$$\zeta = \zeta_a e^{KZ_o} \cos (Kx_o + \omega t) \tag{3.1}$$

in which:

ζ_a = the amplitude of waves,
K = wave number $= \omega^2/g = 2\pi/\lambda$
λ = wave length
ω = circular frequency of wave,

and circular frequency of encounter ω_e is given by

$$\omega_e = \omega + KV = \omega(1 + \omega V/g) \tag{3.2}$$

Assuming Z and θ to be small, the equation (3.1) can be approximately transformed into the following equation with reference to the coordinate system fixed in the ship.

$$\zeta = \zeta_a e^{KZ_b} \cos(Kx_b + \omega_e t) \tag{3.3}$$

Theoretical calculation of heave and pitch was carried out by Fukuda's method [7], which is in principle based on Watanabe's linear strip theory [6]. Two of the coupled second-order differential equations of motions, heave and pitch, are written as follows:

$$\begin{aligned} &(a+\Delta/g)\ddot{Z} + b\dot{Z} + cZ - d\ddot{\theta} - e\dot{\theta} - g_1\theta = \zeta_a(F_1 \cos \omega_e t - F_2 \sin \omega_e t) \\ &(A+J)\ddot{\theta} + B\dot{\theta} + C\theta - D\ddot{Z} - E\dot{Z} - G_1 Z = \zeta_a(M_2 \sin \omega_e t - M_1 \cos \omega_e t) \end{aligned} \tag{3.4}$$

where Δ/g is the mass of the ship, Δ its displacement and J the mass moment of inertia with respect to pitch.

The sectional added mass and the sectional damping coefficient were calculated according to Tasai's method [8),9)].

In the calculation of the hydrodynamic forces in the equations (3.4) the part of bulbous bow protruding from $F.P.$ was not taken into consideration.

Putting $$Z = Z_o \cos(\omega_e t - \varepsilon_z),\ \ \theta = \theta_o \cos(\omega_e t - \varepsilon_\theta) \tag{3.5}$$

we can obtain Z_o, ε_z, θ_θ and ε_θ by solving the equations (3.4).

3-2 Vertical acceleration

The upward displacement $Z(x_b)$ of point Q located at a distance x_b from the center of gravity G is given by $Z(x_b) = Z - x_b\theta$. Using the equation (3.5) the vertical acceleration of Q is given by the following equation.

$$\ddot{Z}(x_b) = C_2 \cos(\omega_e t - \varepsilon_2) \tag{3.6}$$

where
$$\left.\begin{aligned} &C_2^2 = A_2^2 + B_2^2,\ \ A_2 = \omega_e^2(-Z_o \cos\varepsilon_z + \theta_o x_b \cos\varepsilon_\theta), \\ &B_2 = \omega_e^2(-Z_o \sin\varepsilon_z + \theta_o x_b \sin\varepsilon_\theta),\ \varepsilon_2 = \tan^{-1}(B_2/A_2) \end{aligned}\right\} \tag{3.7}$$

This relation is non-dimensionarized into the form

$$\ddot{Z}(x_b)/\Theta_w g = \ddot{Z}(x_b)/\zeta_a\omega^2 = \bar{C}_2 \cos(\omega_e t - \varepsilon_2) \tag{3.8}$$

where $\bar{C}_2 = C_2/\zeta_a\omega^2$ and $\Theta_w = \pi H/\lambda$ is the maximum wave slope.

3-5 Vertical displacement of bow relative to wave surface

The vertical displacement $S(x_b)$ of the point Q relative to the wave surface is

$$S(x_b) = Z - x_b\theta - \zeta \tag{3.9}$$

This can be non-dimentionarized such as

$$S(x_b)/\zeta_a = \bar{C}_{50} \cos(\omega_e t - \varepsilon_{50}) \tag{3.10}$$

where

$$\left.\begin{aligned} &\bar{C}_{50}^2 = A^2 + B^2,\ \ A = \bar{Z}\cos\varepsilon_z - x_b\bar{\theta}K\cos\varepsilon_\theta - \cos Kx_b \\ &B = \bar{Z}\sin\varepsilon_z - x_b\bar{\theta}K\sin\varepsilon_\theta + \sin Kx_b,\ \ \tan\varepsilon_{50} = B/A \end{aligned}\right\} \tag{3.11}$$

$$\bar{Z} = Z_0/\zeta_a,\ \ \bar{\theta} = \theta_0/K\zeta_a \tag{3.12}$$

When a ship runs in still water the vertical position of water surface relative to the hull changes due to its sinkage, trim and waves generated by the ship.

We shall designate the relative elevation of water surface due to sinkage, trim and bow waves $f_s(x_b)$, and the geometrical freeboard of the ship bow $f(x_b)$.

Then the effective freeboard $f'(x_b)$ in still water is given by

$$f'(x_b) = f(x_b) - f_s(x_b) \tag{3.13}$$

When a ship runs in regular waves, she generates the waves other than the aforementioned waves generated in still water. That is, there occurs dynamic swell-up $h_D(x_b)$ of water surface owing to ship motions.

Moreover, $f'(x_b)$ in waves varies with time, though it is the stationary value in still water, because the ship disturbs regular waves. But assuming that even in waves the average of $f'(x_b)$ is approximately equal to that in still water, the relative freeboard in waves $h'(x_b)$ can be expressed by the following equation as Tasaki[10] discussed,

$$\begin{aligned} h'(x_b) &= f(x_b) - f_s(x_b) - h_D(x_b) + S(x_b) \\ &= f'(x_b) - h_D(x_b) + S(x_b) \end{aligned} \tag{3.14}$$

4. Comparison of experiment and theory concerning ship motions in regular waves

4-1 Full load condition

4-1-1 Ship motions and vertical acceleration

Table 1 presents the particulars of N, R-ship for full load condition. These hull forms have the same after body, but there are some differences in their fore body forms as shown in Fig. 2 and Photo. 1.

Theoretically obtained $\bar{\theta} = \theta_0/K\zeta_a$, $\bar{Z} = Z_0/\zeta_a$, ε_θ and ε_z for N-ship are shown in Figs. 5, 6, 7 and 8. The arrow marks in Figs. 5, 6, 7 and 8 are the resonance points obtained by using the calculated natural period for zero forward speed.

Table 1-a Full Load Condition

Description		N - Ship	R - Ship
Length between perpendicular	L	3·0000 m	
Beam	B	0·5012 m	
Depth	D	0·2500 m	
Draft	d	0·1686 m	
Displacement	Δ	206·48 kg	206·38 kg
Block coefficient	C_B	0·815	0·814
Waterplane area coefficient	C_W	0·870	0·869
Prismatic coefficient	C_P	0·822	0·822
Center of buoyancy forward of midship		6·55 cm	6·63 cm
Center of waterplane area forward of midship		-0·10 cm	-0·15 cm
Radius of gyration for pitch		0·235 L	

Table 1-b Particulars of Model Propeller

Diameter	D	0·0804 m
Pitch ratio (constant)	H/D	0·730
Expanded area ratio	a_E	0·575
Boss ratio		0·187
Rake angle		10°
Number of blades		5
Turning direction		Right
Section of blade		Aerofoil

From the comparison of $\bar{\theta}$ for N-ship and R-ship in Fig. 9 it will be found that there is almost no difference between them. As for $\bar{Z}$, ε_z and ε_θ similar results were also obtained.

The calculated natural periods of pitch and heave for zero forward speed are compared with the corresponding experimental values in Table 2.

Table 2 Natural period (Full Load)

		N-Ship	R-Ship
Heave T_z	Calculation	1·117 sec	1·113 sec
	Experiment	1·11 "	1·13 "
Pitch T_θ	Calculation	1·007 "	1·002 "
	Experiment	1·00 "	1·01 "

It is noted that they are in good agreement. It can be further said that there is little difference between the natural periods of both the ship models. The natural period was calculated according to the method of the paper (9). Figs. 10 and 11 show the response functions $\bar{C}_{2F}$, $\bar{C}_{2S}$ for the vertical acceleration of bow and stern of N-ship. As for $\bar{C}_{2F}$ and $\bar{C}_{2S}$, there are also little difference between the calculated values for N-ship and R-ship.

In the Figs. 12-a, b, c and Figs. 13-a, b, c the calculated frequency characteristics of $\bar{\theta}$ and $\bar{Z}$ are compared with the experimental values measured for $H/\lambda = 1/50$.

In the first place the measured and calculated values of $\bar{\theta}$ show good agreement for $\lambda/L \leqslant 1.1$, but the former is larger than the latter for $\lambda/L > 1.1$

In the next place, the measured values of $\bar{Z}$ are larger than the calculated ones for $0.7 < \lambda/L < 1.0$, but for other λ/L it may be said that the calculated $\bar{Z}$ is on the avarage equal to the experimental one.

As seen from Figs. 12 and 13, there is little difference between the motions of N-ship and R-ship.

Figs. 14 and 15 are the experimental results concerning to what extent $\bar{\theta}$, $\bar{Z}$ are influenced by the magnitude of wave slope H/λ.

It seems that, when H/λ is smaller than 1/30, θ_0 and Z_0 increase nearly in proportion to the wave height.

Figs. 16, 17 are the examples of the comparison of the calculation with the experiment for $\bar{C}_{2F}$ and $\bar{C}_{2S}$. As for the vertical acceleration of bow $\bar{C}_{2F}$, the calculation and the experiment are in good agreement, but with that of stern $\bar{C}_{2S}$, there is large difference, especially in case of $0.9<\lambda/L<1.6$.

In the experimental values of vertical acceleration there is no difference between N-ship and R-ship.

4-1-2 Thrust increase in regular waves

Some examples of mean thrust increase ΔT in regular waves are shown in Figs. 18-a and 18-b by using the non-dimensional value $\tau=\Delta T/\rho g H^2 B^2/L$. The increase of number of propeller revolutions and torque shows the same tendency.

According to Maruo's theory [11], the increment of the wave making resistance of the ship in regular waves is proportional to the wave height squared.

Therefore assuming that thrust deduction factor has the same value for in still water and waves, the relation $\Delta T \propto H^2$ will hold.

In our experiments, this relation seems to hold for $H/\lambda \leqslant 1/40$.

4-1-3 Deck wetness in regular waves

The relative freeboard of the ship in head sea condition can be evaluated from the equation (3.14). We shall now discuss about the deck wetness at F. P.

Let l be the distance from G to F. P.

Then we obtain the following expression for the relative freeboard h$'(l)$ at $F. P.$

$$h'(l)=f'(l)-h_D(l)+S(l) \tag{4.1}$$

Concerning shipping water of a ship in head seas, Tasaki studied in detail [10),12)]. Especially in the paper (12) he obtained $h_D(l)$ experimentally.

He measured the relative vertical displacement of water surface to the model ship in the forced oscillation test, in which a model ship was towed in still water and sinusoidal pitching motions was imported to the model. Then the dynamic swell-up $h_D(l)$ was obtained by substracting $f'(l)$ from the measured above.

From this experiment Tasaki [12)] gave the following relation.

$$\bar{h}_D(l)/\bar{h}(l)=k_2\sqrt{\omega_e^2 L/g} \tag{4.2}$$

and also

$$\bar{h}_D(l)/L=k_2\bar{V}_B/\sqrt{Lg} \tag{4.3}$$

where $\bar{h}(l)$ is the vertical displacement of the bow, $\bar{h}_D(l)$ the amplitude of $h_D(l)$ and $\bar{V}_B$ the amplitude of the relative vertical velocity.

The coefficient k_2 depends on the fullness of the ship and is given by the empirical formula

$$k_2 = (C_B - 0.45)/3, \quad 0.60 \leqslant C_B \leqslant 0.80 \tag{4.4}$$

which is derived from the experiments about a cargo ship and a tanker hull form. And he showed that the phase angle hetween h_D and h is about 180 degrees independent of frequency. From these findings he concluded that the results of experiments for the deck wetness in head seas can be explained by assuming the relation

$$h_D(l) = -\bar{k}_D \, \omega_e \, S(l) \tag{4.5}$$

where

$$\bar{k}_D = \frac{1}{3}(C_B - 0.45)\sqrt{L/g} \tag{4.6}$$

According to the calculation upon two dimensional body carried out by Tasai [13], it is evident that the phase angle between h_D and the vertical displacement h becomes 180 degrees when $\omega_e \to \infty$, and in many cases it is about $90^\circ \sim 120^\circ$ for the frequency of ship motions.

Using the two dimensional theory Tasai [14] calculated h_D of the cross section at Station 9 of the model ship on which Tasaki conducted experiments and found that the amplitude h_D shows satisfactory agreement with the empirical formulae (4.2), (4.4), but the phase difference between h_D and h was about 100 degrees. The difference between Tasai and Tasaki's results seems to come from three-dimensional fluid motion in the neighbourhood of *F. P.* and the periodical change of $f'(l)$.

As described before, regular waves are deformed owing to the existence of a ship, even if she does not move, and this deformation has some effects on shipping water. Further basic investigation should be done for the phenomena discussed above.

Assuming that the equations (4.4), (4.5) are applicable to our model ships, we carried out calculation on the deck wetness with taking $h_D(l)$ into account. Using the equation (4.5) we obtain

$$h'(l) = f'(l) + (1 + \bar{k}_D \omega_e) S(l). \tag{4.7}$$

The shipping of green water over the deck at *F. P.* occurs if:

$$h'(l) < 0 \text{ that is } f'(l) < -(1 + \bar{k}_D \omega_e) S(l) \tag{4.8}$$

Let be $(1+\bar{k}_D\omega_e)\, S(l)/\zeta a = \bar{C}_5 \cos(\omega_e t - \varepsilon_5)$. (4.9)

$$\left.\begin{aligned} &\text{where } \bar{C}_5{}^2 = A_5{}^2 + B_5{}^2, \; A_5 = (1+\bar{k}_D\omega_e)(\bar{Z}\cos\varepsilon_Z - l\bar{\theta}'\cos\varepsilon_\theta - \cos Kl) \\ &B_5 = (1+\bar{k}_D\omega_e)(\bar{Z}\sin\varepsilon_Z - l\bar{\theta}'\sin\varepsilon_\theta + \sin Kl),\; \bar{\theta}' = \theta_0/\zeta_a = K\bar{\theta} \end{aligned}\right\} \tag{4.10}$$

Putting $k_D=0$ in the equation (4.9), $\bar{C}_5$ becomes identical to $\bar{C}_{50}$ in the equation (3.11). $\bar{C}_{50}$ and $\bar{C}_5$ for N-ship are shown in Figs. 19 and 20. In these figures we can see that both $\bar{C}_5$ and $\bar{C}_{50}$ have the maximum values at $\omega=4.5$ for the case of $F_n=0.1$, and as for their maximum values the relation $\bar{C}_5 \doteqdot 1.3\ \bar{C}_{50}$ holds.

In Fig. 21 the results of observation are plotted in the form a little different from Newton's expression [15]. In the figure the dotted line is the experimentally determined critical line for deck wetness.

$f'(l)$ was obtained from the wave profiles photographed at self-propulsion tests in still water. For example, $f'(l)=120.4$ mm at $F_n=0.130$.

We calculated theoretically the critical line of deck wetness by using $\bar{C}_{50}\zeta_a$, $\bar{C}_5\zeta_a$ and $f'(l)$, and the results are shown by solid lines in Fig. 21.

It will be evident from this figure that the calculated value differs from the experiments, provided that $h_D(l)$ is not taken into consideration.

On the other hand, if $h_D(l)$ is taken into account, the calculation and experiments show satisfactory agreement for $0.9<\lambda/L<1.5$.

This facts confirms Tasaki's point of view. [10]

4-2 Ballast condition

In Table 3, principal particulars of two ship forms, N and R at their ballast condition are summarized. Their longitudinal radius of gyrations for this condition are a little larger than for full load condition.

Center of buoyancy lies at afterward of midship and center of floatation at forward of midship, and these particulars are quite different from those in the case of full load condition.

Table 3 Ballast Condition (55% $\triangle_F$)

Description		N-Ship	R-Ship
Draft at fore perpendicular	d_f	6·66 cm	6·70 cm
Draft at midship	$d_{\text{⊠}}$	9·66 cm	9·70 cm
Draft at aft perpendicular	d_a	12·66 cm	12·70 cm
Trim		6 cm	
d_f/L		2·22 %	2·23 %
Displacement	Δ	113·56 kg	113·45 kg
Block coefficient	C_B	0·782	0·778
Waterplane area coefficient	C_W	0·840	0·846
Center of buoyancy forward of midship		−2·89 cm	−3·412 cm
Center of waterplane area forward of midship		4·90 cm	6·291 cm
Radius of gyration for pitch		0·265 L	

4-2-1 Ship motions

Calculated $\bar{Z}$, $\bar{\theta}$, ε_Z and ε_θ of R-ship are shown in Figs. 22~25. The arrow marks in the figures give the resonance points obtained by using the calculated natural period for zero forward speed.

In Table 4, experiments of the natural period for zero forward speed are compared with the calculation. The results of calculation for N-ship are almost in agreement with the ones for R-ship. T_Z is 6% larger in experiments than in calculation. T_θ obtained for R-ship by experiments is larger than that for N-ship.

The reason why the calculation and experiments are not in agreement is probably that the bulb part protruding from F.P. are not taken into consideration in calculation. We can deduce that T_Z, T_θ of R-ship is larger than that of N-ship because added mass and added mass moment of inertia for R-ship are larger than those for N-ship owing to the difference in their bulbous bow forms.

Table 4 Natural period (Ballast condition)

		N-Ship	R-Ship
Heave T_Z	Calculation	0·979 sec	0·971 sec
	Experiment	0·914 "	0·928 "
Pitch T_θ	Calculation	0·931 "	0·932 "
	Experiment	0·910 "	0·947 "

4-2-2 Coupling effect of ship motions for full and ballast condition

Coefficients in the equations (3.4) are non-dimensionarized as follows:

$$\left.\begin{aligned} a/(\Delta/g) &= a',\ b/\Delta\sqrt{gL} = b',\ c/(\Delta/L) = c_0', \\ d/(\Delta L/g) &= d',\ e/\Delta L\sqrt{gL} = e',\ g_1/\Delta = g_1' \end{aligned}\right\} \tag{4.11}$$

and also, putting

$$Z = Z_1\zeta_a,\ \theta = \zeta_1\zeta_a/L,\ t = t_1\sqrt{L/g} \tag{4.12}$$

the non-dimensional form of the first equation of (3.4) will be

$$(1+a')\ddot{Z}_1+b'\dot{Z}_1+c_0'Z_1-d'\ddot{\zeta}_1-e'\dot{\zeta}_1-g_1'\zeta_1 = (F_1'\cos qt_1-F_2'\sin qt_1) \tag{4.13}$$

where

$$F_1' = F_1L/\Delta,\ F_2' = F_2L/\Delta,\ q = \omega_e\sqrt{L/g} \tag{4.14}$$

and $\ddot{Z}_1$, $\dot{Z}_1$ means d^2Z_1/dt_1^2, dZ_1/dt_1.

The second equation of (3.4) is non-dimensionarized in the same manner as the first equation, namely:

$$(\mu+\bar{A}')\ddot{\zeta}_1+B'\dot{\zeta}_1+C_1'\zeta_1-D'\ddot{Z}_1-E'\dot{Z}_1-G_1'Z_1=(M_2'\sin qt_1-M_1'\cos qt_1) \quad (4.15)$$

Dividing both the sides of the equation (4.13) and (4.15) by $(1+a')$ and $(\mu+\bar{A}')$ respectively, we obtain the following expression:

$$\left.\begin{aligned} \ddot{Z}_1+b_0\dot{Z}_1-\bar{c}_0Z_1-d_0\ddot{\zeta}_1-e_0\dot{\zeta}_1-g_{10}\zeta_1 &= F_{10}\cos qt_1-F_{20}\sin qt_1 \\ \ddot{\zeta}_1+B_0\dot{\zeta}_1+C_{10}\zeta_1-D_0\ddot{Z}_1-E_0\dot{Z}_1-G_{10}Z_1 &= M_{20}\sin qt_1-M_{10}\cos qt_1 \end{aligned}\right\} \quad (4.16)$$

Coefficients of these differential equations when λ/L is 0.8, 1.0, 1.2, 1.5 and 2.0 with $Fn=0.13$ are shown in Table 5.

The following facts will be found from Table 5.

(1) b_0, B_0, $\bar{c}_0$, C_{10}, D_0, E_0, F_0, M_0 for ballast condition are larger than the ones for full load condition, and e_0 is larger for full load condition.

Table 5

Full	λ/L	0.8	1.0	1.2	1.5	2.0
	b_0	0.597	0.816	0.969	1.117	1.208
	$\bar{c}_0$	9.676	9.923	9.974	9.873	9.396
	d_0	-0.001	-0.002	-0.004	-0.005	-0.006
	e_0	-0.108	-0.107	-0.105	-0.103	-0.100
	g_{10}	-0.274	-0.306	-0.328	-0.345	-0.348
	F_{10}	-0.742	-0.236	1.467	2.969	4.453
	F_{20}	-0.169	-0.064	0.195	0.576	0.964
	F_0	0.762	0.245	1.480	3.024	4.556
	B_0	0.836	1.061	1.195	1.341	1.330
	C_{10}	11.869	11.995	11.925	11.880	10.931
	D_0	-0.013	-0.041	-0.063	-0.093	-0.112
	E_0	0.428	0.404	0.420	0.503	0.618
	G_{10}	-3.671	-3.709	-3.688	-3.678	-3.391
	M_{10}	0.794	-2.032	-3.986	-5.475	-5.475
	M_{20}	5.462	14.685	19.731	22.542	20.656
	M_0	5.519	14.825	20.130	23.197	21.369
Ballast	λ/L	0.8	1.0	1.2	1.5	2.0
	b_0	1.423	1.610	1.693	1.714	1.637
	$\bar{c}_0$	13.215	13.016	12.727	12.139	11.229
	d_0	0.023	0.024	0.024	0.025	0.026
	e_0	-0.026	-0.020	-0.019	-0.022	-0.030
	g_{10}	0.183	0.150	0.130	0.111	0.095
	F_{10}	-0.950	0.335	1.839	3.625	5.314
	F_{20}	-0.450	0.638	1.504	2.189	2.454
	F_0	1.052	0.720	2.376	4.235	5.853
	B_0	1.567	1.682	1.724	1.705	1.597
	C_{10}	13.630	13.312	12.900	12.306	11.354
	D_0	0.387	0.397	0.403	0.414	0.421
	E_0	2.386	2.413	2.414	2.417	2.391
	G_{10}	6.125	5.986	5.807	5.546	5.127
	M_{10}	-7.694	-12.201	-12.485	-10.327	-6.244
	M_{20}	5.839	16.969	22.807	25.560	24.028
	M_0	9.659	20.900	26.001	27.567	24.826

$(F_0^2 = F_{10}^2+F_{20}^2,\ M_0^2 = M_{10}^2+M_{20}^2)$

(2) Any of d_0, D_0, g_{10}, G_{10} are negative for full load condition, but they are positive for ballast condition.

Fukuda and others [16] carried out the calculation of the motions for the ballast condition of a ship with $L/B = 6.98$, $C_B = 0.795$. In their calculation g_{10} and G_{10} show the same tendency as those in ours.

In Figs. 26 ~ 29, the solutions of coupled equations (3.4) or (4.16) are compared with those of uncoupled equation. For $\bar{\theta}$ value of full load condition in Fig. 27 their difference is very small. Such a phenomenon in full load condition was found in Gerritsma's research [17].

For ballast condition, however, their difference is very small in $\bar{Z}$ as well as in $\bar{\theta}$ as shown in Figs. 28 and 29. The coupled solution $\bar{Z}$ for full load condition is larger than that for ballast condition when $\lambda/L>0.9$, but it is quite contrary when $\lambda/L<0.9$. On the other hand, the values of pitching amplitude in full load and ballast conditions are much the same.

Now we investigated the following items by the equation of motions (4.16).

i) the reason why the coupling effect of heave on pitch is small

ii) the reason why the difference in $\bar{\theta}$ is small for both cases of full load and ballast conditions

iii) the reason why the coupling effect of pitch on heave for full load condition is different from that for ballast condition

We put here

$$Z_1 = \bar{Z}_1 \cos(qt_1-\varepsilon_Z),\quad \zeta_1 = \bar{\zeta}_1 \cos(qt_1-\varepsilon_\theta)$$
$$\bar{Z}_1 = \bar{Z} = Z_0/\zeta_a,\quad \bar{\zeta}_1 = \bar{\theta}2\pi L/\lambda \tag{4.17}$$

The dominant term of the coupling effect of heave on pitch is $G_{10}Z_1$.
In many cases, the phase difference between heave and pitch is nearly equal to 90° ~ 120°, and therefore we can estimate the coupling effect by comparing $B_0\dot{\zeta}_1$ with $G_{10}Z_1$ in (4.16).

Using the value given in Table 5 we can obtain that $G_{10}\bar{Z}$ is of order 20 ~ 30% of $B_{10}q\bar{\zeta}_1$. It signifies that the coupling effect of heave on pitch is small.

In the next place, we can discuss item (ii) without large error by considering the uncoupled equation of motion, as seen from Figs. 27 and 29.

The solution of the uncoupled equation of pitch is given by

$$\bar{\zeta}_1 = M_0/\sqrt{(C_{10}-q^2)^2+B_0^2q^2}$$

M_0, C_{10}, B_0, given in Table 5 are larger for ballast condition, and because of this fact there is no large difference in $\bar{\theta}$ between full load and ballast condition.

Thirdly we discuss item (iii). As seen from Fig. 26 the coupling effect is predominant in $1.0<\lambda/L<1.5$. In this range the phase difference between heave and pitch is 90 degrees ~ 120 degrees. Hence the coupling effect of $g_{10}\zeta_1$ upon $b_0\dot{z}_1$ is large. g_{10} of full and ballast condition has an opposite sign of each other and the absolute value of the former is about twice that of the latter when $\lambda/L=1.0$.

Now we consider the case of $\lambda/L=1.0$.

When λ/L is 1.0, ε_θ-ε_Z is nearly equal to 120 degrees and the component of $b_0\dot{Z}_1$-$g_{10}\zeta_1$ in the equation (4.16) with the same phase as $\dot{Z}_1$ is given by

$$-(qb_0\bar{Z}_1+g_{10}\bar{\zeta}_1\cos 30°)\sin(qt_1-\varepsilon_Z)$$

In an attempt to calculate this value with data given in Table 5, for the case of full load condition the damping force of heave decreased to 1/2.5 and for the ballast condition it increased to 1.2 times in comparison with the damping force $b_0\dot{Z}_1$. It is because g_{10} has large negative value and b_0 is so small that the damping force of heave is small for the full load condition. Ballast condition is the case contrary to the full load condition.

The coefficient g_1 is given by

$$g_1=\rho g\int 2y_w x_b dx_b-Vb \tag{4.18}$$

where y_w is the half breadth of water plane.
The sign of g_1 at the lower speed may be determined by the first term on the right hand side. After all, for the ballast condition at which the center of floatation lies at forward of center of buoyancy, g_1 becomes positive and for the full loard condition it becomes negative, because the center of floatation lies at afterward of center of buoyancy.

It is a matter of course that the terms $e_0\dot{\zeta}_1$ and $d_0\ddot{\zeta}_1$ should be taken into account, but it is supposed that the main reason of the item (iii) is the difference of the coupling effect due to $g_{10}\zeta_1$.

4-2-3 Phase lag and slamming

One of the important problems caused by ship motions at the ballast condition is a slamming phenomenon. Hence we tried to investigate the phase lag ε_θ, ε_Z which are important about slamming.

ε_Z and ε_θ shown in Figs. 24 and 25 are much different from ordinary ones.

Fig. 30 and Fig. 31 show the relation of tuning factor $\Lambda_\theta=T_\theta/T_e$, where T_θ is 0.932 sec and T_e is period of encounter, and $\theta_0\omega_e/K\zeta_a$ or ε_θ. The quantity $\theta_0\omega_e$ is proportional to the downward velocity of the stem due to pitching.

As seen from Figs. 25 and 31, ε_θ does not reach 180° when $\Lambda_\theta=1.0$. ε_θ attains its maximum value at $\Lambda_\theta=1.0$ and decreases again as Λ_θ increases. Fukuda [16] obtained the similar phase curve.

When $Fn=0.1$ and 0.13, ε_θ has its maximum value 120°, 142° respectively.

That ε_θ is smaller than 180° for $\lambda/L \doteqdot 1.0$ means that the part of the bow bottom which has emerged from water is small, namely, a ship is on safe side with respect to slamming.

Since ε_θ of full load condition shown in Fig. 7 becomes 180° at $\Lambda_\theta \doteqdot 1.0$, the tendency of ε_θ in Figs. 25 and 31 is found to be the characteristics of the ballast condition.

From the Gerritsma's experiments [17], which were conducted upon the model ships of Todd 60 series with $C_B = 0.60$, 0.70 and 0.80 for full load condition, the following facts can be derived.

a) ε_θ becomes 180° at $\Lambda_\theta \fallingdotseq 1.0$ in any cases of these three ship forms.

b) $\theta_0\omega_e/K\zeta_a$ reaches its maximum value at $\Lambda_\theta \fallingdotseq 0.9$.

c) Under the condition of a constant Froude number, the fuller a ship form is, the smaller $\theta_0\omega_e/K\zeta_a$ at $\varepsilon_\theta = 180°$, and this value is larger at a high speed.

The results of Y-ship, which was of a high speed cargo ship form, were compared with our results of R-ship. When $Fn = 0.1$, ε_θ of Y-ship is 180° at $\Lambda_\theta \fallingdotseq 1.0$ for both full load and ballast conditions (Fig. 32-a), but ε_Z is not equal to 90° at $\Lambda_Z \fallingdotseq 1.0$ for ballast condition, and furthermore, the properties of ε_Z-ω curve are similar to those of R-ship (Fig. 32-b).

From the aforementioned comparison and consideration of the theoretical and experimental results it is inferred that ε_θ of R, N-ship is representative of the characteristics of full ship forms at ballast condition.

In the next place we investigated the factors which have an influence upon the characteristics of ε_θ.

The coupling effect of heave on pitch is not large and so we will consider here the uncoupled equation of motion. We can obtain such an uncoupled equation from the equation (3.4) as follows,

$$(J+A)\ddot{\theta}+B\dot{\theta}+C\theta = \zeta_a M_0 \cos(\omega_e t-\beta) \tag{4.19}$$

and putting $\theta = \theta_0 \cos(\omega_e t-\varepsilon_\theta)$, $J+A = A'$ we get

$$\left.\begin{aligned} \tan\varepsilon_\theta &= \frac{(C-A'\omega_e^2)\sin\beta+B\omega_e\cos\beta}{(C-A'\omega_e^2)\cos\beta-B\omega_e\sin\beta} \\ \tan\beta &= \frac{M_2}{-M_1} \end{aligned}\right\} \tag{4.20}$$

If $\beta \fallingdotseq 0$, ε_θ becomes nearly equal to 90° under the condition of $C-A'\omega_e^2 \fallingdotseq 0$ and if $\beta \fallingdotseq 90°$, ε_θ becomes about 180° under the similar condition.

Table 6 shows the difference of β and ε_θ between full load and ballast conditions in the neighbourhood of the resonance point.

Table 6

		Ballast		Full	
Fn		0·10	0·10	0·10	0·13
λ/L		0·75	0·70	0·80	0·80
β		25·7°	-3·7°	93·9°	98·8°
ε_θ	uncoupled	118°	99°	-161°	-132°
	coupled	129°	107·5°	-160°	-131°

Table 7

Fn	0·10	0·13	0·16	0·20
Λ_θ	0·98	1·03	1·075	1·13
$\theta_0\omega_e/K\zeta_a$	1·00	1·12	1·25	1·38
λ/L	0·78	0·80	0·83	0·84
ε_θ	126°	142°	160°	178°

It is because of small β that ε_θ does not reach 180° at the ballast condition.

In Table 7 are shown the values Λ_θ, $\omega_e\theta_0/K\zeta_a$ and λ/L, where ε_θ is at the maximum. As seen from this table it is at $\lambda/L \doteqdot 0.8$ that ε_θ reaches its maximum and $\theta_0\omega_e/K\zeta_a$ is of an order of 1.0 at $\lambda/L = 0.8$. In the case of aforementioned ship Y, $\theta_0\omega_e/K\zeta_a$ has nearly equal to 3.0 at $\Lambda_\theta = 1.0$ for the speed of $Fn = 0.10$ (Fig. 32-c).

From these considerations the typical phenomena at ballast condition are summarized into the two following points.

i) For $Fn < 0.20$ at any λ/L in the range of $0.5 < \lambda/L < 2.0$ ε_θ does not attain 180°. When $\Lambda_\theta \doteqdot 1.0$, ε_θ has its maximum value but cannot attain 180°. It is because the phase angle β between the exciting moment and the wave is small.

ii) ε_θ becomes its maximum at much smaller $\theta_0\omega_e/K\zeta_a$ than the one of high speed ships.

In the experiments in regular waves the emergence of the bow bottom from water occurred most frequently for $0.7 < \lambda/L < 1.0$. This fact supports the aforementioned consideration concerning the relation between the maximum ε_θ and λ/L.

4-2-4 Vertical acceleration and relative bow motion

$\bar{C}_{2F}$ is much smaller than for full load condition but $\bar{C}_{2S}$ is not so smaller. $\bar{C}_{50}$ (relative bow motion without dynamic swell-up at Station 9½) is shown in Fig. 33.

4-2-5 Comparison of calculation and experiment concerning ship motions and vertical acceleration

The calculated results of $\bar{Z}$ and $\bar{\theta}$ are compared with the experimental ones for $H/\lambda = 1/50$ in Figs. 34 and 35 respectively.

As for $\bar{Z}$, the calculation and the experiment are in good accord with each other when $\lambda/L > 1.0$, but the latter has not such a minimum value as found in the former. This is the same case with full load condition. When $\lambda/L = 0.9$, the experimental value is larger than twice of the calculated value, though the value itself is quite small. The calculated ε_Z and experimental one agree with each other for $\lambda/L = 0.7$ $(H/\lambda = 1/30)$, but there is a large discrepancy between them for $\lambda/L = 0.9$ $(H/\lambda = 1/50)$ (shown in Table 8). This difference in case of $\lambda/L = 0.9$ is thought to be owing to the difference in exciting force.

Table 8

λ/L		0·70 (H/λ = 1/30)		0·90 (H/λ = 1/50)
Fn		0·100	0·130	0·100
ε_Z	Exp.	−112°	−101°	−126°
	Cal.	−104°	−86°	−50°
ε_θ	Exp.	80°	114°	
	Cal.	107°	86°	

As for $\bar{\theta}$ the theory and experiment are in considerable good accord, and as shown in Table 8, this is also the case with ε_θ. In the experiment for $H/\lambda = 1/30$ (the figures are omitted), we obtained the similar results to the ones in the case of $H/\lambda = 1/50$ for both $\bar{\theta}$, $\bar{Z}$.

If $H/\lambda \leqslant 1/30$, θ_0 and Z_0 increase generally in proportion to the wave height, as in the case of full load condition.

Though N-ship and R-ship are not different in $\bar{Z}$, non-dimensional amplitude of pitch $\bar{\theta}$ of R-ship is a little larger than that of N-ship for $0.8 < \lambda/L < 1.0$ at the speed of $Fn > 0.130$ (Fig. 35). This seems to be because $J+A$ for R-ship is a little larger as described in the discussion about the natural period.

As for $\bar{C}_{2F}$, the calculation and experiment show good agreement, but for $\bar{C}_{2S}$ the latter is smaller than the former as in the case of full load condition.

4-2-6 Thrust increase in regular waves

In Figs. 36, 37 the coefficients of thrust increase in regular waves $\tau_0 = \Delta T/(\rho g \zeta_a^2 B^2/L)$ obtained by experiments are shown for N-ship and R-ship.

In these figures it is found that there are large differences between τ_0 value of N-ship and R-ship when $\omega > 4.8 (\lambda/L < 1.0)$. When the wave height H is small it is very difficult to measure H accurately and therefore it is apprehended that τ_0 may include the error of measurement.

5. Ship motions and vertical acceleration in irregular waves

5-1 Irregular waves and calculation of mean values

5-1-1 Theoretical calculation method

In many cases the wave elevation measured from mean free surface level is considered as a stochastic stationary Gaussian process.

The power spectral density $S_{\zeta\zeta}(\omega)$ of waves is defined as the mean square values of the amplitudes of component waves with the circular frequency ω,

and the power spectrum is given by $S_{\zeta\zeta}(\omega)d\omega = \sum_{\omega}^{\omega+\delta\omega} \zeta^2{}_{an}/2$ (5.1)

and we have the following relations:

$$\left.\begin{array}{ll} \text{Variance} & \sigma^2 = \int_0^\infty S_{\zeta\zeta}(\omega)\,d\omega = m_0 \\ \text{Standard deviation} & \sigma = \sqrt{m_0} \end{array}\right\} \tag{5.2}$$

When the wave spectrum is of narrow band, probability density for the apparent amplitude ζ_a of the wave elevation is given by the Rayleigh formula and the probability P of ζ_a being between a and b is given by:

$$P[a<\zeta_a<b] = \frac{1}{m_0}\int_a^b \xi e^{-\xi^2/2m_0}\, d\xi \tag{5.3}$$

From this equation we can obtain the significant wave height as follows:

$$\bar{H}_{1/3} \fallingdotseq 4\sqrt{m_0} \tag{5.4}$$

Ship motions in irregular waves, if the phenomenon is a stochastic stationary Gaussian process, can be determined as usually by the linear superposition of the ship response to the individual regular wave components[18),19)].

Let us consider, for example, pitching motion for which the amplitude response function is given by $|H_{\theta\zeta}(\omega_e)|$. Then the power spectrum of pitching motion is defined as follows:

$$S_{\theta\theta}(\omega_e)d\omega_e = |H_{\theta\zeta}(\omega_e)|^2\ S_{\zeta\zeta}(\omega_e)d\omega_e$$

Making use of the relation $\int S_{\theta\theta}(\omega_e)d\omega_e = \int S_{\theta\theta}(\omega)d\omega$, $m_{0\theta}$, $m_{2\theta}$ and $m_{4\theta}$

are given by

$$m_{0\theta} = \int_0^\infty S_{\theta\theta}(\omega_e)d\omega_e = \int_0^\infty S_{\zeta\zeta}(\omega)\,|H_{\theta\zeta}(\omega)|^2\,d\omega$$

$$m_{2\theta} = \int_0^\infty S_{\theta\theta}(\omega_e)\,\omega_e^2 d\omega_e = \int_0^\infty S_{\zeta\zeta}(\omega)\,|H_{\theta\zeta}(\omega)|^2\,(\omega+\omega^2V/g)^2 d\omega$$

$$m_{4\theta} = \int_0^\infty S_{\theta\theta}(\omega_e)\,\omega_e^4 d\omega_e = \int_0^\infty S_{\zeta\zeta}(\omega)\,|H_{\theta\zeta}(\omega)|^2(\omega+\omega^2V/g)^4 d\omega \tag{5.5}$$

The narrowness ε and mean period $\bar{T}_2$ derived from zero-up crossing of a spectrum are given as follows:

$$\varepsilon = \sqrt{(m_0m_4-m_2^2)/m_0m_4},\quad \bar{T}_2 = 2\pi\sqrt{m_0/m_2} \tag{5.6}$$

In the case of small ε, the significant value of the double amplitude of pitching may be obtained as follows:

$$2\tilde{\theta}_{0\,1/3} = 4\sqrt{m_{0\theta}} \tag{5.7}$$

As long as the corresponding spectra are narrow, the above mentioned relations are also valid for other motions and phenomena.

5-1-2 Irregular waves used for experiments

We can generate irregular waves in our tank by driving the wave-maker at a constant amplitude and changing the driving period of wave-maker by every one cycle. In the experimental tank there can be many sequences of driving periods of wave-maker for the generation of irregular waves with a given power spectrum.

For our experiments two kinds of sequences of periods, as shown in Fig. 38, were used. Sequence A is one as random as possible and B is a sequence in which periods are gradually changed. It is of course that the histogram of A and B is identical.

A spectrum of Moskowitz-Pierson type may be most suitable for our experiments, however on this research not the spectrum of M-P type but the spectrum which was easily generated by our apparatus was selected. (Experiment with M-P spectrum is planned now).

Six kinds of irregular waves, namely, two kinds of sequences of driving periods with three kinds of significant wave heights, were generally used, but the waves with the spectrum of different mean period were used when necessary. In Table 9, irregular waves used for the experiment of R-ship at ballast conidtion are presented and some of these irregular waves are shown in Fig. 39.

Table 9 Irregular Waves

	Sequence	$\tilde{H}_{1/3}$ (mm)	$\bar{\tilde{T}}_2$ (sec)	ε
No. 6	A	98·0	1·067	0·384
No. 7	B	97·0	1·082	0·401
No. 9	A	160·0	1·177	0·383
No. 10	B	154·0	1·199	0·400
No. 12	A	208·0	1·196	0·400
No. 13	B	215·0	1·204	0·365

We can not always generate an irregular wave with the same $\tilde{H}_{1/3}$ and $\bar{\tilde{T}}_2$, because there may be small errors in setting the amplitude of the wave-maker and a small daily drift of the driving period of the wave-maker.

Therefore we measured waves for every condition of our experiments and the power spectrum obtained from these measurements was applied to the analysis of model experiments.

5-1-3 Examination of Gaussian and Rayleigh distribution

In the derivation of power spectra of waves, ship motions and acceleration etc., the sampling period was 0.1 second, the number of sampling were $600 \sim 900$ and the maximum lag number was 60.

Wave spectra thus obtained and the Gaussian distribution are compared in Fig. 40-a, and b. No. 6 wave looks like the Gaussian distribution, but when wave height becomes larger, there occurs such deviation as shown in Fig. 40-b.

In comparison with Rayleigh distribution some examples show good agreement while others give considerable discrepancy.

5-2 Ship motions and vertical acceleration for ballast condition

5-2-1 Mean value of pitch and heave

Experiments were carried out at various speed of $Fn = 0.100, 0.130, 0.145$ for waves of No. 6, 7, at speed $Fn = 0.056,\ 0.070,\ 0.100$ for waves of No. 9, 10 and at speed $Fn = 0,\ 0.056$ for waves of No. 12, 13.

We carried out one experiment three times, and the average of the significant values of pitch or heave amplitude obtained from the three experimental results was adopted as one experimental value.

In Fig. 41 the theoretical calculation of amplitude of pitch and heave are compared with the experimental results. The significant value of double amplitude of pitch was calculated from the equations (5.5), (5.7) by using the theoretical response function given in Fig. 24. This calculated value shows good agreement with the experimental one.

As for heave, the theoretical value obtained by applying theoretical response function is smaller than experimental one by 30%. This is due to the facts that the theoretical response function is smaller than experimental one at $0.7 < \lambda/L < 1.0$ and the mode frequency of wave spectrum is just in the range of the frequency corresponding to $0.7 < \lambda/L < 1.0$.

Accordingly, we calculated the heave amplitude by using the response function obtained by experiments in regular waves as shown in Fig. 35. The results of this modified calculation and the experimental results in irregular waves almost agreed.

Summarizing the aforementioned descriptions, it may be said that the significant mean values of pitch and heave, which were calculated from the theoretical response function for pitch and from the experimental values of $\bar{Z}$ in regular waves for heave, are nearly in accord with the experimental ones.

Wave slope $\overset{\frown}{H}_{1/3}/\lambda_2 (\lambda_2 = g\overset{\frown}{T}_2{}^2/2\pi)$ is 1/19 for waves No. 6, 7 and 1/13.2 for waves of No. 9, 10 and 1/11.0 for waves of No. 12, 13.

As seen from Fig. 41, the linear superposition principle holds for such a steep wave as $\overset{\frown}{H}_{1/3}/\lambda_2 = 1/13.2$.

Though pitch and heave in irregular waves of R-ship and N-ship were compared in the form of $2\overset{\frown}{Z}_{0\frac{1}{3}}/\overset{\frown}{H}_{\frac{1}{3}}$ and $2\overset{\frown}{\theta}_{0\frac{1}{3}}/\overset{\frown}{H}_{\frac{1}{3}}$, no distinct difference was found between them. But it may be said from Fig. 35 that pitch amplitude of N-ship is a little smaller than that of R-ship at a higher speed, and such a property is also found in Fig. 42.

5-2-2 Vertical acceleration of bow and stern

We can assess the acceleration in irregular waves by the calculation using the theoretical response function for the acceleration of bow and the experimental response function for the one of stern.

5-3 Full load condition

We can compute the significant values of pitch, heave and acceleration in irregular waves by the method similar to that for the ballast condition and its results nearly agrees with the results of experiment. Examples of A_F, A_S are shown in Fig. 43-a and 43-b.

6. Thrust increase in irregular waves

According to the reference (20) the average increase of thrust in irregular waves can be calculated by the equation

$$\varDelta T_W = 2\int_0^\infty S_{\zeta\zeta}(\omega)\varDelta T(\omega)/\zeta_a{}^2 d\omega \tag{6.1}$$

In Fig. 44 the measured $\varDelta T_W$ and the calculated one obtained by using τ given in Figs. 18-a, 18-b, etc. and the equation (6.1) are compared with respect to the case of full load condition of N-ship. It will be found that the calculation and the measurement are considerably in good accord with each other except for a speed $Fn = 0.056$. In Fig. 45 a similar comparison is made on ballast condition of N-ship and R-ship.

For R-ship the calculation and the experiment show fairly good agreement and the difference is within $\pm$ 10% of them. On the contrary, for N-ship their difference is sometimes considerably large, for instance, being 80%.
This large discrepancy is supposed to come from the error in the measurement of the response function for $\lambda/L \leqslant 0.8$.

In the next place we compared $\varDelta T_W/\overset{\frown}{H}{}^2_{\frac{1}{3}}$ of N-ship with that of R-ship for ballast condition in such waves of which $\overset{\frown}{T}_2$ and significant wave height $\overset{\frown}{H}_{\frac{1}{3}}$ are almost identical. The result in No. 6 wave is shown in Fig. 46 as an example. From this figure it is known that the thrust increase of R-ship is smaller than that of N-ship.

With No. 9, 10 waves which have large $\overset{\frown}{H}_{\frac{1}{3}}$, however, there was little difference between both ships.

7. Slamming for ballast condition

Photos. 3 and 4 show the behaviour of R-ship and N-ship in the experiments for ballast condition.

7-1 Frequency of bottom emergence of bow

Generally slamming does not occur if bow bottom does not emerge from water.

In this research we investigated the emergence of a point on the bottom at Station 9½ (R in Fig. 47 shows this point). Horizontal distance from R to the center of gravity G is l_1.

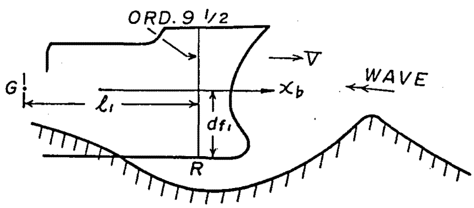

Fig. 47

The relative elevation $S(l_1)$ of the point R to the wave surface is given by $S(l_1) = Z - l_1\theta - \zeta = C_{50}\cos(\omega_e t - \varepsilon_{50})$ as described in 3-3.

Though bow wave and dynamic swell-up should be generally taken into consideration, we neglected them since, in many cases, the bow wave cancells out the dynamic swell-up when the bow is moving upward.

Then we assumed the condition of the bow bottom emergence from water as follows:

$$S(l_1) > df_1 \tag{7.1}$$

where df_1 denotes the draft at Station 9½.

Assuming that $S(l_1)$ in irregular waves is described approximately as stationary Gaussian process, we can obtain the probability of time during which the bow bottom is out of water.

Namely the probability of $S(l_1) > df_1$ is given by

$$P[S(l_1) > df_1] = \frac{1}{\sqrt{2\pi}} \int_{df_1/\sqrt{m_{0s}}}^{\infty} e^{-\xi^2/2} d\zeta \tag{7.2}$$

where

$$m_{0s} = \int_0^\infty \bar{C}_{50}^{\,2}\, S_{\zeta\zeta}(\omega)\, d\omega \tag{7.3}$$

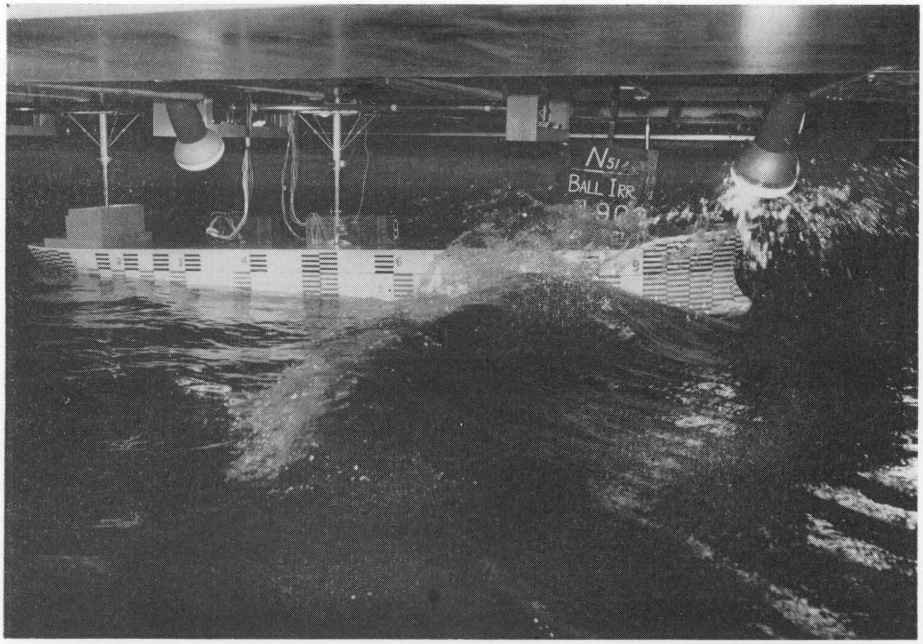

Photo. 3 Tank experiment for N-ship ballast condition in irregular waves of No. 9; Fn=0.10

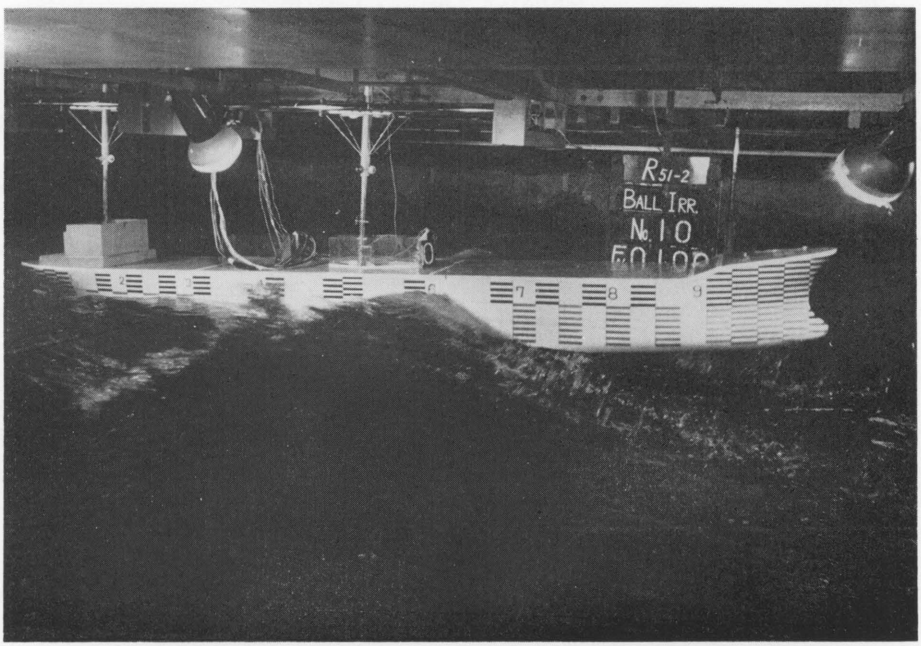

Photo. 4 Tank experiment for R-ship ballast condition in irregular waves of N. 10; Fn=0.10

(*Facing p.* 394)

On the other hand, the frequency of the emergence is rather important for slamming.

If the power spectrum of $S(l_1)$ is of narrow band and the probability density for maxima and minima of $S(l_1)$ is given by Rayleigh distribution, the probability of the bow bottom emergence will be given as follows:

$$P_e[\breve{S}(l)>df_1]=\int_{df_1}^{\infty}\frac{\xi}{m_{0s}}e^{-\xi^2/2m_{0s}}d\xi=e^{-df_1{}^2/2m_{0s}} \tag{7.4}$$

The mean period of the bow emergence or immersion caused by irregular motions of a ship will be given by $\breve{T}_2=2\pi\sqrt{m_{0s}/m_{2s}}$.
Since it is thought that the maximum value $\breve{S}(l_1)$ of $S(l)$ occurs only once in $\breve{T}$, the times N_1 of $\breve{S}(l)$ occurred in time T_A, the total time of one run, is given by the equation

$$N_1=T_A/2\pi\sqrt{m_{0s}/m_{2s}}$$

Therefore, the number of the bow emergence N_e per unit time is

$$N_e=\frac{1}{2\pi}\sqrt{\frac{m_{2s}}{m_{0s}}}\,e^{-df_1{}^2/2m_{0s}} \tag{7.5}$$

where

$$m_{2s}=\int_0^\infty \bar{C}_{50}{}^2\ \omega_e{}^2\ S_{\zeta\zeta}(\omega)d\omega \tag{7.5$'$}$$

The equation similar to the equations (7.3), (7.4), and (7.5) was applied to statistic calculation concerning slamming and shipping of green water by Tick [21], Tasaki [12], Ochi [22] and Fukuda [19].

From the records of ship motions and the emergence of the point R, we obtained an effective time of one run T_A, number of wave encounters W, the times of the bow emergence N_B, and the total time T_B during which the bow bottom is not in water. Experimental values of P and N_e will be given by $P=T_B/T_A$ and $N_e=N_B/T_A$ respectively. We compared the results thus obtained with the theoretical calculation by the equations (7.3), (7.5) using $\bar{C}_{50}$ value at Station 9½ given in Fig. 33.

This comparison is shown in Figs. 48-a, b. As seen in these figures, the experimental value is larger than the calculated one both for P and N_e. Such a result is quite reasonabe since dynamic swell-down is not taken into account. However their difference becomes smaller for large $\breve{H}_{1/3}$.

7-2 Criterion of slamming

It was stated before that in regular waves impact pressure seldom occured even for $H/\lambda=1/30$. In irregular waves, however, impact pressure frequently occurred. In Figs. 49-a, b, c and d are shown some examples of measurements concerning the motions, the vertical acceleration of bow and stern, and the pressure at bow bottom of R-ship. The records shown in these figures are the results obtained when the model ship was run at $Fn=0.100$ in No. 9 wave of Sequence A.

In Figs. 49-a, b the relation of waves with pressure is shown, in which waves are measured by wave height meter B. It should be noted that this wave meter progresses with the towing carriage and the position of the wave meter is not fixed with reference to a model ship. In the case of these figures, the longitudinal position of wave height meter B is averagely sideward of Station 9½ and therefore the record generally shows the wave height at Station 9½. Fig. 49-c shows the relation of waves and the ship motions, and Fig. 49-d is the record of A_F and A_S.

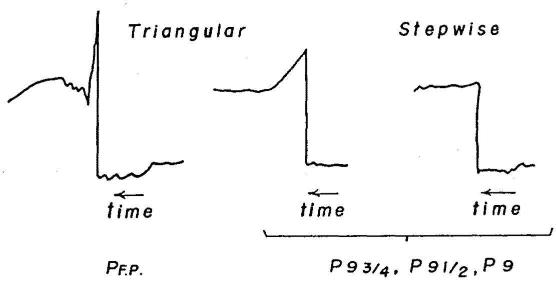

Fig. 50-a

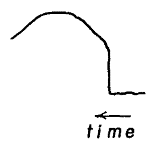

Fig. 50-b

We can find the following facts from these records on R-ship.

(a) The duration of impact pressure at $F.P.$ is so short as 0.01~0.03 second.

(b) At Station 9¾, 9½ and 9 the duration are comparatively long and have triangular form. And there are some examples of stepwise impact pressure (Fig. 50-a). In addition, the forms of the pressure at Station 9¾ have easy slopes in many cases. (Fig. 50-b)

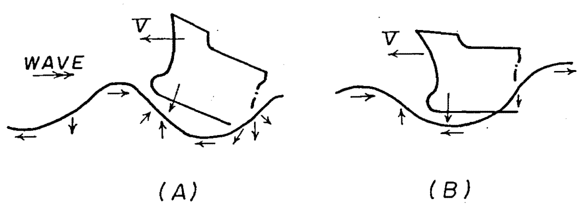

Fig. 51-a

(c) The large pitching motion does not necessarily generate the large impact pressure (point c in Fig. 49-a).

(d) When the ship bottom strikes against a slope of wave surface (the wave orbital velocity is upward, Fig. 51-a-(A)) or a flat surface (the upward component of wave orbital velocity is zero, Fig. 51-a-(B)) with large pitching velocity, the violent impact pressure occurs.

(e) As seen from Fig. 49-c, the decrement of a model speed is considerably large if a violent impact pressure acts successively.

(f) The records of acceleration show an abrupt change at the points B, C, and D at the moment of impact. These facts are found more clearly in Fig. 59-c, which was employed by Ochi [22] to detect the occurrence of slamming.

(g) Generally the impact pressure travels with time from Station 9 to $F. P.$, but it sometimes occurs simultaneously at all stations. In the latter case, the impact pressure and the abrupt change of acceleration are very large.

Ochi [22] regarded that slamming occurred when the acceleration made an oscillatory change at the moment of the bow immersion.

In this paper, however, the auther distinguishes slamming from impact pressure as follows.

(1) When the pressue is of the triangular type or makes stepwise variation with time, it is considered to be an impact pressure.

(2) When the impact pressure defined in (1) acts simultaneously at four stations $F. P.$, 9¾, 9½ and 9 and, in addition, these pressures exceed 8.0cm water head, it is regarded that slamming has occured.

Table 10 Impact Pressure and Slam

Ord.	F. P.	9¾	9½	9	Slam
No. 1	25·1	/	/	/	no
No. 2	73·0	15·0	28·3	18·4	yes
No. 3	20·2	11·1	14·3	15·4	yes
No. 4	27·8	/	/	10·3	no

Some examples of impact pressure or slamming which were obtained fror pressure records in accordance with the aforementioned definitions (1) an (2) are presented in Table 10, where the magnitude of pressure is expressed i water head in cm. No. 2 and No. 3 in Table 10 are considered to be slamming. The examinations of all the records of the pressure lead us to a conclusion that, even when there occurs no impact pressure at Station 9½, occasionally A_F and A_S make an oscillatory change with impact pressure on Station F. P., 9¾ and 9. Whenever we defined the occurrence of slamming, however, A_F and A_S showed an oscillatory change.

7-3 Probability of occurrence of slamming

When the bow bottom of a ship enters the water with large velocity v and, in addition if the angle α between the bow bottom and the water surface is small (Fig. 51-b), then large impact pressure will occur, as discussed by Watanabe [23] and Szebehely [24].

The emergence of the bow bottom from the water is the first requirement

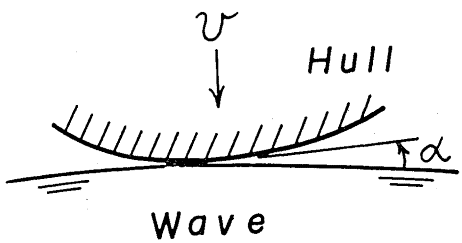

Fig. 51-b

for slamming occurrence, but, even when this requirement has been fulfilled, slamming does not necessarily occur as long as v and β $(=\pi/2-\alpha)$ remain small.

Watanabe [25] showed according to the theory of Wagner [26] that the mean impact pressure of the bottom in the case of the normal impact (In the reference (23) two types of impact, normal impact and oblique one, are defined by Watanabe, and the normal impact is a type of (B) in Fig. 51-a) is given by the following equation

$$P_m = \frac{\rho\pi^2}{4} v_d^2 \tan\beta \tag{7.6}$$

where v_d is the vertical downward velocity of the bow. Moreover he compared the severity of slamming in the form of non-dimensional coefficient n expressed as follows by using draft of full load condition d_{Full}.

$$n = P_m/\rho g d_{Full} = \pi^2 v_d^2 \tan\beta/4gd_{Full} \tag{7.7}$$

Tick [21] gave the theoretical formula for the probability P_s of occurrence of slamming under the condition that the relative vertical speed v_{dr} of the bow with respect to the wave surface exceeds a critical value v_o when the bow bottom enters the water again and the angle α which a keel of a ship makes with the wave surface is very small.
If the condition upon α is taken into account, the formula becomes rather complicated and so he also showed the following simplified expression excluding α.

$$P_s = exp\left[-(df_1^2/2m_{0s}+v_0^2/2m_{2s})\right] \tag{7.8}$$

where m_{0s} and m_{2s} are given by the equatios (7.3) and (7.5)$'$.
Therefore the number of slamming per unit time is given by

$$\mathrm{N}_s = \frac{P_s}{2\pi}\sqrt{m_{2s}/m_{0s}} \tag{7.9}$$

Ochi [22] and Fukuda [19] used the equations (7.8) and (7.9).

Ochi [25] gave the threshold velocity v_0 for five ship models, the average of which was expressed as follows:

$$v_0 \fallingdotseq 0.09\sqrt{gL} \tag{7.10}$$

Using a record of A_F we integrated the acceleration from the time of bow up to the instant of impact and obtained v_d at Station 9½. The relation between $P_{F.P.}$ and v_d is illustrated in Fig. 52. As seen from this figure, slamming seems to occur for $v_d \geqslant 0.3$m/sec. And the validity of the relation $P_{F.P.} \propto v_d^2$ is doubtful. That is to say, it should be thought that the impact pressure is related to the square of relative vertical velocity v_{dr} which includes the wave orbital velocity. Watanabe [23] did not take v_{dr} into account, probably because he wished to simplify the method of the calculation and make easy the analysis of structural damage due to ship slamming. m_{2s} is a variance of

$$-l_1\theta_0\omega_e \sin(\omega_e t-\varepsilon_\theta)+Z_0\omega_e \sin(\omega_e t-\varepsilon_z)-\zeta_a\omega_e \sin(Kl_1+\omega_e t) \tag{7.11}$$

but this should be defined as variance of the correct v_{dr} [27] given by

$$\begin{aligned} v_{dr} &= l_1\dot{\theta}-\dot{Z}+V\dot{\zeta}-V\theta \\ &= -l_1\theta_0\omega_e \sin(\omega_e t-\varepsilon_\theta)+Z_0\omega_e \sin(\omega_e t-\varepsilon_z) \\ &\quad -\zeta_a\omega \sin(Kl_1+\omega_e t)-V\theta_0 \cos(\omega_e t-\varepsilon_\theta) \end{aligned} \tag{7.12}$$

In the table of Fig. 53 the probability of impact pressure prob. [impact], the probability of slamming prob. [slam] = P_s and the maximum impact pressure P_{max} are shown for the cases of $Fn=0.10$ in No. 9 and 10 waves.

Fig. 54-a and Fig. 54-b show a P_{max} distribution along the ship length. As seen from Figs. 53 and 54, any of Prob. [impact], P_s and P_{max} is larger in Sequence B (No. 10 wave) in spite of smaller significant wave height.

The results of the experiment concerning P_s are given in Figs. 55-a, b and Fig. 56. Though P_s has different values according as the waves are of sequence A or B, P_s for the waves of one sequence is not always larger than P_s for those of the other sequence. Since this is also found in the case of P_{max}, therefore in this paper we adopted the mean value for both the sequences as P_s and P_{max}.

Fig. 57 shows one example of P_s calculation based on the equation (7.8). We looked for v_0 at which P_s obtained from the analysis of experiment (in Figs. 55-a, b and Fig. 56) coincided with the one calculated (Fig. 57) by the equation (7.8). This v_0 is shown in Fig. 58, and it can be concluded from this figure that threshold velocity v_0 is not constant but decreases as Fn becomes larger. On the other hand, we can derive $v_0 = 0.5$m/sec from the equation (7.10) and this value seems to give the mean value of the experiments.

Figs. 59-a, b, c are examples of the records of slamming for *N*-ship, where wave height meter *B* is installed on the average at the side of Station 9 of a model ship.

These records for *N*-ship are different from that for *R*-ship in the following points:

1) Impact pressure is small at *F. P.* but large at Station 9½ and 9.
2) In many cases the duration of impact pressure at *F. P.*, Station 9½ and 9 is short.
3) In many cases impact pressure occurs almost simultaneously at *F. P.*, Station 9¾, 9½ and 9.

As seen from Fig. 59-c, A_x as well as A_F and A_S, (A_x is the surging acceleration measured in the neighbourhood of the center of gravity G) make an oscillatory change.

In analyzing the experimental results we applied the same method as in the case of *R*-ship for determination of occurrence of slamming.

In Fig. 60, P_s for *R*-ship is compared with the one for *N*-ship. P_s for *N*-ship has a maximum value at $Fn = 0.130$ and a little smaller value at $Fn = 0.145$. It does not mean, however, as will be discussed later, that running with $Fn = 0.145$ is safer from the view point of slamming than with $Fn = 0.130$.

7.4 Impact pressure

Figs. 61 and 62 show examples of the histogram of slamming impact pressure for *R*-ship and *N*-ship. Although there is no large difference in P_s between *R*-ship and *N*-ship, its distribution along the ship length is quite different.

In Fig. 63 the variation of the histogram of impact pressure at Station 9 with the ship speed is shown, and from this figure we can find that high impact pressure occurs more frequently as the ship speed increases. And the probability of the impact pressure at Station 9 amounting to 48∼56cm water head is 1.9% (0.317 × 8 × 0.75) at $Fn = 0.13$, whereas it is 4.6% (0.255 × 8 × 2.25) at $Fn = 0.145$. The probabilitie of P ⩾ 34cm, that is n ⩾ 2, is presented in Table 11. As seen from this table, P_s is smaller at $Fn = 0.145$ than at $Fn = 0.130$, whereas the probability n ⩾ 2 is larger at $Fn = 0.145$. This fact implies that the higher the ship speed is the more dangerous the ship is from the view point of slamming.

Taelb 11 Ps of N-Ship

Fn	0·056	0·070	0·100	0·130	0·145
Ps	0·067	0·168	0·206	0·322	0·255
Prob. [P9½ > 34cm]	0·047	0·051	0·048	0·185	0·216
Prob. [P9 > 34cm]	0·071	0·208	0·263	0·434	0·588

Ochi theoretically deduced that slamming impact pressure obeys the truncated exponential law given by

$$f(P) = \frac{1}{2CR'_{\dot{r}}}\exp\left[-(P-P_*)/2CR'_{\dot{r}}\right] \tag{7.13}$$

where $R'_{\dot{r}} = 2 \times$ variance of v_{dr} (by equ. 7.11) $(ft/\mathrm{sec})^2$

$C =$ a constant dependent upon the sectional form $(P.S.I. - \mathrm{sec}^2/ft^2)$

$P_* =$ threshold velocity $= 2Cv_0^2$

$f(P) = \%/P.S.I.$

and he stated that it is in good agreement with experiment. The histogram of Fig. 63 resembles to the equation (7.13) in form for small Froude number, though quite different at high speed.

Figs. 64–a, b show the P_{max} distribution along the ship length for R-ship in No. 6, 7 waves. P_{max} attains its maximum at $F.P.$ like in Figs. 55–a, b. Figs. 65 and 66 are the distribution of P_{max} for N-ship. In this case, P_{max} is small at $F.P.$, and it increases to a very large value at Station $9\frac{1}{2}$ and 9. In order to examine the pressure at Station $8\frac{1}{2}$ we carried out another experiment, in which the afore-mentioned pressure was known to be very small, as shown in Fig. 66.

As shown in Figs. 65, 66, P_{max} is almost independent of Froude number and the same property is found in the case of R-ship. This is chiefly because pitching amplitude does not increase, but decrease slightly as Froude number increases. The waves, of which spectrum and mean period are different from those of the waves used in our experiments, bring about the another relation of Froude number and P_{max} which is different from our conclusion.

In Figs. 67 and 68 the P_{max} distribution is compared for N-ship and R-ship. From this comparison it is found that the impact pressure for R-ship is small at Station 9, $9\frac{1}{2}$ and $9\frac{3}{4}$ and large at $F.P.$, whereas for N-ship, the pressure is small at $F.P.$ and large at Station $9\frac{1}{2}$ and 9.

In the next place we will consider the difference in P_{max} distribution for N-ship and R-ship.

From the equation (7.12) the following expression is obtained,

$$v_{dr}/\zeta_a\omega = \bar{C}_3 \cos(\omega_e t - \varepsilon_3) \tag{7.14}$$

where

$$\bar{C}_3 = \sqrt{\bar{A}_3^2 + \bar{B}_3^2}$$
$$\bar{A}_3 = (l_1\theta_0\omega_e \sin\varepsilon_\theta - Z_0\omega_e \sin\varepsilon_z - \zeta_a\omega\sin Kl_1 - V\theta_0\cos\varepsilon_\theta)/\zeta_a\omega$$
$$\bar{B}_3 = (l_1\theta_0\omega_e \cos\varepsilon_\theta - Z_0\omega_e \cos\varepsilon_z + \zeta_a\omega\cos Kl_1 + V\theta_0\sin\varepsilon_\theta)/\zeta_a\omega \tag{7.15}$$

Using the equations (7.14), (7.15) we can calculate the relative velocity v_{dr0} at the instant that the bottom of each Station touches the surface of the regular wave.

Table 7 shows that, for $Fn = 0.130$, ε_θ has its maximum value at $\lambda/L = 0.8$. Taking this fact into account, we computed v_{dr0} of R-ship and N-ship in regular waves of $\lambda/L = 0.8$ and $H/\lambda = 1/15$, the results of which are shown in Fig. 69.

As seen from this figure there is little difference in v_{dr0} between the cases of $Fn = 0.100$ and 0.130. The factors which have dominant influence upon $\bar{C}_3$ are pitching motion and orbital motion of waves.

We also obtained tan β_e from the lines of the ship following Watanabe's method [23] and calculated $v_{dr0}^2 \tan \beta_e$ for $Fn = 0.130$. In the Watanabe's method [23] it is defined that $\tan \beta_e = b_0/\eta$ and $\tan \beta_e \leqslant 11.43$, where b_0 is the half breadth of a section at the height $\eta = 0.0025\ L$ from the keel line.

The calculated results are shown in Table 12 and Fig. 70. The numbers written in brackets of Table 12 denote exact tan β_e and $v_{dr0}^2 \tan \beta_e$. These results are shown with dotted lines in Fig. 70.

As seen from this figure, the pressure is a little larger in the case of R-ship at $F.P.$ and much larger in the case of N-ship at Station 9½ and 9. This relation in the magnitude of the pressure is similar to the experimental results shown in Figs. 67 and 68. In our experiment, however, the pressure for R-ship is particularly large at $F.P.$, and on the other hand, at Station 9½ and 9 it is 1/2~1/3 of that for N-ship. With such a theoretical calculation as shown in Fig. 70, we cannot explain the above experimental facts.

Table 12

	Ord.	F. P.	9¾	9½	9	8½
N-Ship	tan βe	3·2	6·0	10·3	11·43 (20·0)	11·43 (26·6)
	$v_{dr0}^2 \tan\beta e$	2·1	3·8	6·0	5·0 (8·4)	3·4 (7·8)
R-Ship	tan βe	3·7	2·4	6·9	11·43 (16·9)	11·43 (24·0)
	$v_{dr0}^2 \tan\beta e$	2·5	1·3	3·4	4·5 (6·7)	2·7 (5·7)

In the begining, we will discuss on the first point.

The bulbous bow of R-ship is a raised-up one. Through the calculation of v_{dr0} for $\lambda/L = 0.8$ we found that the bottom at $F.P.$ touches the wave surface where the wave slope is nearly equal to its maximum and the upward component of orbital velocity of waves is almost the largest.

The resultant velocity v of v_{dr0} given in Fig. 69 and ship speed $V = 0.72$ m/sec ($Fn = 0.130$) is 1.15m/sec, and consequently, $v^2 \tan\beta e$ becomes twice as large as the value given in Table 12.

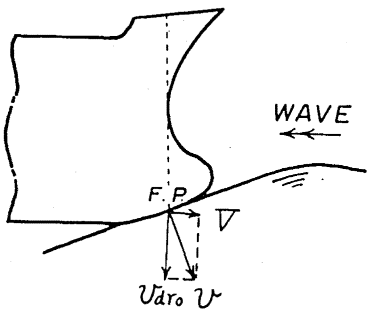

Fig. 71

We can infer as follows. At *F. P.* of *R*-ship there is much possibility that the ship bottom strikes normally against the wave surface (as shown in Fig. 71) with the aforementioned large resultant velocity v, and therefore, the impact pressure at *F. P.* becomes large at the instant of impact. This inference is in accord with the experimental results in (d) of Chapter 7-2.

The calculution of Fig. 70, was carried out under an assumption that a two-dimensional normal impact occurs at each section of a ship. From the pressure variation with time for *R*-ship of Fig. 49, we can find that in many cases the impact pressure travels forward from Station 9 to *F. P.* and that it has long duration at Station 9 and 9½. This seems to mean that the impact at Station 9 and 9½ of *R*-ship is not a normal impact but an oblique impact.

Watanabe [23] asserted that the pressure of oblique impact is not more than a half of the normal impact.

Fig. 72 is the comparison of dead flat forms and water plane forms at $\eta = 0.0025L$ of both ships and this figure shows that the half breadth of dead flat part for *R*-ship is less than a half of that for *N*-ship at Station 9 and 9½.

The fact that an impact on *R*-ship at Station 9½ and 9 is of oblique impact and its magnitude is $1/2 \sim 1/3$ of that on *N*-ship is thought to be owing to the difference in hull forms, especially dead flat form.

The relationship of form and size of dead flat part of a ship to the magnitude of the impact pressure should be investigated in future.

7-5 Mean period of waves and slamming severity.

There can be other waves with the same type of spectrum and significant wave height as used in our experiment, with different mean period $\overset{\approx}{T}_2$.
We calculated the waves of spectra with $\overset{\approx}{T}_2 = 0.8,\ 1.0,\ 1.4,$ and 1.8 seconds and the significant values of *R*-ship motions shown in Fig. 73-a. $2\overset{\approx}{Z}_{0\,1/3}$ and $2\overset{\approx}{\theta}_{0\,1/3}$ increase as $\overset{\approx}{T}_2$ becomes longer. This fact may be a matter of course judging from the characteristics of responce function for pitch and heave.

We calculated the probability P_s and frequency N_s of slamming for waves of $\overline{\overline{T}}_2 = 1.0, 1.4$ seconds and No. 9 wave with the equations (7.8) and (7.9). The results are shown in Fig. 73-b. From this figure it is found that the probability of occurrence of slamming for the case of $Fn = 0.07 \sim 0.10$ becomes the largest at the mean period $\overline{\overline{T}}_2$, which is nearly equal to that of No. 9 wave. In order to confirm this experimentally another experiments were conducted on two kinds of waves 9-A, and 9-B which had almost the same significant wave height as No. 9's one but different $\overline{\overline{T}}_2$. First, P_s of N-ship was calculated for No. 9, 9-A and 9-B wave respectively at $Fn = 0.070$, 0.100 and 0.130.

The results for $Fn = 0.100$ are given in Fig. 74-a, which shows that P_s becomes the largest for No. 9 waves under a constant V_0. Though the figures are not given here we can obtain similar results for $Fn = 0.070$ and 0.130. Secondly, these kinds of waves were generated in the tank and model experiments were conducted.

Fig. 74-b is the result of these experiments, which shows a good agreement with the aforementioned calculation with the maximum P_s in the neighbourhood of $\overline{\overline{T}}_2$ of No. 9 wave in it.

There is no distinct difference among the three waves in the experimentally obtained P_{max}. But the probability of the magnitude of pressure at Station 9 coming to $n \geqslant 2$ is 0.434, 0.265, and 0.400 for No. 9, 9-A and 9-B wave respectively at $Fn = 0.130$. In case of $Fn = 0.100$ it is 0.263, 0.160 and 0.180 respectively. It can be said from these results that the spectra used for our experiments have the average periods $\overline{\overline{T}}_2$ wihch give rise to the severest slamming against these ship models.

7-6 Ship speed in waves and maximum slamming pressure

In order to assess the maximum of slamming pressure it is indispensable to know the speed loss in winds and waves of an actual ship corresponding to a given model ship, that is to say, Nominal Loss of Speed. Leaving the calculation of the loss of speed to an another chance, we tried to estimate by applying wave spectra used in the experiments in this paper the maximum value of slamming pressure under the following assumptions.

Assumption:

(1) The ship speed in still water is $Fn = 0.170$.
(2) We can neglect the wind resistance. That is, the resistance increase is due to waves only.
(3) The ship progresses in head waves with a spectrum used in this paper.
(4) Propulsive efficiency is identical in still water and in waves.

Under these assumptions we can calculate the speed at which E. H. P. of a ship in waves is equal to that at $Fn = 0.170$ in still water by using the results of resistance and self propulsion test in still water and irregular waves. In the case of R-ship we obtained $Fn \doteqdot 0.124$ for No. 6 and 7 waves, and $Fn \doteqdot 0.086$ for No. 9 and 10 waves.

P_{max} at these Froude number were evaluated from Figs. 64-a, b with the results as shown in Table 13, where P_{max} was the mean value over $Fn = 0.11 \sim 0.12$ for No. 6 and No. 7 wave and over $Fn = 0.07 \sim 0.09$ for No. 9 ~ No. 10 wave. Table 13 shows also that it is more severe case on the magnitude of n when a ship runs in No. 9 or 10 wave.

Table 13 n-max of R-Ship

	F. P.	$9^3/4$	$9^1/2$	9
No. 6, 7 Wave	2·3	1·0	0·8	0·6
No. 9, 10 Wave	4·2	1·2	1·2	1·2

When the ship length Lpp is 300m, 350m and 400m, No. 9 ~ No. 10 waves correspond to waves of $\tilde{H}_{1/3} = 16$m, 18.6m and 21.3m respectively. Since Yamanouchi [28] reported that $\tilde{H}_{1/3}$ seldom exceeds 15m, head waves of $\tilde{H}_{1/3} = 15$m was considered to be practically the most severe condition. Assuming that n is proportional to $\tilde{H}^2_{1/3}$ and $\tilde{H}_{1/3} \leqslant 15$m we calculated n-max of an actual ship running in No. 9, 10 waves at speed $Fn = 0.08$ by the interpolation from Figs. 64-a, b. Table 14 gives the results. P_{max} shows little variation with Froude number as shown in Fig. 66 and therefore n-max has always the same magnitude over $Fn = 0.07 \sim 0.100$. Fig. 75 is n-max distribution for ships with Lpp = 250m, 350m presented in Table 14.

In our experiments the data were recorded continuously for 80 seconds at $Fn = 0.08$, and this time length corresponds to 15 minutes in an actual ship of Lpp = 350m. That is, n-max given in Table 14 is the maximum value which may occur in 15 minutes.

Table 14 n-max

Lpp (m)	$\tilde{H}_{1/3}$ (m)	λ_2 (m)	$\tilde{H}_{1/3}/\lambda_2$	n_{max}				
				R - Ship		N - Ship		
				F.P.	$9^3/4$, $9^1/2$, 9	F.P., $9^3/4$	$9^1/2$	9
200	10·6	144	1/13·2	4·2	1·2	1·0	2·6	3·4
250	13·3	179	1/13·2	4·2	1·2	1·0	2·6	3·4
300	15·0	216	1/14·4	3·8	1·2	1·0	2·1	2·7
350	15·0	253	1/17·0	3·2	1·2	1·0	1·7	1·8
400	15·0	287	1/19·0	2·8	1·2	1·0	1·5	1·4

7-7 Method of n-calculation proposed by Structure Committee of the Society of Naval Architects of West Japan[4]

By using the method[4] (it is called W. J. method henceforth) we also evaluated n-max distribution at $Fn = 0.10$ for a ship of R-ship form with Lpp

= 313m and 210, 000 D. W. T. This distribution is given by (A) curve in Fig. 76. On the other hand, (B) curve in this figure shows the results calculated by a modified W. J. method using T_θ obtained from our experiments and calculation of pitching motion (Fig. 24). The magnitude of (A) is much larger than that of (B). The reason why (A) is much larger than (B) is firstly that Froude-Kriloff's theory was applied to the calculation of pitching exciting moment in (A), which is 3. 0, 1. 9, 1. 5 and 1. 4 times as large as the calculated ones in the case of (B) for $\lambda/L = 0.7$, 0. 8, 0. 9 and 1. 0 respectively. And $(\theta_0\omega_e)^2$ derived from W. J. method is abouta quadruple of that of (B) for $\lambda/L = 0.8$. For instance, at $Fn = 0.130$, n-value computed by W. J method is 5. 03, 2. 56, 8. 95, 11. 00 and 7. 03 at Station *F. P.*, 9¾, 9½, 9 and 8½ respectively, on the other hand n-value obtained from the modified W. J. method is 1. 67, 0. 62, 1. 27, 0. 85 and 0. 30.

Following the W. J. method and assuming that P_{max} acts statically upon a bottom panel with its all edges built-in, we evaluated the maximum stress in the panel with the same aspect ratio and thickness as panel plate of a ship of Lpp = 313m and obtained $\sigma_s = 60\text{kg/mm}^2$ on Stations 9 ～ 9¾ in the case of n = 4. If we assume that the bottom damage occurs when σ_s exceeds 30 kg/mm², the bottom should be sufficiently reinforced from the viewpoint of (A), though such a reinfocement is unnecessary from the viewpoint of (B).

The formula of n-value calculation by W. J. method is

$$n = \left\{\frac{\pi^2}{4g}\cdot\frac{L^2}{d_{Full}}\cdot\theta_0{}^2\bar{\omega}_e{}^2\right\}\left\{1-\left(\frac{d\varepsilon}{L\varepsilon\theta_0}\right)^2\right\}\varepsilon^2\tan\beta_e \tag{7.16}$$

Where ε is x_b/L and $d\varepsilon$ is the draft at this position, and $\bar{\omega}_e = 0.9\left(\frac{2\pi}{T_\theta}\right)$.

The term $\left\{1-\left(\frac{d\varepsilon}{L\varepsilon\theta_0}\right)^2\right\}$ is apt to change sensitively with the slight variation of θ_0 if $\varepsilon\theta_0$ is small, and therefore, in such calculation as the W. J. method, θ_0 must be carefully estimated.

(C) of this figure is the experimentally obtained n-max in No. 6, 7 waves and at $Fn = 0.100$, and (D) curve is the interpolated one from the data of Table 14. It may be sure judging from Fig. 64-b that this (D) curve is considered to be also n-max at $Fn = 0.100$. (C), (D) is similar to (B), qualitatively in its distribution, but not quantitatively. Fig. 75 is the results of the application of the W. J. method for the calculation of n-value of *R*-ship and *N*-ship with Lpp = 350m.

This result for *N*-ship is much larger than the value estimated from our experiments in spite of the similarity in their shape of distribution. As for *R*-ship the calculated n-value almost agrees with the one obtained from our experiments at F. P. and Station 9¾, though it does not at Station 9½ and 9, as in Fig. 76.

The aforementioned facts will be summarized as follows.

(1) For a large full ship, W. J. method gives too large θ_0 and consequently very large n-max.

(2) From (B) curve based on the modified W. J. method which was derived by using more correct θ_0, it can be said that n-value becomes very small, and there is no danger of damage with a ship with $Lpp \geqslant 300$m.
(3) The conclusions obtained from (A) and (B) curves contradict each other. The future investigation is neccessary for ascertaining this contradiction.
(4) If we take a measure to counter the damage at *F. P.* for *R*-ship and at Station 9 and 9½ for *N*-ship with taking into account the results in Table 14, they will be almost free from any danger of damage.

8. Deck wetness and impact pressure

8-1 Frequency of deck wetness

The number of deck wetness at F. P. per unit time Nw is derived as follows in a similar manner as in the equation (7. 5),

$$N_w = \frac{1}{2\pi}\sqrt{\frac{m_{2w}}{m_{0w}}}e^{-f\cdot(l)^2/2m_{ow}} \tag{8. 1}$$

where

$$m_{ow} = \int_0^\infty \bar{C}_5{}^2 S_{\zeta\zeta}(\omega)d\omega, \quad m_{2w} = \int_0^\infty \omega_e{}^2 \bar{C}_5{}^2 S_{\zeta\zeta}(\omega)d\omega \tag{8. 2}$$

The equation (8. 1) is of the same type as used in the calculation by Fukuda [19], though he did not take $f_s(l)$ and dynamic swell-up $h_D(l)$ into consideration. Fig. 77 is a comparison of the experimentally obtained Nw in irregular waves No. 6 ~ 13 and the theoretical one calculated with the equation (8. 1).

For No. 6and 7 waves the calculated Nw is not zero, though very small, whereas in the experiment, it was zero. For No. 6~13 waves the theory and experiment show fairly good agreement. In this figure the calculated Nw with no consideration given to $h_D(l)$ is also shown for No. 9 and 10 waves and this is found to be less than half of experimental N_w or that calculated by the equation (8. 1). This N_w will be smaller if $f_s(l)$ is excluded. As stated above, it was known that the experimental result of N_w can be interpreted by the calculation in which $h_D(l)$ given by Tasaki [12] and measured $f_s(l)$ are used.

In Fig. 77 are shown the results of *R*-ship in No. 10 wave, which seem to be a little amaller as compared with that of *N*-ship. It is perhaps because $h_D(l)$ of *R*-ship is a little smaller than that of *N*-ship, since there is no difference in $f(l)$, $f_s(l)$ and motions between both ship models.

8-2 Impact pressure on deck

The impact pressure due to green shipping water was measured on the center line of deck at five stations *F. P.* Station 9¾, 9½, 9 and 8¾ when *N*-ship model ran in irregular waves with full load condition. Let N be the number of times at which the magnitude P' of the impact pressure exceeds 2cm water head, and W the total number of times of pitching motion (about 110 times at $Fn = 0.056$). We calculated the probalility of $P' \geqslant 2$cm water head by N/W, where P' is an impact pressure acting on the deck. The results in No. 9 wave are shown in Fig. 78.

The probability of impact pressure increases for $F.P.$ and Station 8¾ as the ship speed increases, for Station 9½, though the influence of the ship speed is obscure. At Station 9¾ and 9, P' is smaller than 2cm water head.

Fig. 79 shows the relationship between P'_{max} and ship speed. As seen from this figure, P'_{max} at $F.P.$ increases with Froude number but shows no variation at Station 8¾. And P'_{max} at Station 9½ decreases as speed becomes higher.

Judging from the photographs the pressure owing to the fall down of pile-up waves seems to be effective at $F.P.$. At Station 8¾ the impact pressure acts at the moment when the flown up water above the forecastle deck falls down again. P'_{max} of Table 15 was obtained from Fig. 79 assuming $Fn = 0.08$. This P'_{max} corresponds to 7ton/m^2, 7ton/m^2 and 10ton/m^2 at $F.P.$, Station 9, and 8 respectively for a ship with $Lpp = 300$m in No. 10 wave of $\bar{\bar{H}}_{1/3} = 16$m, $\bar{\bar{T}}_2 = 11 \sim 12$ second.

Table 15

	F.P.	9½	8¾
P'_{max}	7 cm	7 cm	10 cm
$n = P'_{max} / \rho g d_{Full}$	0·4	0·4	0·6

9. Conclusion

We investigated the seakeeping qualities of full ship forms with the coefficients $L/B = 6.0$, $C_B = 0.815$ by applying the model experiment and theoretical consideration. For this investigation two ship forms were adopted and their seakeeping qualities were compared in order to examine how the differences in the ship form exert influence upon seakeeping qualities. These two ship-forms are the same in their after bodies but different in their fore bodies and bulbous bows. From this investigation we could derive the following conclusions.

9-1. Ship motions in regular waves

1) Heaving motion for full load condition generally has amplitude larger than that for ballast condition. On the other hand, there is almost no difference in pitching amplitude between full load and ballast conditions.
2) The coupling term g_1 in restoring forces has a negative value for full load condition and a positive one for ballast condition, and in addition,

the absolute value of the former is larger than that of the latter. Therefore the coupling effect of pitching upon heaving motion is comparatively small for ballast condition and very large for full load condition.

3) ε_θ of ballast condition does not amount to 180° at $\Lambda_\theta \doteqdot 1.0$. This fact is owing to the phase angle between the exciting moment and the regular waves. ε_θ has its maximum value at $\lambda/L \doteqdot 0.8$ and in this case $\theta_0\omega_e/K\zeta_a \doteqdot 1.0 \sim 1.1$. The maximum value of $\theta_0\omega_e/K\zeta_a$ is about one third of that for high speed ship with $C_B = 0.64$ (70% load) at the same speed.

9-2 Comparison of theoretical calculation and experiment concerning ship motions in regular waves

1) As regards pitching motions theoretical calculations and experiments show good agreement at ballast condition, but experimental amplitude is a little larger at full load condition for $\lambda/L > 1.1$.
2) As for heaving motions the experimental amplitude is more than twice of the theoretical one for $0.7 < \lambda/L < 1.1$, but for the other λ/L both are in good agreement.
3) The amplitude of pitch and heave are almost proportional to the wave height when H/λ is smaller than 1/30.
4) As for the vertical acceleration of the bow, theory and experiment are in good accord, but experimental value is smaller in case of the one of the stern.
5) Mean thrust increase ΔT is almost proportional to the square of the wave height for $H/\lambda = 1/50 \sim 1/40$.

9-3 Ship motions and others in irregular waves

1) We calculated pitching motions and A_F by using the response function derived from theoretical calculations, and heaving motions and A_S by using the responce function obtained from the experiments in regular waves of $H/\lambda = 1/50$. The significant mean values thus obtained generally agree with the experimental ones.
2) Even for such a steep wave as the wave slope $\overset{\infty}{H}_{1/3}/\lambda_2$ amounts to 1/13.2 ($\lambda_2 = g\overset{\infty}{T}_2{}^2/2\pi$) a linear superposition principle generally holds.
3) In some cases, the experimental values of the mean thrust increase in irregular waves are in fairly good accord with the estimated values by using the response functions in regular waves of $H/\lambda = 1/50$, but they does not always in all cases agree. This disagreement is supposed to be owing to the error in the measurement of the response function for λ/L <0.8.

9-4 Emergence of bow bottom and slamming

1) As for the frequency N_e per unit time of bow bottom emergence from the water the calculated value is fairly smaller than the experimental one for the waves with cmparatively small significant wave height, but the

larger the significant wave height becomes, the smaller their difference is.

2) When the impact pressure acts simultaneously on $F.P.$, Station $9\frac{3}{4}$, $9\frac{1}{2}$ and 9, the magnitude of impact pressure attains its maximum and the oscillating variation of acceleration becomes larger.
3) When bow bottom strikes against the slope of wave surface at which the upward component of wave orbital velocity is nearly maximum, there occurs violent impact pressure.
4) Threshold velocity obtained from our experiments varies with Froude number in contrast with Ochi's [25] result, where threshold velocity does not depend on Froude number in the case of a constant ship length.
5) For $0.07 \leqslant Fn \leqslant 0.13$ the magnitude of slamming impact pressure and its distribution along the ship length are almost independent of Froude number. At a higher speed, however, the probability of high impact pressure becomes larger. It may be therefore said from the view point of slamming that it is more dangerous at a higher speed than at a lower speed.
6) The impact pressure of R-ship with a raised-up bulbous bow is largest at $F.P.$ and smaller at Station $9\frac{3}{4}$, $9\frac{1}{2}$ and 9. On the contrary, the impact pressure of N-ship is very large at Station $9\frac{1}{2}$ and 9, and small at $F.P.$ and Station $9\frac{3}{4}$. That is to say, their distributions have an opposite tendency.
7) The reason why the impact pressure of R-ship is large at $F.P.$ is that the ship bottom strikes normally against the wave surface with the resultant velocity of its relative downward velocity with respect to the wave and the ship speed V. The fact that the pressure at Station 9 and $9\frac{1}{2}$ is less than half of the pressure in N-ship is supposed to be due to the reason that the area of dead flat part in the R-ship bottom is less than half of that in N-ship and that there occurs the oblique impact called by Watanabe [17].
8) In the method proposed by the Structure Committee of the Society of Naval Architects of West Japan [4] the pressure of full ship forms is overestimated. This may be ascribed to the fact that the exciting pitching moment is computed based on the Froude-Kriloff's assumption.
9) Full ship forms are exposed to small impact pressure in spite of their large $\tan\beta_e$ in the bow bottom. One reason for it is because their ship motions are of small amplitude and the another is because ε_θ does not come to 180° at the resonance point.

9-5 Deck wetness and water pressure on deck

1) Using the empirical formula of dynamic swell-up given by Tasaki [12], occurrence of deck wetness obtained from our experimente in regular waves and in irregular waves can be well explained. When dynamic swell-up h_D is neglected, then the calculated value becomes less than half of the experimental one, and therefore, h_D should be taken into consideration, especially for the case of full ship.
2) The mechanism by which green sea comes up over deck is so complicated

that it is very difficult to understand. In our models large impact pressure was exerted upon the deck at *F. P.* and Station 8¾.

9-6 Comparison of *N*-ship and *R*-ship

We can compare *N*-ship and *R*-ship by applying many results obtained in this research from the view point of the concept "optimum ship form in waves" which was proposed in the Introduction. Here both ship forms are supposed to be actual ships with length more than 200m.

1) There is little difference in ship motions, vertical accelerations and thrust increase at full load condition between both ships.
2) Frequency of deck wetness is a little higher in *N*-ship for full load condition than that in *R*-ship.
3) For ballast condition both ships have almost the same amplitude of heave. But pitching and vertical acceleration of *N*-ship are a little smaller than those of *R*-ship for $Fn \geqslant 0.130$ and $0.8 < \lambda/L < 1.2$.
4) In the case of *N*-ship, we must take care of the structual strength at Station 9 and 9½ against slamming impact pressure. As for *R*-ship in which oblique impact is apt to happen, there may be no danger of damage due to slamming if the structure at *F. P.* and bulbous bow are strengthened.
5) We can find from our experiment that the thrust increase is smaller in *R*-ship than in *N*-ship under moderate sea condition, though there is no difference between them under severe sea condition.

Which ship form of *R*-ship or *N* is better in seakeeping quality or in which sea area they are most suitable to run, the author dare not decide immediately only with the support of the results obtained from our researches.

The author hopes to study further on the problems of whipping. He also wishes to do his best to find out the method to obtain the optimum ship form under a sea condition on the basis of the present investigation and the results of observation made on actual ships.

Acknowledgments

The author wishes to express his deepest appreciation to Emeritus Professor Y. Watanabe of Kyushu University for his kind guidance. He is indebted to Associate Professor R. Yamazaki of Kyushu University, Professor S. Hatano, Associate Professor M. Nakato of Hiroshima University and Lecturer M. Okusu of Kyushu University for the helpful discussions and Dr. M. Takagi of Technical Research Labaratory, Hitachi Shipbuilding & Engineering Co., Ltd. for the offering of his calculation results.

The author is indebted to Mr. M. Kurihara, H. Arakawa, K. Kawasumi and T. Kita for their cooperation throughout this research.

Particular thanks are due to Mr. A. Tashiro, M. Yasunaga, M. Inada, K. Watanabe and Miss Y. Okazaki, F. Mori, K. Yagi, K. Marubayashi, M. Hohjoh who cooperated with the author in carrying out experiment and numerical calculation.

References

1) Lewis, E.V.: "Ship Speeds in Irregular Seas" S.N.A.M.E., 1955.
2) Ochi, M.K.: "Performance of Two Hull Forms (U and V) in Irregular waves" Symposium on" Some Effects on Hull Form on Ship Performance in a Seaway", New York, October 10, 1967.
3) Takezawa, S: "A Study on the Large Bulbous Bow of a High Speed Displacement Ship, Part 2, Performance in Waves", Journal of the Society of Naval Architects of Japan, Vol. 111, June, 1962.
4) Report of the Structure Committee of the Society of Naval Architects of West Japan: "Slamming Damage and a Prevention Method", Lectured at the 35th Meeting of the Society of Naval Architects of West Japan, October, 1967.
5) Tasai, F.: "Experiments on Heaving and Pitching Motions of a Ship Model in Regular Longitudinal Waves", Bulletin of Research Institute for Applied Mechanics, Japanese) No. 26, 1967.
6) Watanabe, Y.: "On the Theory of Heaving and Pitching Motions", Thechnology Report of the Faculty of Engineering, Kyushu University, Vol. 31, No. 1, 1958.
7) Fukuda, J.: "Computer Program Results for Response Operators of Wave Bending Moments in Regular Oblique Waves", Journal of the Society of Naval Architects of West Japan, No. 32, July, 1966.
8) Tasai, F.: "Damping Force and Added Mass of Ships Heaving and Pitching", Reports of Research Institute for Applied Mechanics, Kyushu University, Vol. VII, No. 26, 1959.
9) Tasai, F.: "Damping Force and Added Mass of Ships Heaving and Pitching (Continued)", Reports of Research Institute for Applied Mechanics, Kyushu University, Vol. VIII, No. 31, 1960.
10) Tasaki, R.: "On the Shipping Water in Head Waves ", Journal of the Society of Naval Architects of Japan, Vol. 107, July, 1960.
11) Maruo, H.: "On the Increase of the Resistance of a Ship in Rough Seas (1)", Journal of the Society of Naval Architects of Japan, Vol. 101, August,, 1957.
12) Tasaki, R.: "On Shipping Water", Monthly Report of Transportation Technical Research Institute, Vol. 11, No. 8, August, 1961.
13) Tasai, F.: "Wave Height at the Side of Two-Dimensional Body Oscillating at the Surface of a Fluid", Reports of Research Institute for Applied Mechanics, Kyushu University, Vol. 9, No. 35, 1961.
14) Tasai, F.: "Note on the Shipping Water", Bulletin of Research Institute for Applied Mechanics (Japanese), No. 18, 1961.
15) Newton, R. N: "Wetness Related to Freeboard and Flare", T.I.N.A., 1959.
16) Fukuda, J., Shibata, J. and Toyota, H.: "On the Longitudinal Strength of a Supertanker in Regular Head Waves", Journal of the Society of Naval Architects of West Japan, No. 26, September, 1963.
17) Gerritsma, J.: "Ship Motions in Longitudinal Waves", TNO Report, No. 35 S, 1960.
18) St. Denis, M. and W.J. Pierson,: "On the Motions of Ships in Confused Seas", S.N.A.M.E., Vol. 51, 1953.
19) Fukuda, J. and Shibata, J.: "Some Problems Associated with the Ship Motions in Rough Seas, and the Effects of Ship length on Them", Journal of the Society of Naval Architects of West Japan, No. 30, August, 1965.
20) Gerritsma, J.: "Behaviour of a Ship in a Seaway", TNO Report, No. 84 S, 1966.

21) Tick, Leo J.: "Certain Probabilities associated with Bow Submergence and Ship Slamming in Irregular Seas", Journal of Ship Research, 1958.
22) Ochi, M. K.: "Extreme Behaviour of a Ship in Rough Seas--Slamming and Shipping of Green Water", S. N. A. M. E., 1966.
23) Watanabe, Y.: "On the Properties of Hydrodynamic Impact on Ship Bottom and Whipping "and" A Judging of Slamming Occurrence and its Relation to Foredraft", Journal of the Society of Naval Architects of West Japan, No. 32, July, 1966.
24) Szebehely, V. G.: "Progress of Theoretical and Experimental Studies of Ship Slamming", Ships and Waves.
25) Ochi, M. K.: "Prediction of Occurrence and Severity of Ship Slamming at Sea", 5th Syposium on Naval Hydrodynamics, Bergen, Norway, 1964.
26) Wagner, H.: "Uber Stoss und Gleitvorgänge an der Oberfläche von Flüssigkeiten", Z. A. M. M., 1932.
27) Fukuda, J.: "A Practical Method of Calculating Vertical Ship Motions and Wave Loads in Regular Oblique Waves", Note Presented in the Rome Meeting of the Committee 2 on "Wave Loads, Hydrodynamics", ISSC, August, 1968.
28) Yamanouchi, Y.: "Extreme Condition of Waves", Japan Shipbuiding & Marine Engineering, Vol. 2, No. 2, March, 1967.

(Received December 9, 1968)

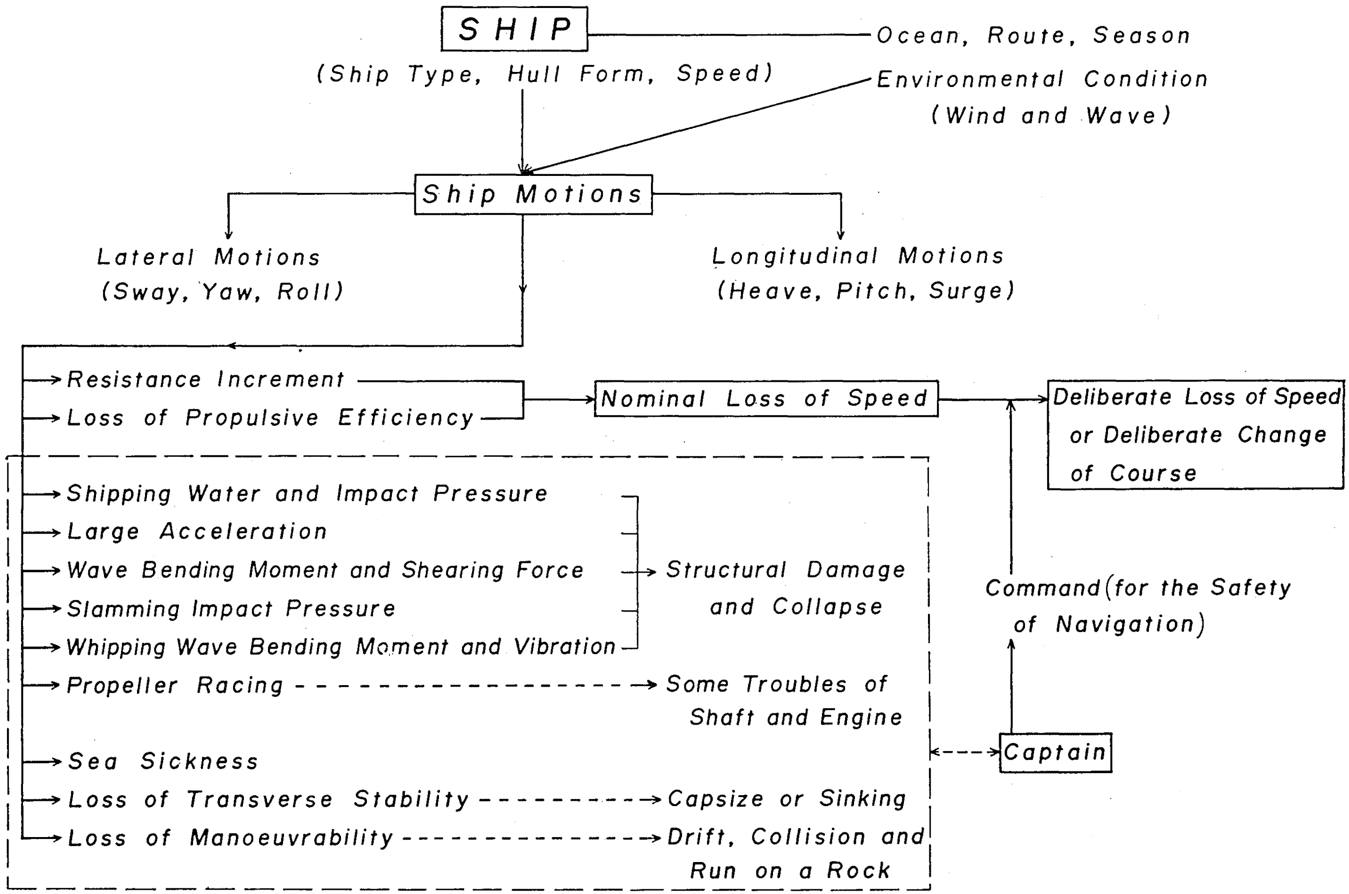

Fig. 1 Seakeeping qualities

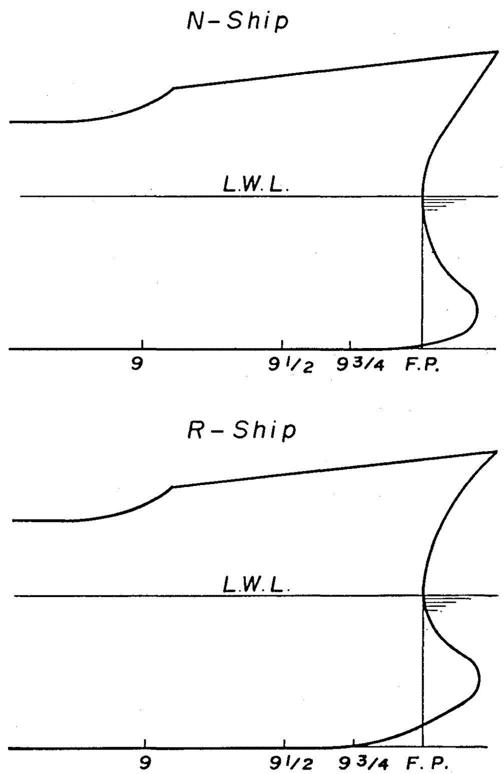

Fig. 2 Profiles of bow forms

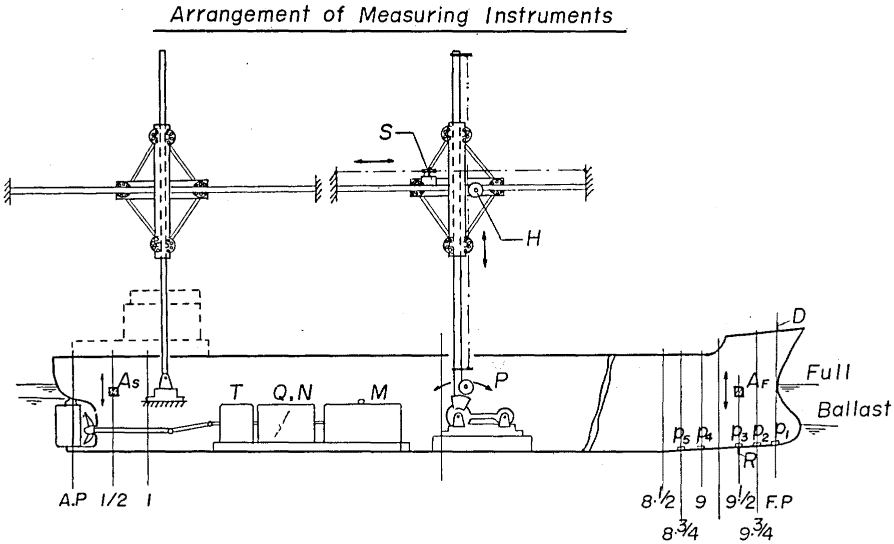

Fig. 3 Arrangement of Measuring Instruments

S : Potentiometer for Surge
P : Potentiometer for Pitch
A_S, A_F : Accelerometer
Q : Torque Meter
M : Driving Motor
D : Deck Wetness Sensor
H : Potentiometer for Heave
P_1, P_2, P_3, P_4, P_5 : Pressure Gauge
T : Thrust Meter
N : Revolution Counter
R : Bow Emergence Sensor

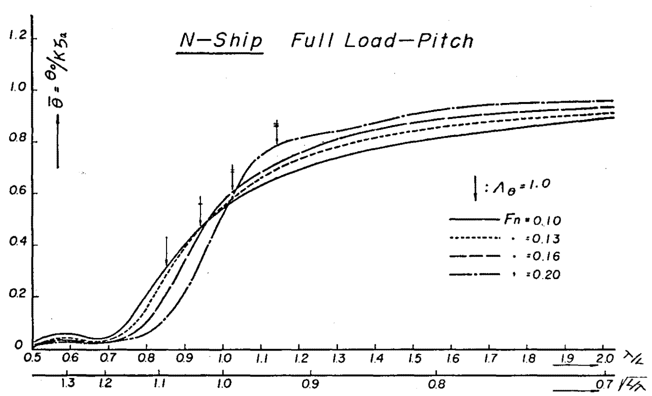

Fig. 5 Calculated frequency characteristics of pitch amplitude

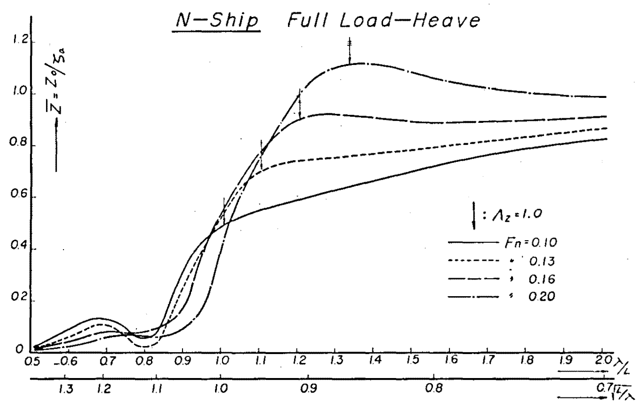

Fig. 6 Calculated frequency characteristics of heave amplitude

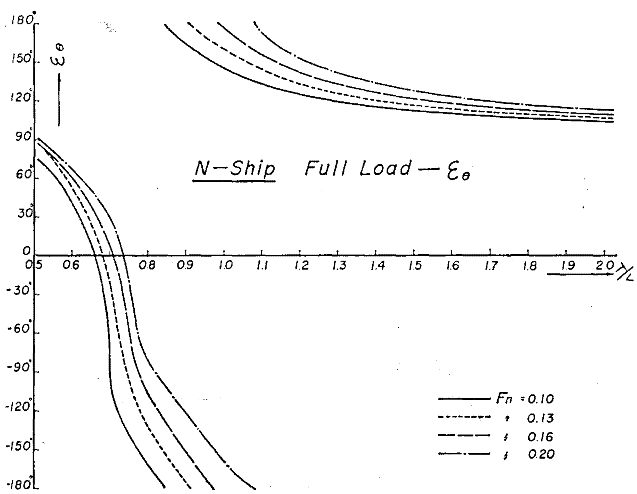

Fig. 7 Calculated frequency characteristics of phase angle between pitch and waves

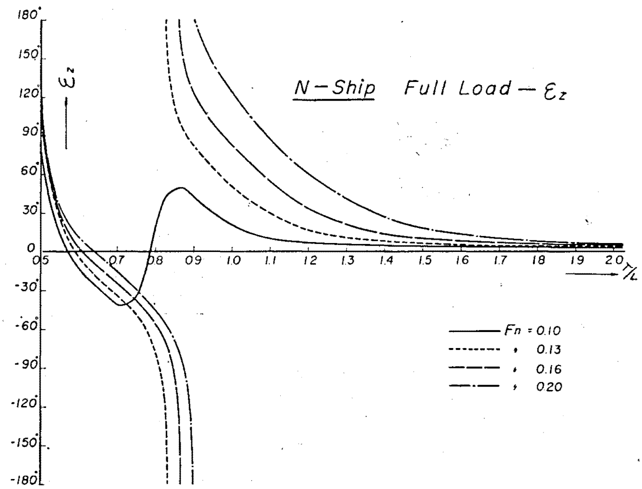

Fig. 8 Calculated frequency characteristics of phase angle between heave and waves

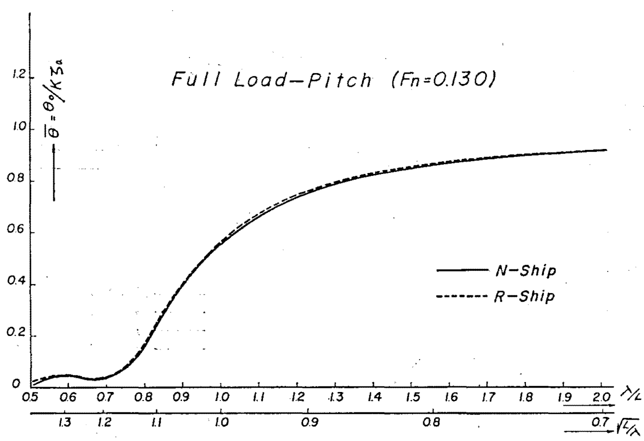

Fig. 9 Comparison of amplitudes of pitch for N-ship with those for R-ship

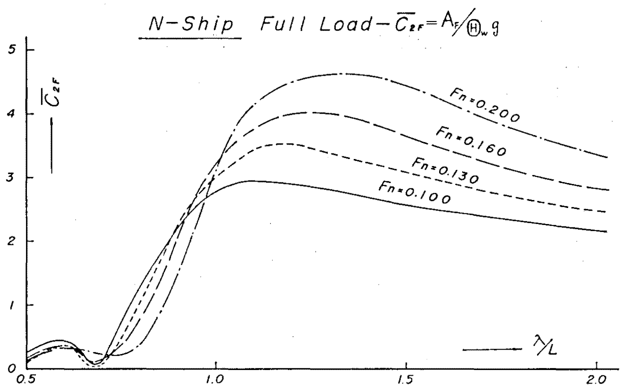

Fig. 10 Frequency characteristics of vertical acceleration of bow

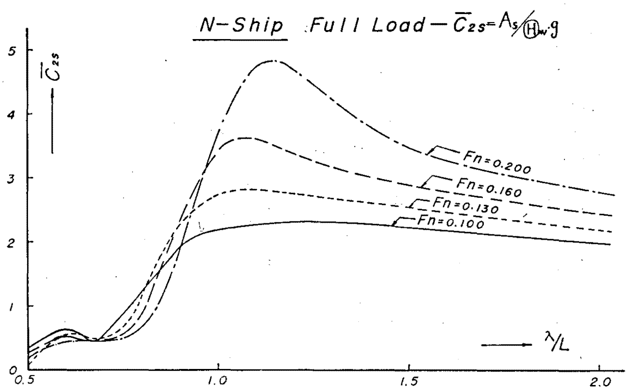

Fig. 11 Frequency characteristics of vertical acceleration of stern

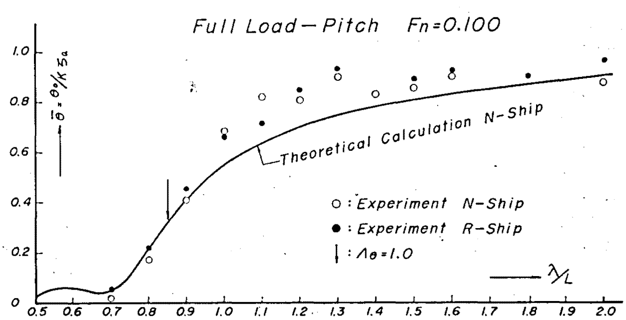

Fig. 12–a Comparison of calculated and measured amplitude of pitch; Fn=0.10

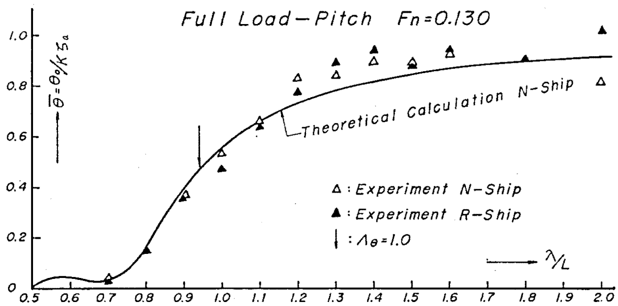

Fig. 12-b Comparison of calculated and measured amplitude of pitch; Fn=0.13

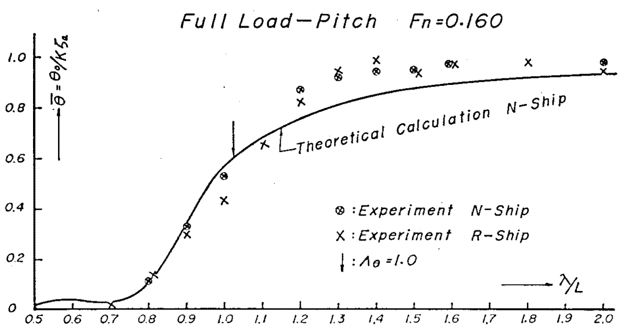

Fig. 12-c Comparison of calculated and measured amplitude of pitch; Fn=0.16

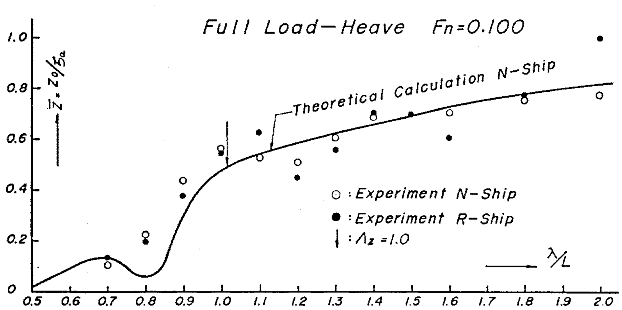

Fig. 13-a Comparison of calculated and measured amplitude of heave; Fn=0.10

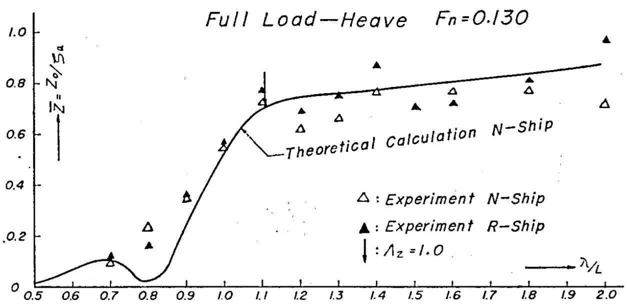

Fig. 13-b Comparison of calculated and measured amplitude of heave; Fn=0.13

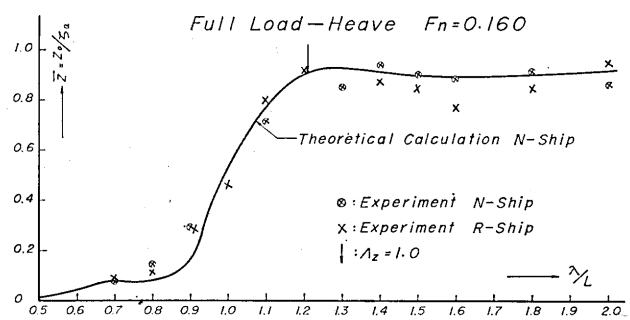

Fig. 13-c Comparison of calculated and measured amplitude of heave; Fn=0.16

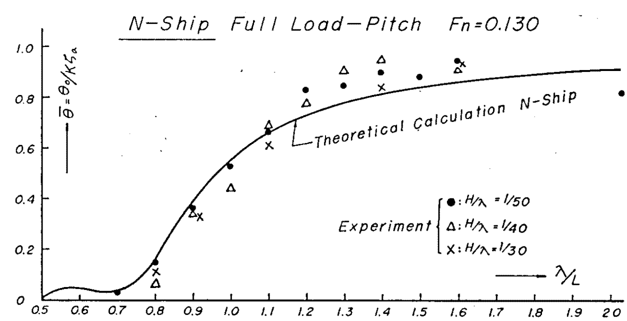

Fig. 14 Measured amplitudes of pitch in regular waves of different steepness H/λ

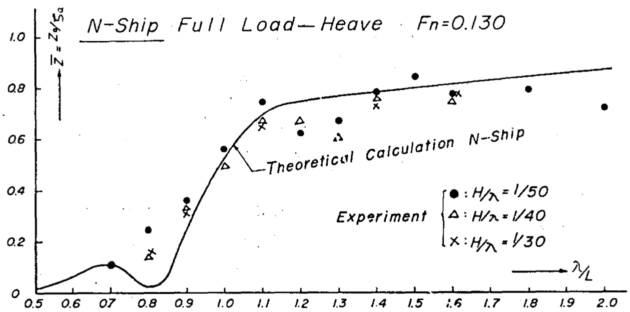

Fig. 15 Measured amplitudes of heave in regular waves of different steepness H/λ

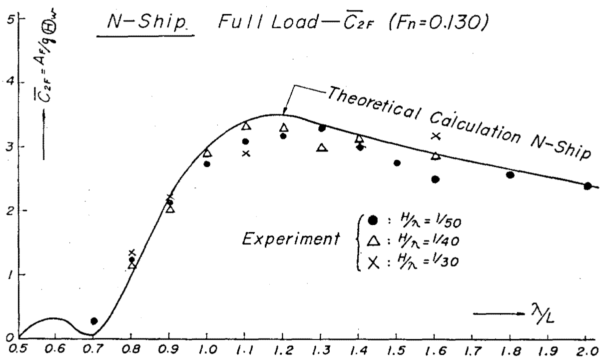

Fig. 16 Measured amplitudes of vertical acceleration of bow in regular waves of different steepness H/λ

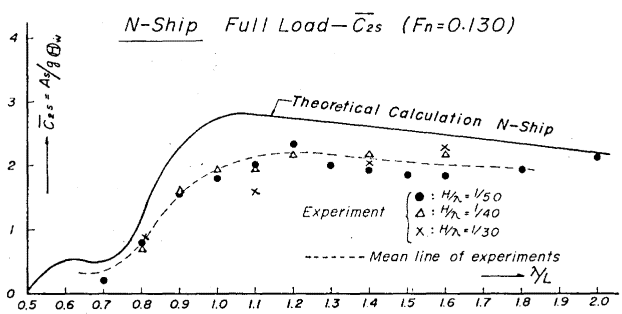

Fig. 17 Measured amplitudes of vertical acceleration of stern in regular waves of different steepness H/λ

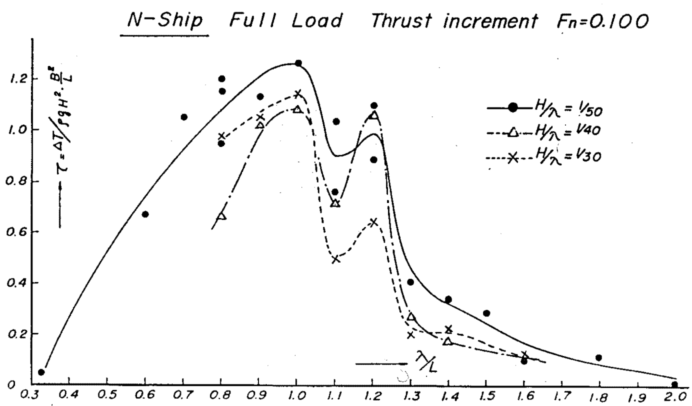

Fig. 18-a Mean increase of thrust measured in regular waves of different steepness H/λ; Fn=0.10

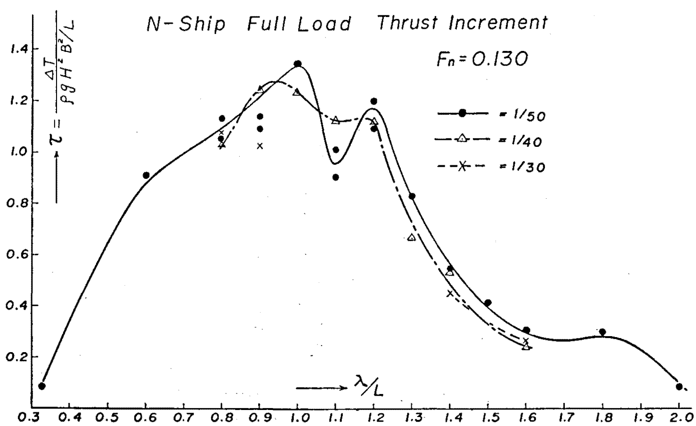

Fig. 18-b Mean increase of thrust measured in regular waves of different steepness H/λ; Fn=0.13

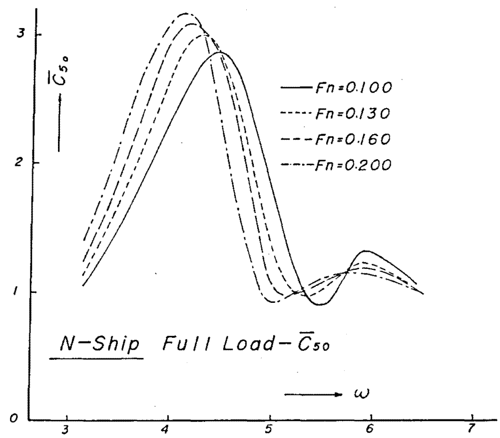

Fig. 19 Amplitude characteristics of the relative bow motion at the forward perpendicular —— without dynamic swell-up

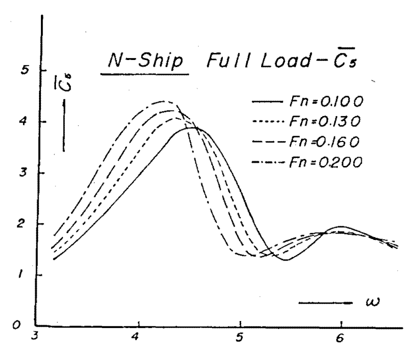

Fig. 20 Amplitude characteristics of the relative bow motion at the forward perpendicular —— with dynamic swell-up

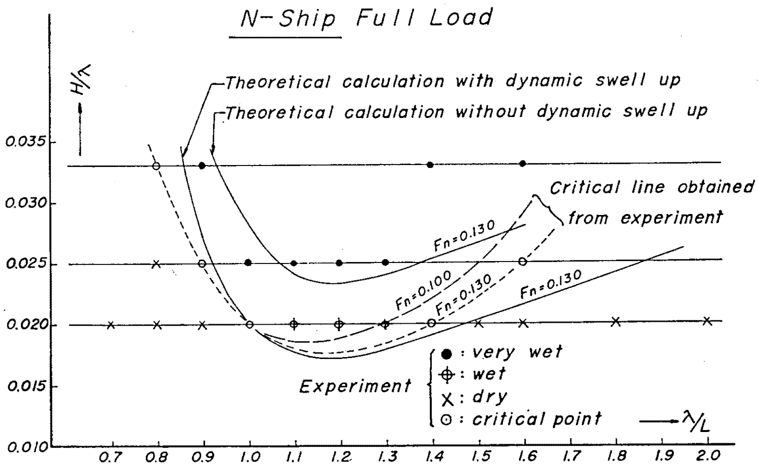

Fig. 21 Observed wetness of deck and calculated critical lines of wetness at the forward perpendicular

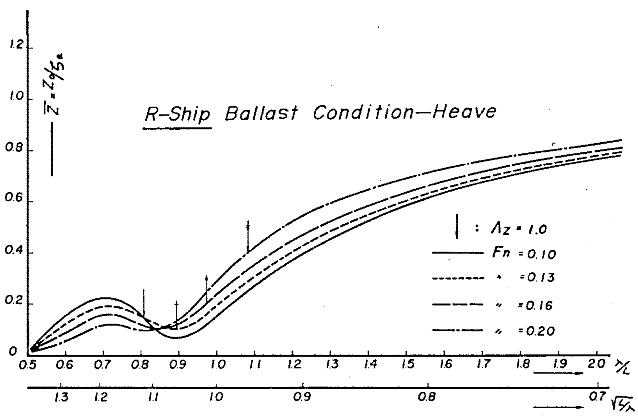

Fig. 22 Calculated frequency characteristics of heave amplitude

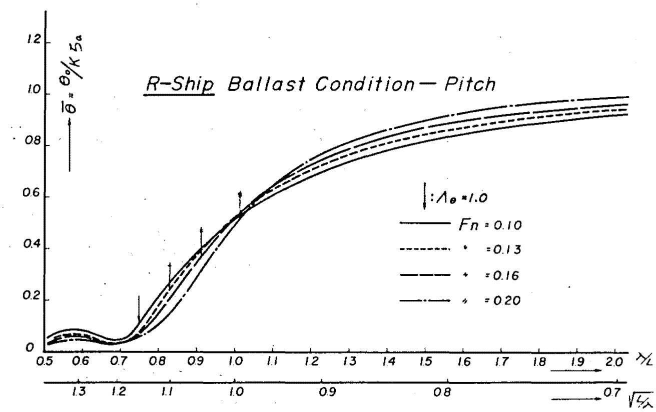

Fig. 23 Calculated frequency characteristics of pitch amplitude

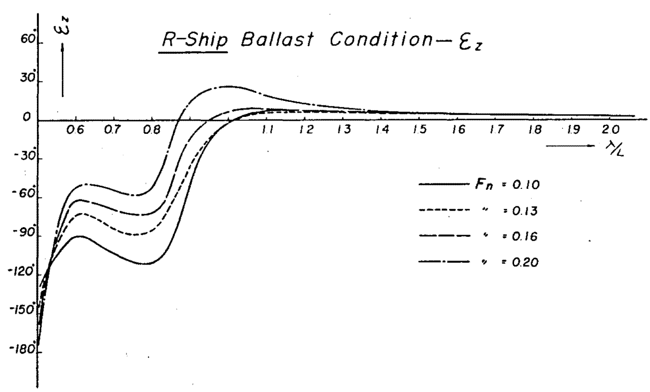

Fig. 24 Calculated frequency characteristics of phase angle between heave and waves

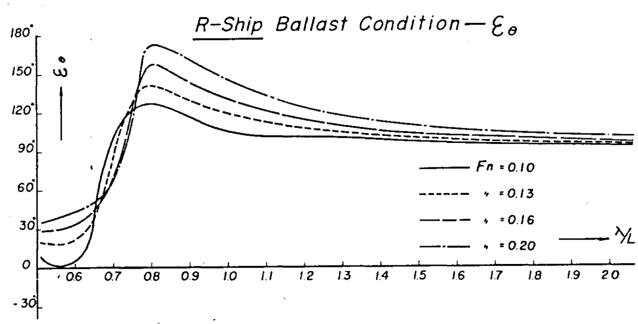

Fig. 25 Calculated frequency characteristics of phase angle between pitch and waves

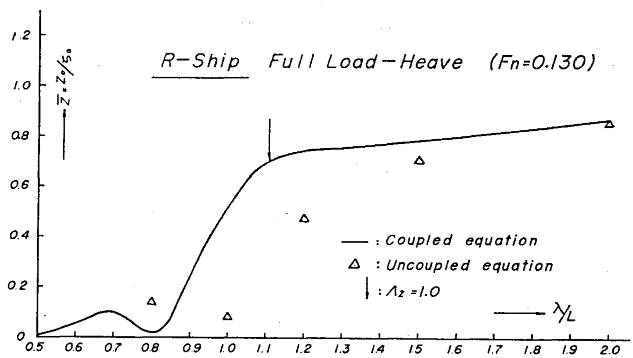

Fig. 26 Comparison of solutions by coupled equations and those by uncoupled equation for heave —— Full Load

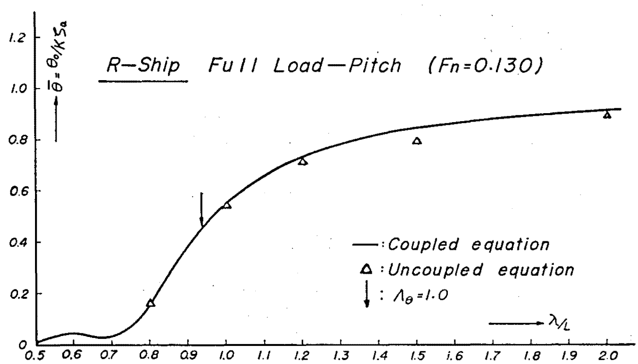

Fig. 27 Comparison of solutions by coupled equations and those by uncoupled equation for pitch —— Full Load

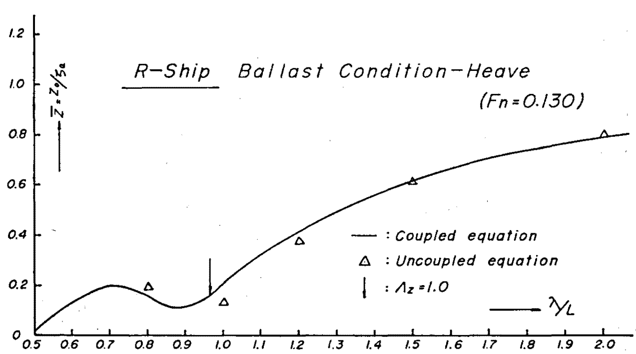

Fig. 28 Comparison of solutions by coupled equations and those by uncoupled equation for heave —— Ballast Condition

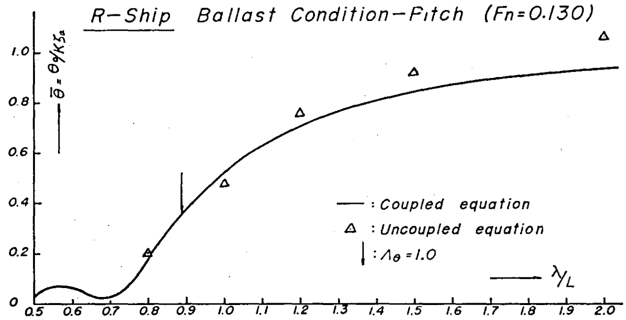

Fig. 29 Comparison of solutions by coupled equations and those by uncoupled equation for pitch —— Ballast Condition

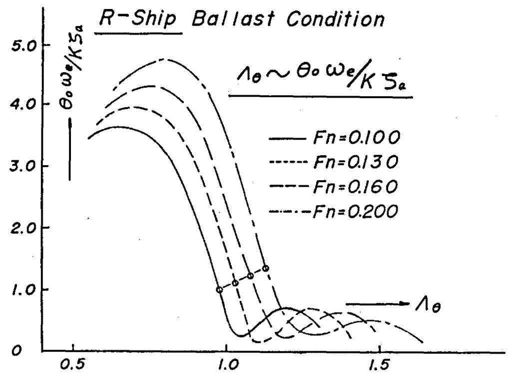

Fig. 30 Calculated $\theta_0\omega_e/K\zeta_a$ versus tuning factor Λ_θ

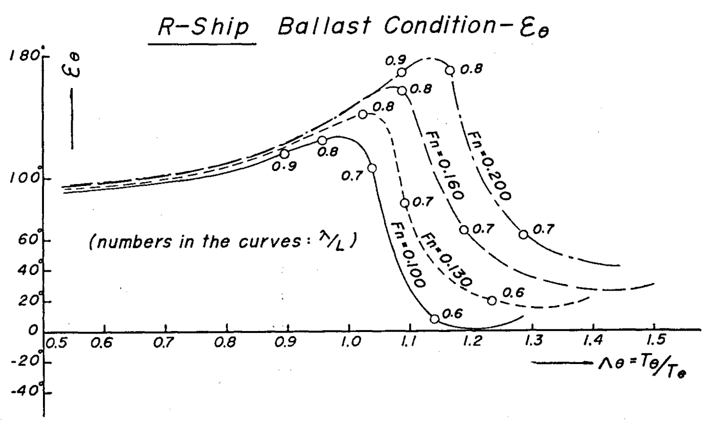

Fig. 31 Frequency characteristics ε_θ versus tuning factor Λ_θ

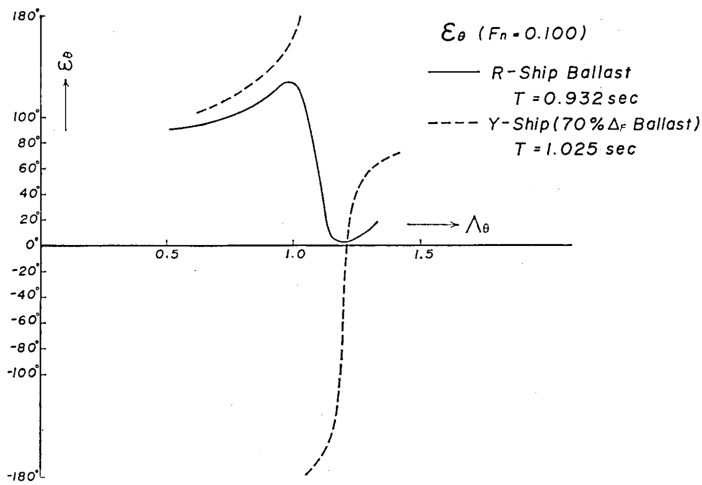

Fig. 32–a

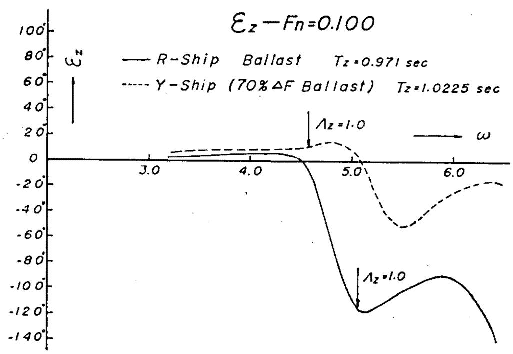

Fig. 32–b

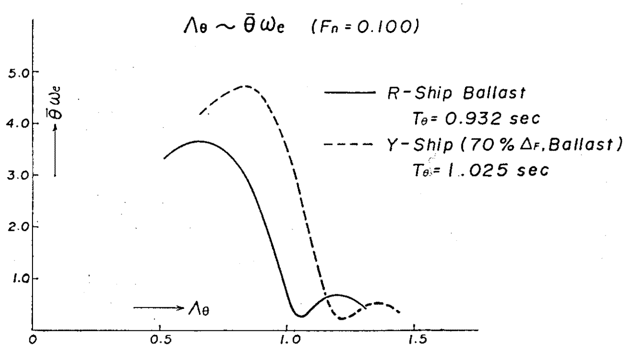

Fig. 32–c

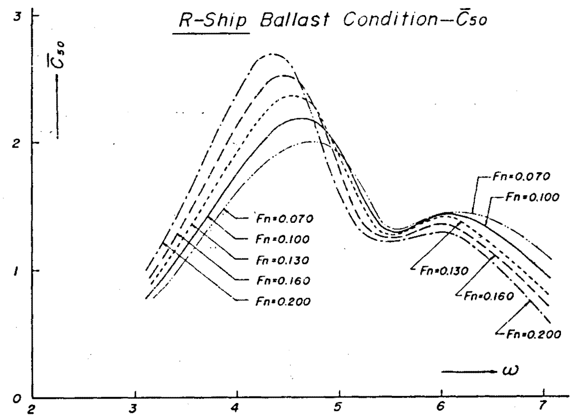

Fig. 33 Calculated amplitude characteristics of relative bow motion at Station 9½

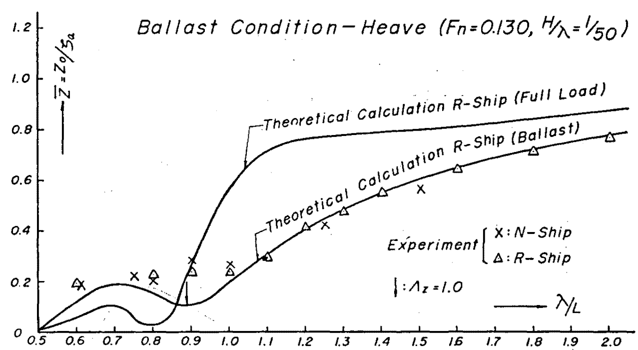

Fig. 34 Comparison of calculated and measured amplitude of heave

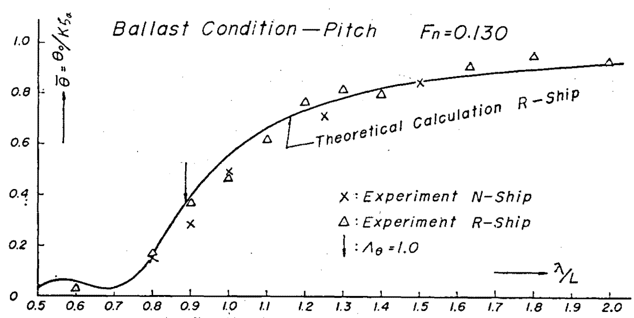

Fig. 35 Comparison of calculated and measured amplitude of pitch

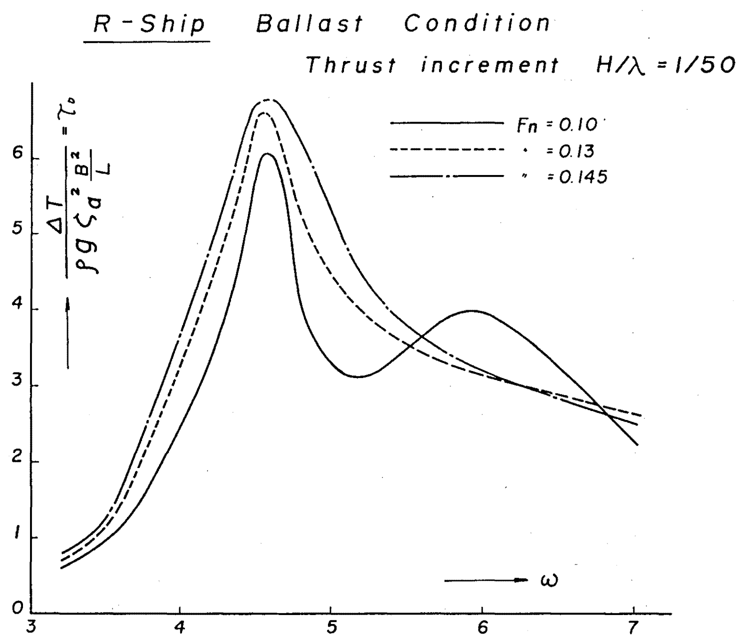

Fig. 36 Mean thrust increase for R-ship in regular waves

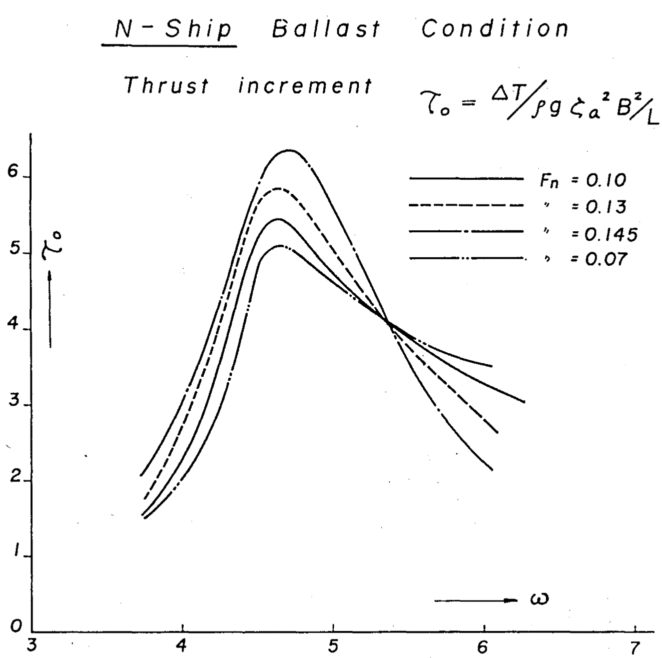

Fig. 37 Mean thrust increase for N-ship in regular waves

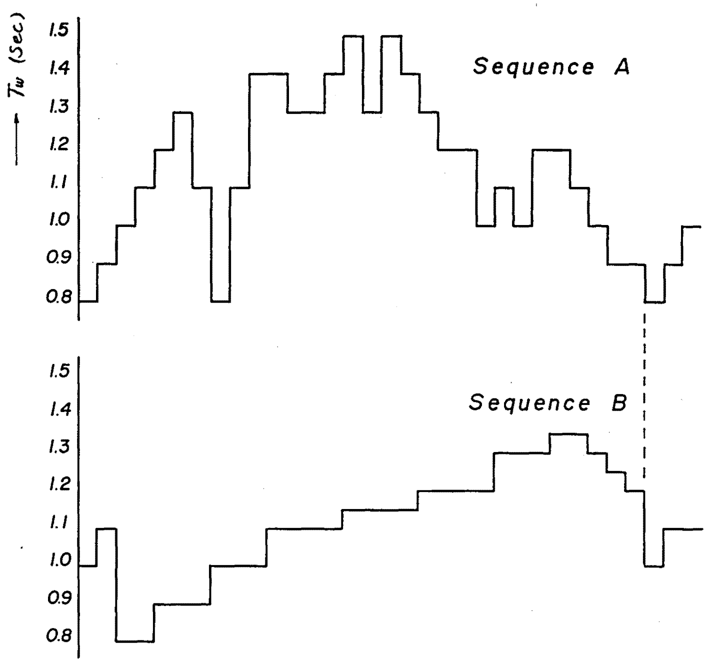

Fig. 38 Sequence of driving periods of wave-maker

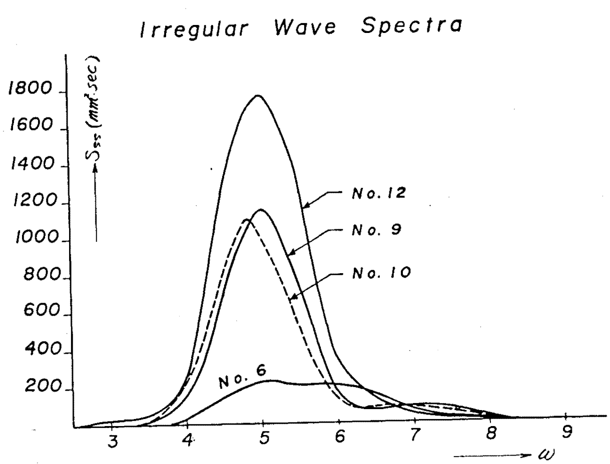

Fig. 39 Some examples of irregular wave spectra used for the experiment

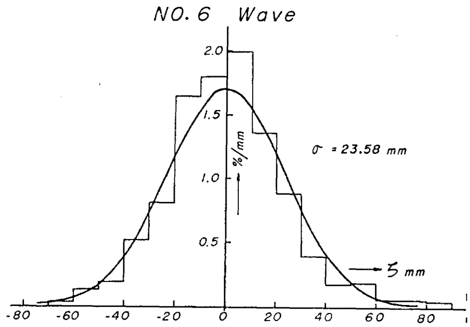

Fig. 40-a Comparison of Gaussian distribution and measured results

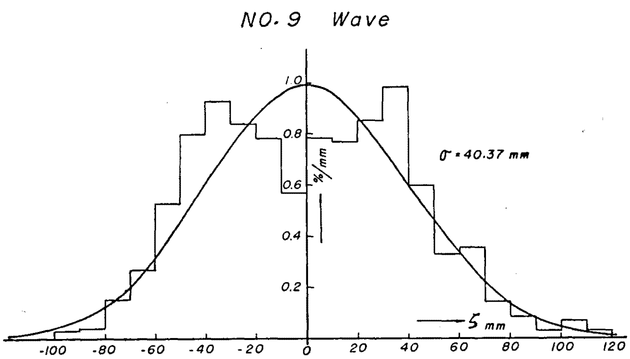

Fig. 40-b Comparison of Gaussian distribution and measured results

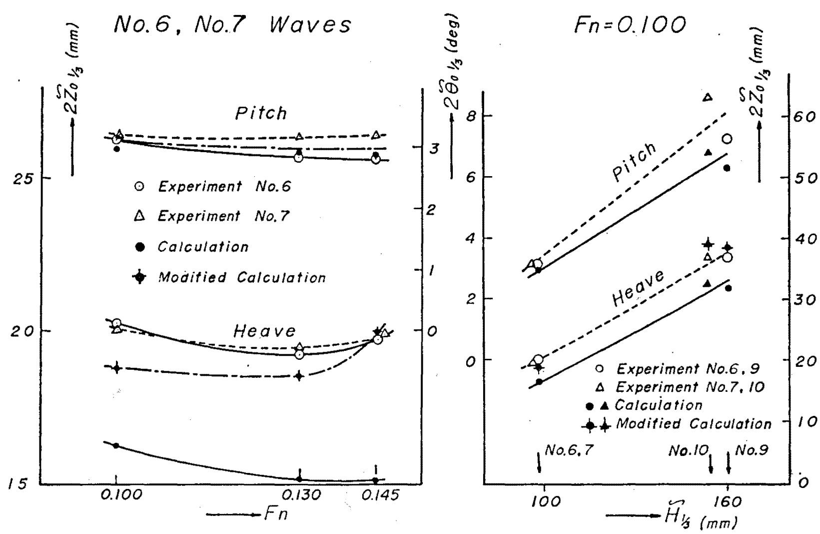

Fig. 41 Comparison of calculated and measured significant values of double amplitude of heave and pitch

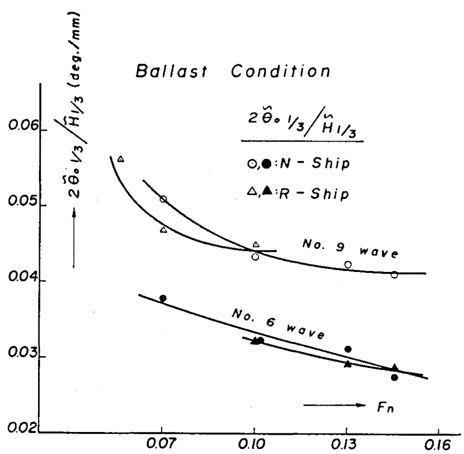

Fig. 42 Comparison of pitching amplitude in irregular waves for R-ship and N-ship

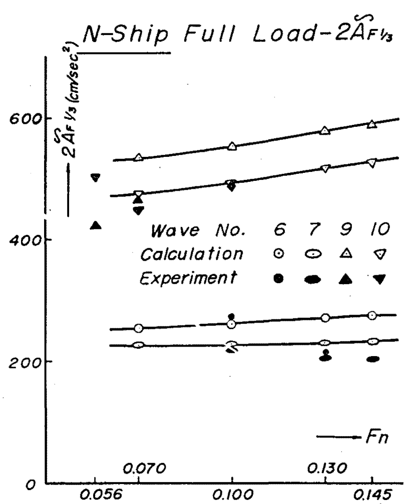

Fig. 43-a Comparison of calculated and measured significant values of vertical acceleration at Station 9½

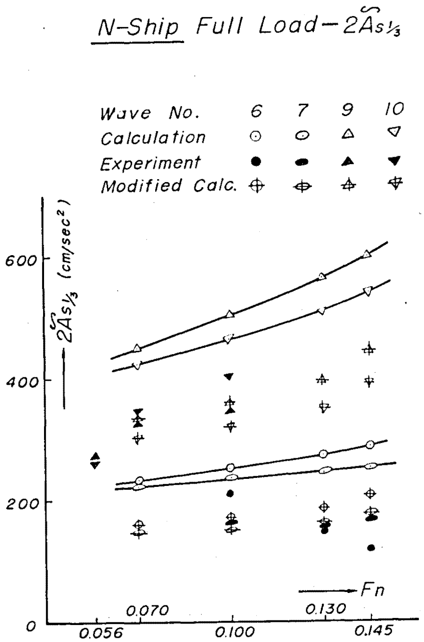

Fig. 43-b Comparison of calculated and measured significant values of vertical acceleration at Station ½

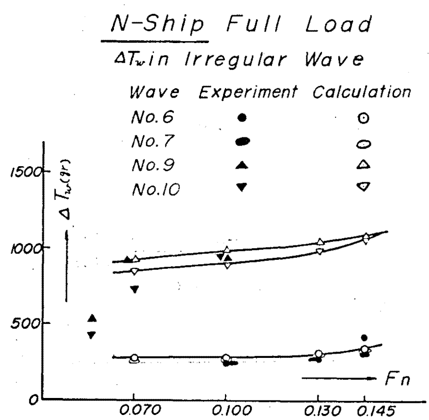

Fig. 44 Comparison of measured and calculated mean increase of thrust in irregular waves —— Full Loard

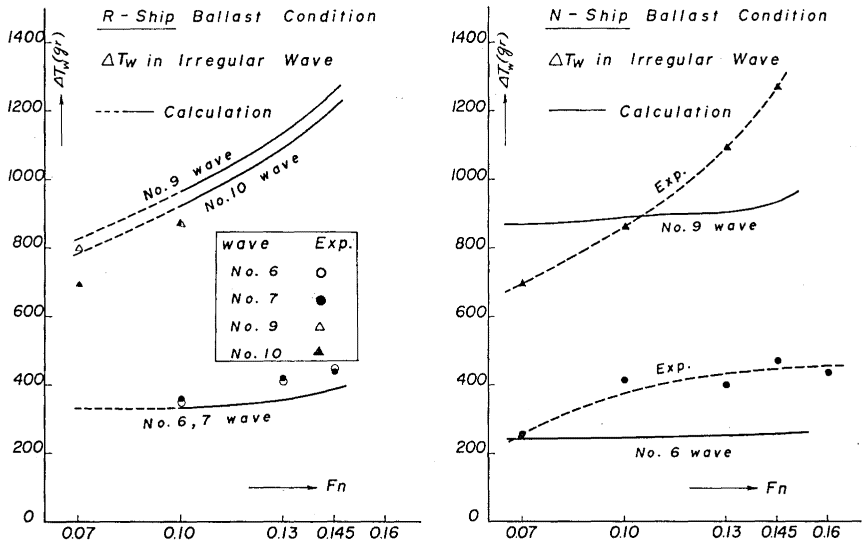

Fig. 45 Comparison of measured and calculated mean increase of thrust in irregular waves —— Ballast Condition

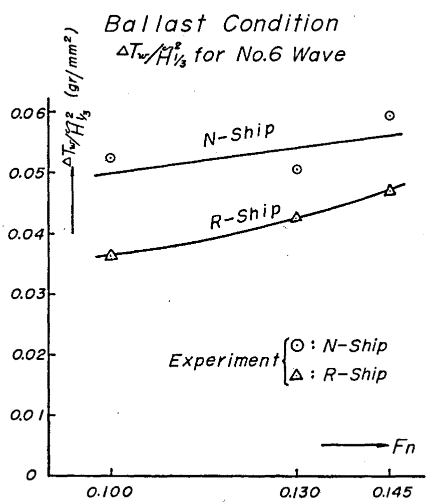

Fig. 46 Comparison of mean increase of thrust in irregular waves for R-ship and N-ship

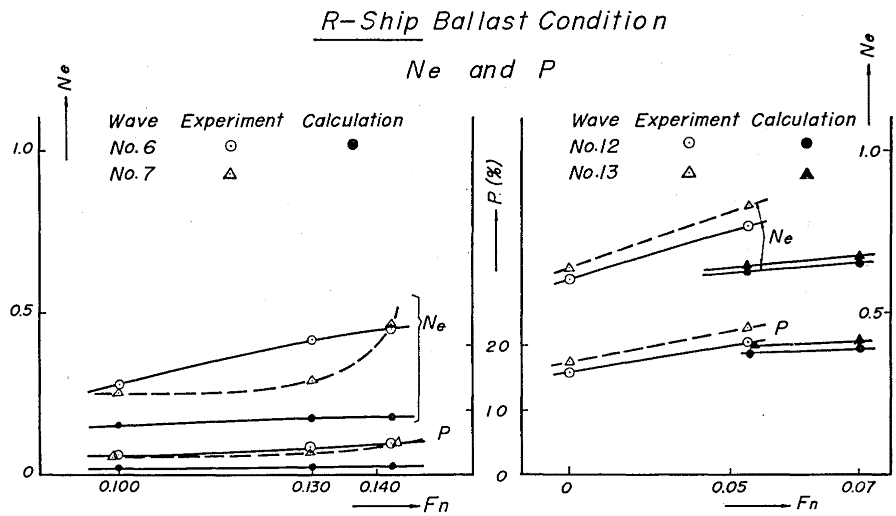

Fig. 48–a Comparison of calculated and measured frequency of bow emergence *Ne* and probability of time of bow emergence *P*

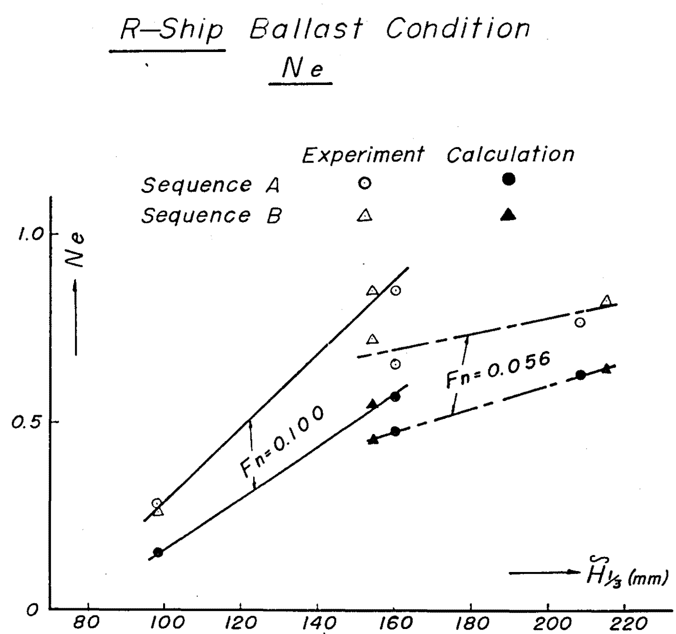

Fig. 48–b Comparison of calculated and measured frequency of bow emergence *Ne*

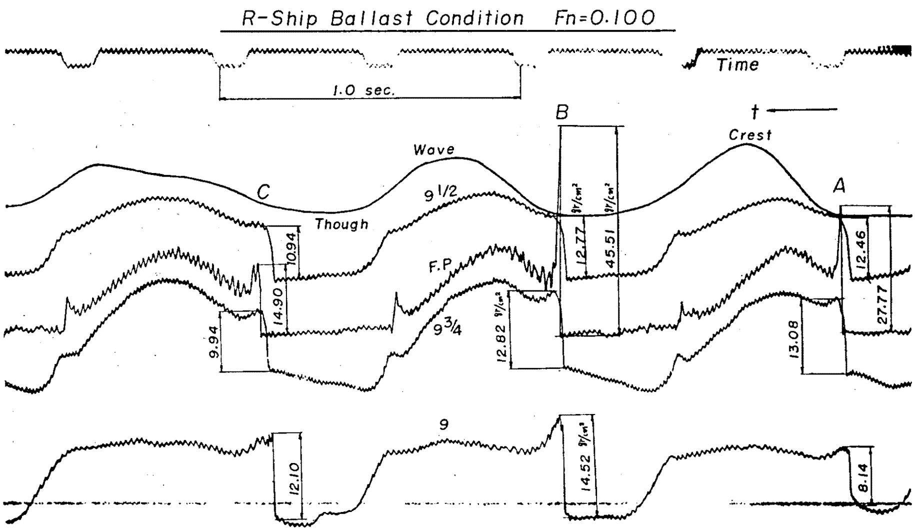

Fig. 49-a

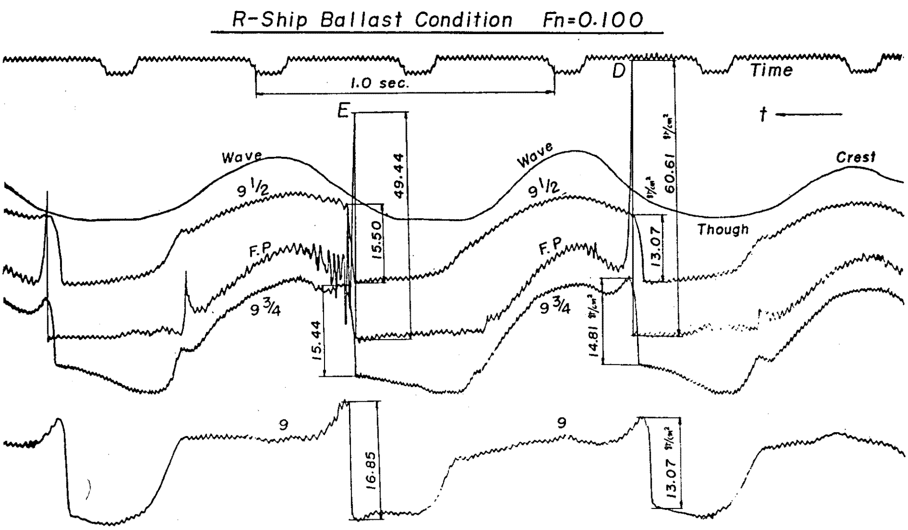

Fig. 49-b Records of slamming impact pressure measured for R-ship

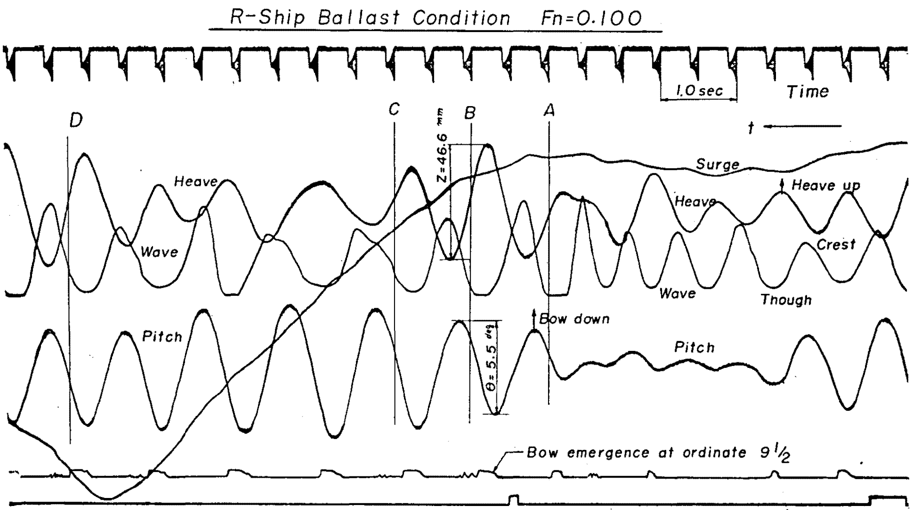

Fig. 49-c Records of longitudinal motions in irregular waves

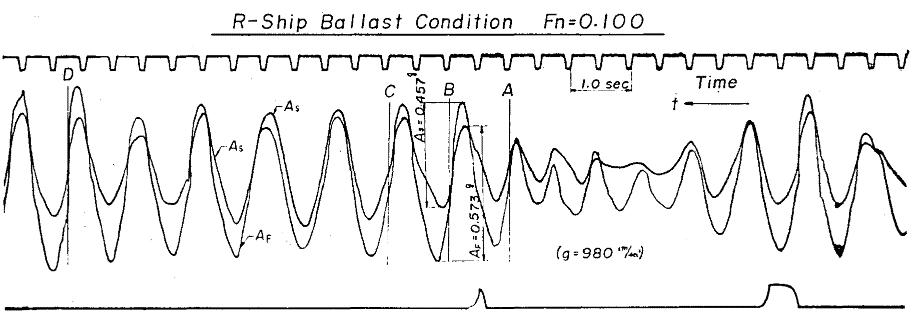

Fig 49-d Records of vertical accelerations of bow and stern in irregular waves

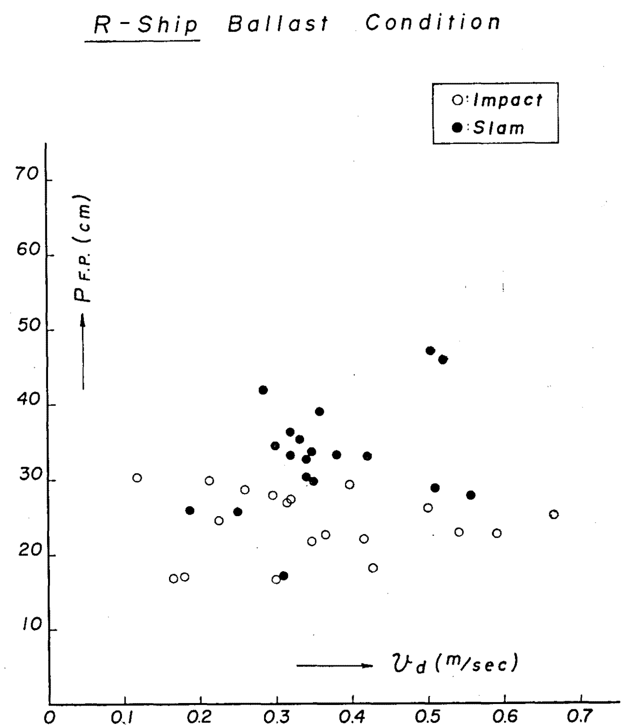

Fig. 52 Impact pressure experienced at F. P. and the downward velocity of bow at Station 9½

R–Ship Ballast Condition — Fn=0.100													
Sequence	Wave No.	W*	Prob. [Impact]				Prob. [Slam]	Pmax				$\widetilde{H}_{1/3}$ (mm)
			F.P	9·¾	9·½	9		F.P	9·¾	9·½	9	
(1) A	9	59	0.831	0.475	0.186	0.424	0.169	53.4	18.6	17.3	16.4	160.0
(2) A	9	68	0.852	0.324	0.235	0.414	0.176	50.5	18.0	17.3	16.2	
(3) A	9	60	0.683	0.382	0.233	0.333	0.216	50.7	19.8	17.5	17.5	
Mean			0.789	0.394	0.218	0.390	0.187	51.5	18.8	17.4	16.7	
(1) B	10	72	0.888	0.500	0.264	0.389	0.250	70.6	16.6	17.0	14.5	154.0
(2) B	10	68	0.853	0.559	0.324	0.500	0.324	73.5	15.2	16.8	17.3	
(3) B	10	69	0.855	0.493	0.348	0.478	0.333	53.1	16.4	18.3	21.6	
Mean			0.865	0.520	0.312	0.456	0.302	65.7	16.1	17.3	17.8	
* W is total number of pitch in the experiment.												

Fig. 53 Examples of probability of occurrence of slamming and maximum impact pressure

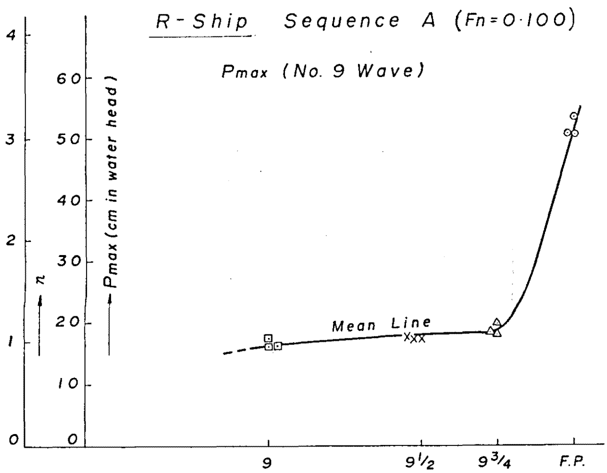

Fig. 54-a Maximum impact pressure experienced along ship length; R-ship, No. 9 wave, Sequence A

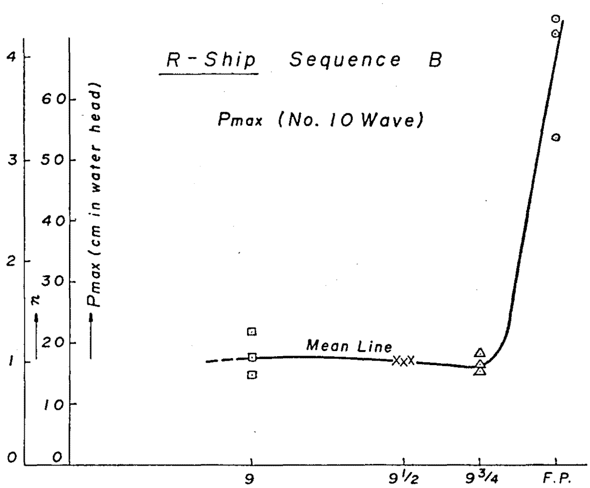

Fig. 54-b Maximum impact pressure experienced along ship length; R-ship, No. 10 wave, Sequence B

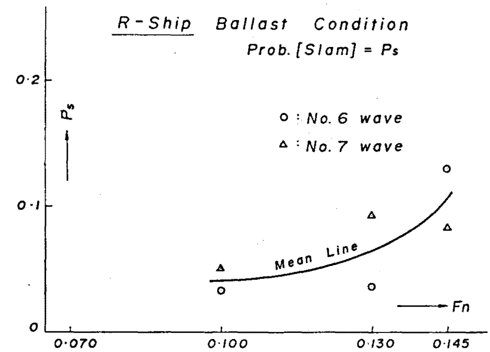

Fig. 55–a Probability of occurrence of slamming at various ship speed; R-ship, No. 6 and 7 waves

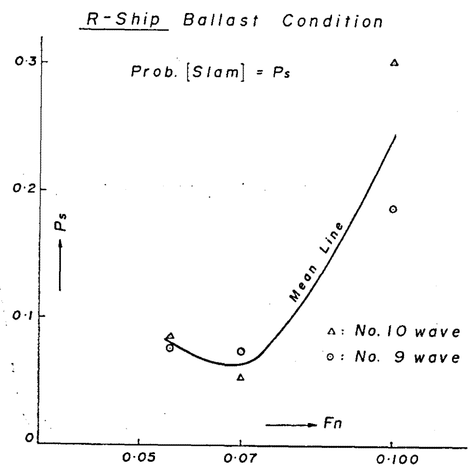

Fig. 55–b Probability of occurrence of slamming at various ship speed; R-ship, No. 9 and 10 waves

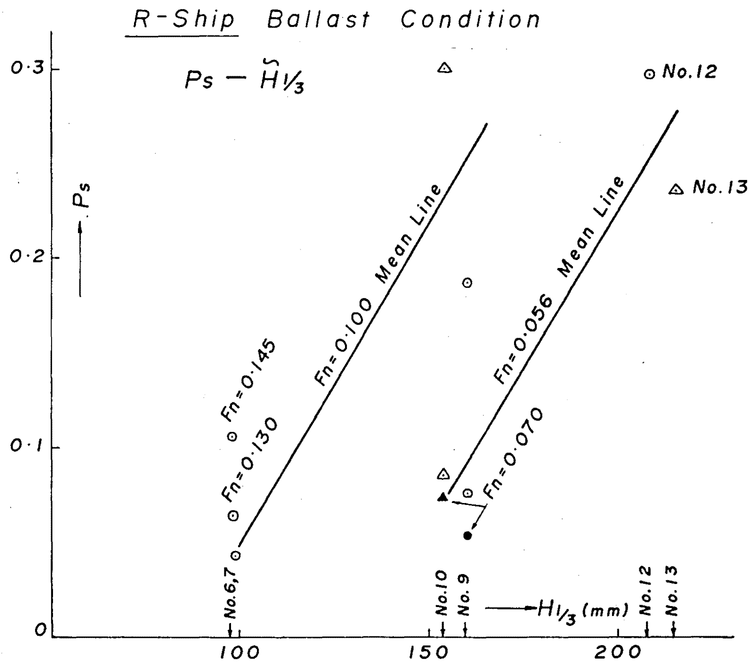

Fig. 56 Probability of occurrence of slamming at various significant wave height; R-ship

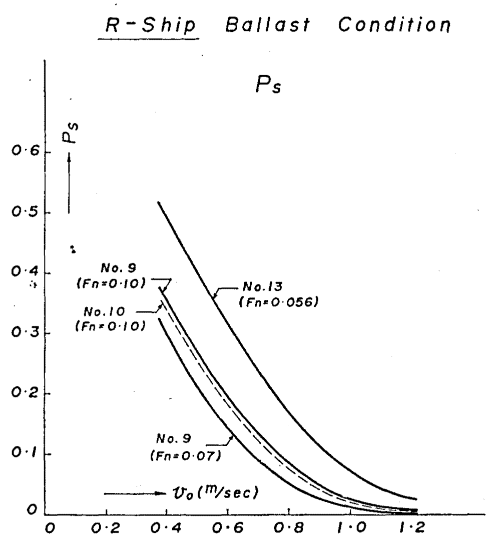

Fig. 57 Calculated probability of occurrence of slamming for R-ship

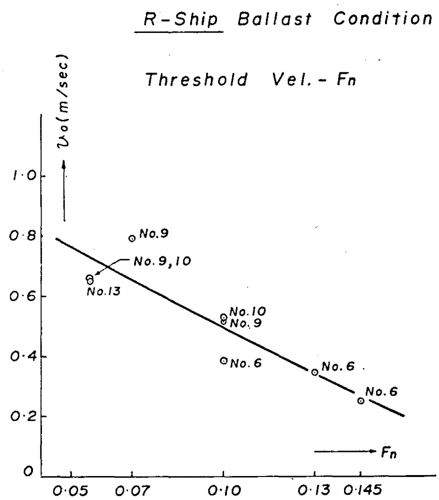

Fig. 58 Threshold velocity derived from the theoretical calculation and experimental results of P_s

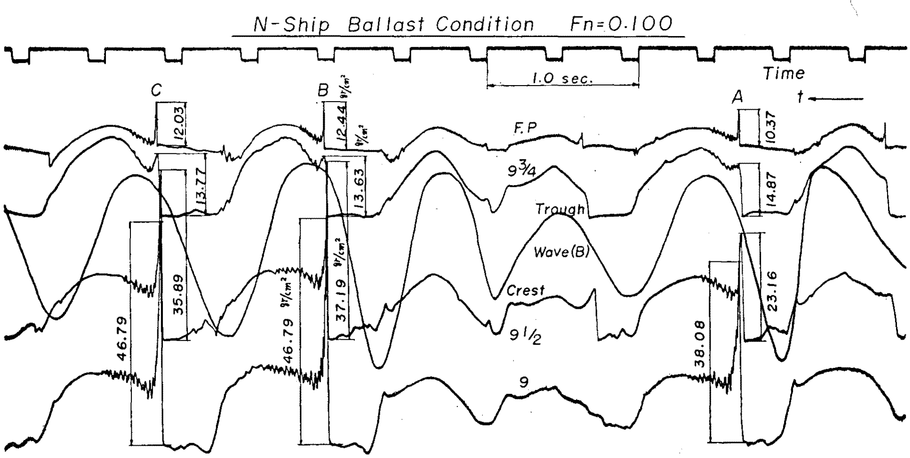

Fig. 59-a Records of slamming impact pressure for N-ship

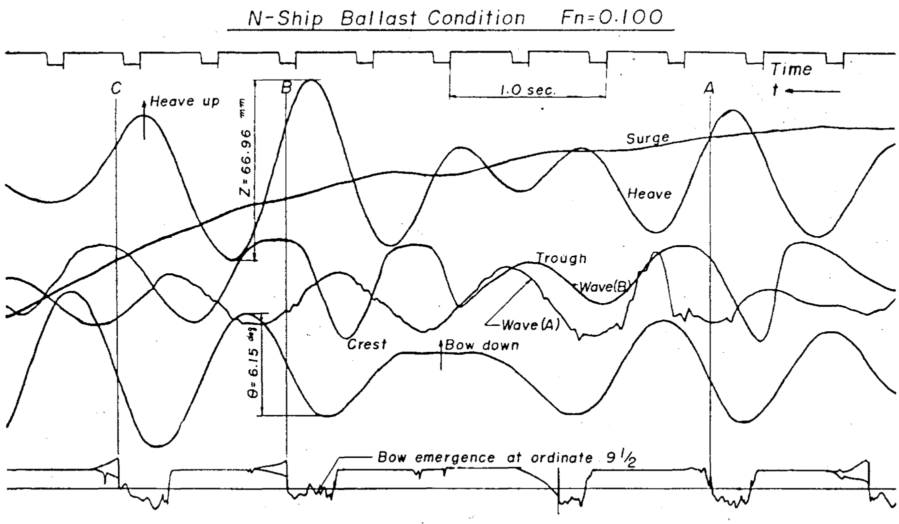

Fig. 59-b Records of longitudinal motions in irregular waves, N-ship

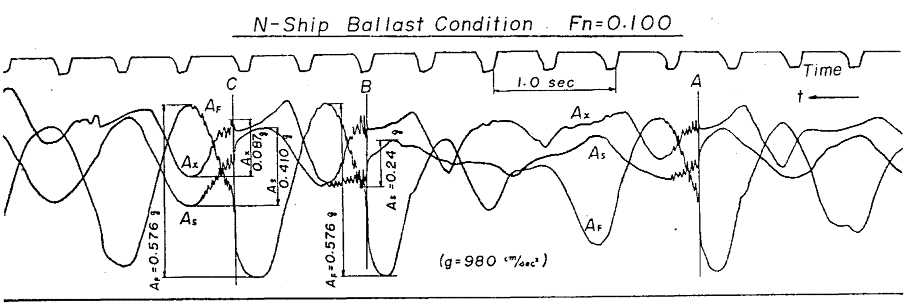

Fig. 59-c Records of vertical acceleration of bow and stern, and surging acceleration

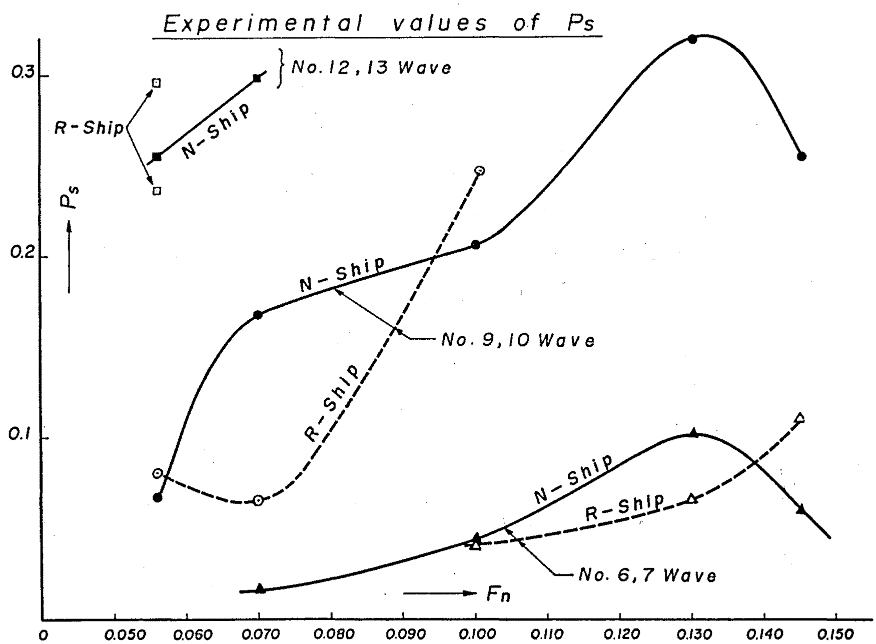

Fig. 60 Comparison of probability of occurrence of slamming for R-ship and N-ship

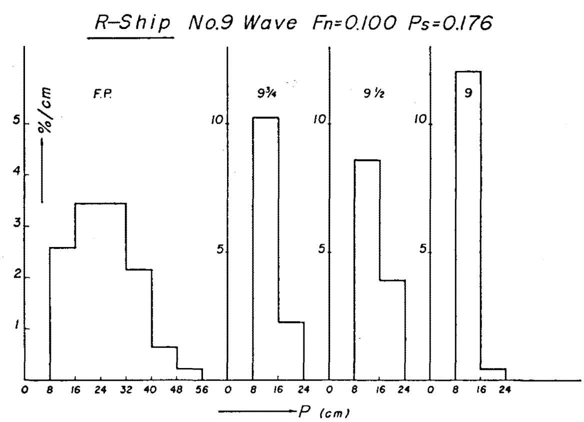

Fig. 61 Histograms of impact pressure obtained at F.P., Station 9¾, 9½ and 9; R-ship

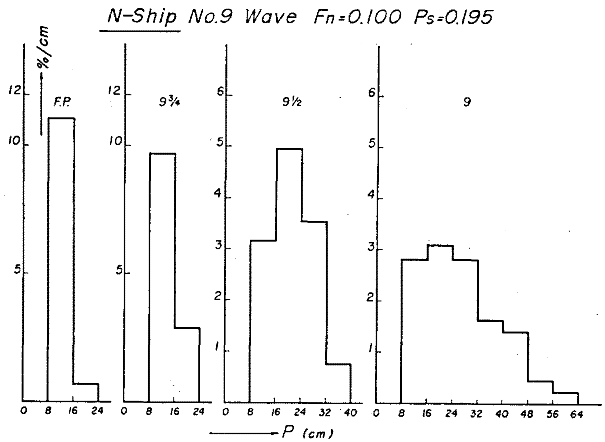

Fig. 62 Histograms of impact pressure obtained at F.P. Station 9¾, 9½ and 9; N-ship

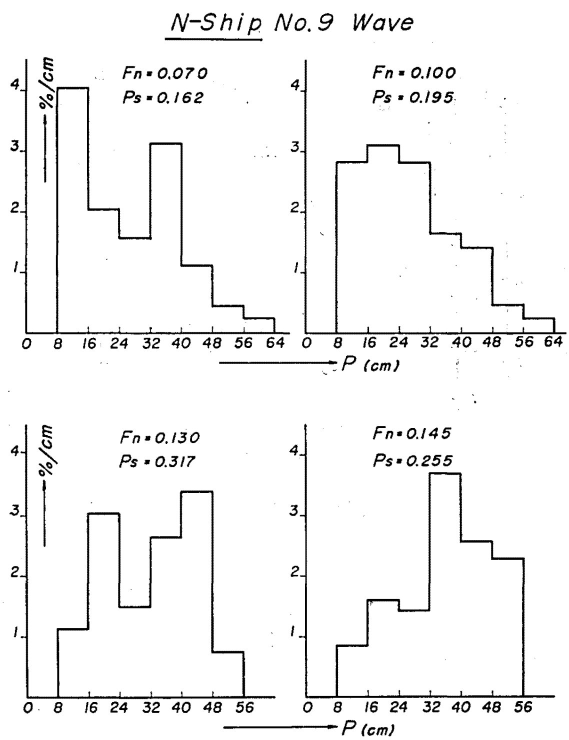

Fig. 63 Variation of histograms of impact pressure at Station 9 with ship speed; N-ship

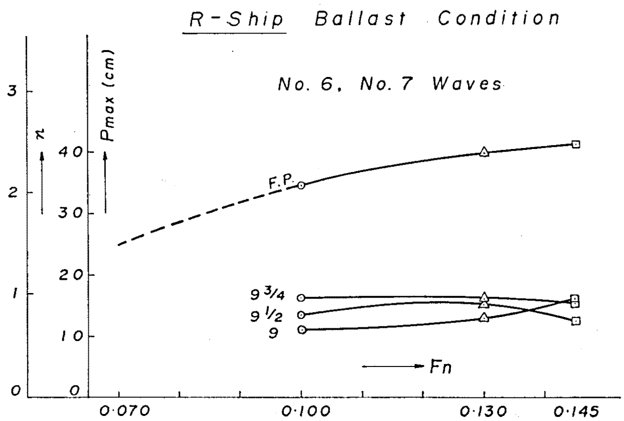

Fig. 64-a Maximum impact pressure of R-ship in No. 6 and No. 7 waves

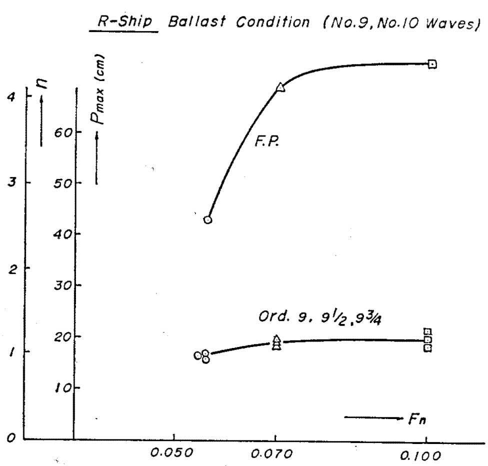

Fig 64-b Maximum impact pressure of R-ship in No. 9 and No. 10 waves

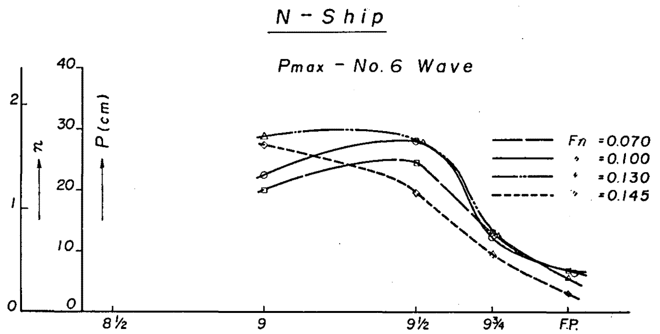

Fig. 65 Maximum impact pressure distribution of N-ship along ship length for, No. 6 wave

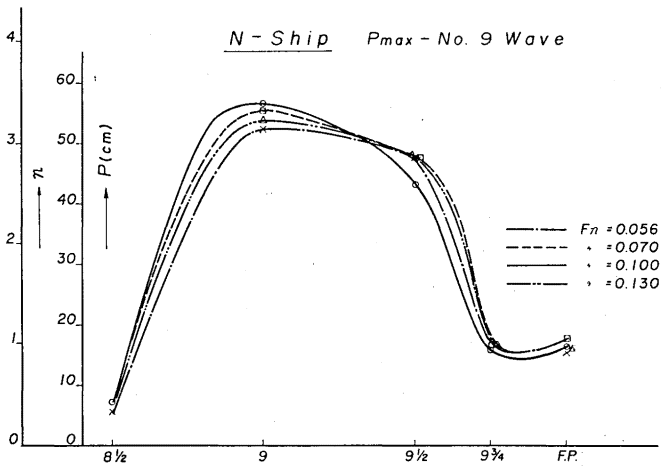

Fig. 66 Maximum impact pressure distribution of N-ship along ship length for No. 9 wave

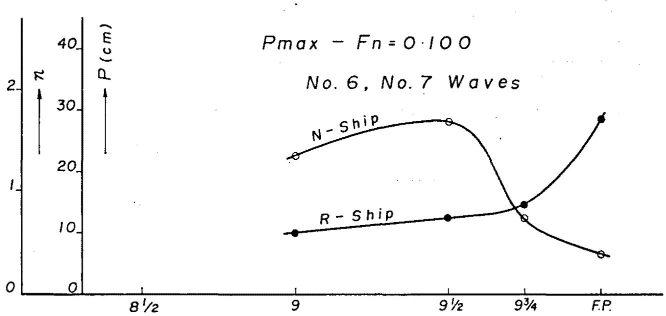

Fig 67 Comparison of pressure distribution along ship length for R-ship and N-ship; No. 6 and No. 7 waves

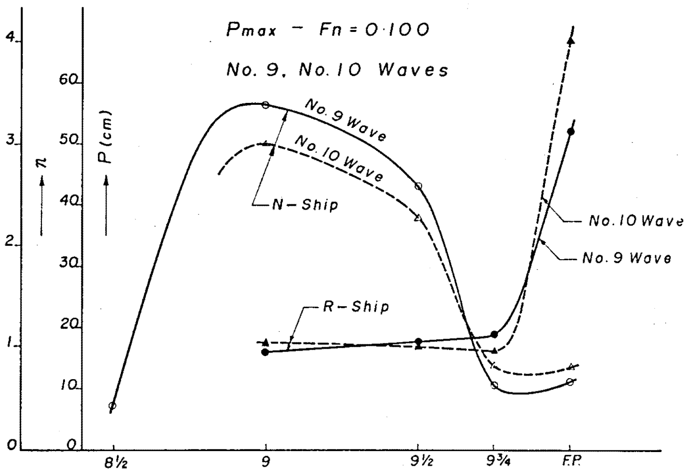

Fig. 68 Comparison of pressure distribution along ship length for R-ship and N-ship; No. 9 and No. 10 waves

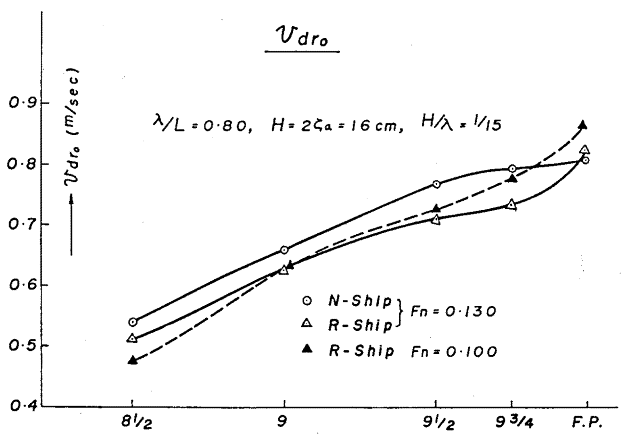

Fig. 69 Relative vertical downward velocity at the instant that the bottom of every station touches the surface of regular wave

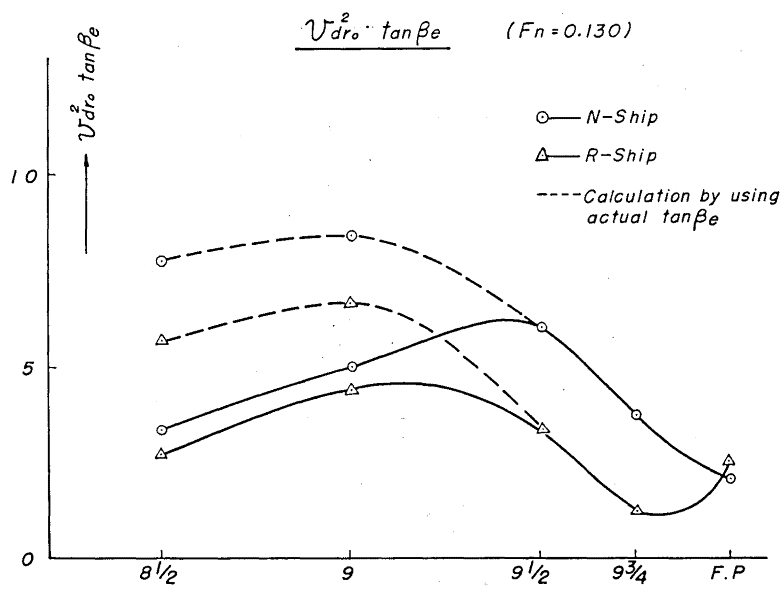

Fig. 70

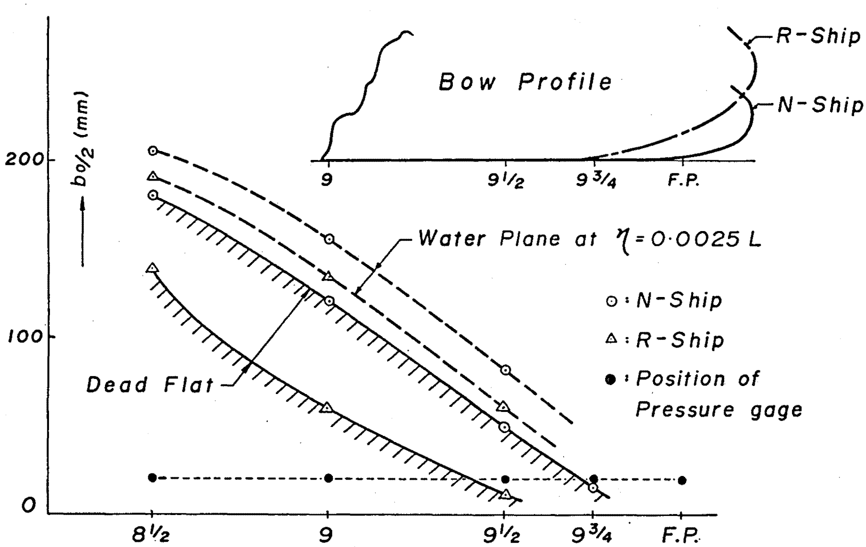

Fig. 72 Comparison of the shape of dead flat for R-Ship and N-Ship

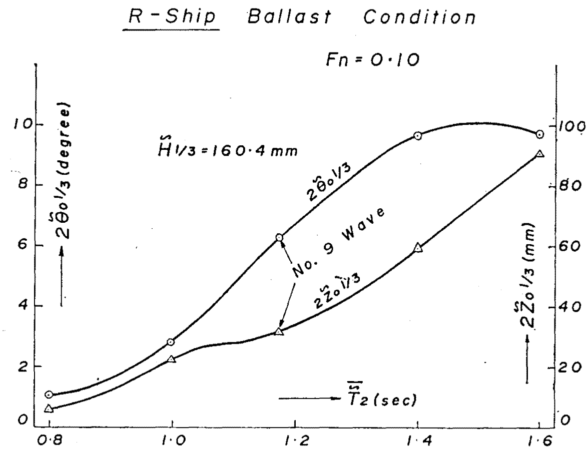

Fig. 73-a Calculated significant amplitudes of pitch and heave in irregular waves with various mean periods of wave spectra and the same significant wave height

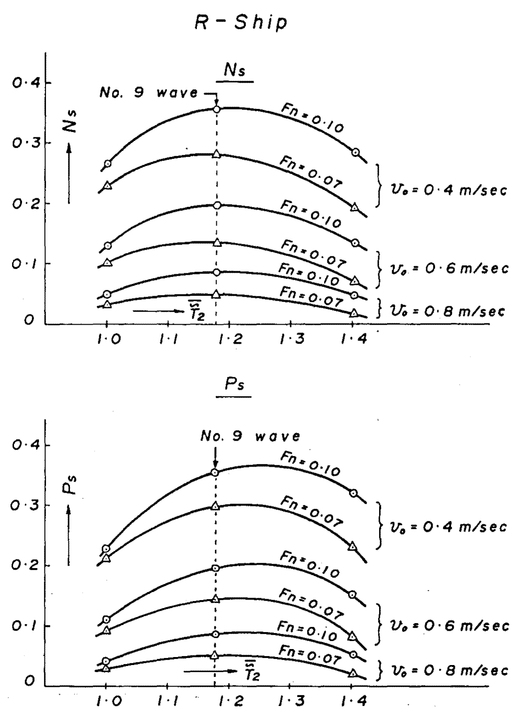

Fig. 73-b Variation of *Ps* and *Ns* with mean period of irregular waves

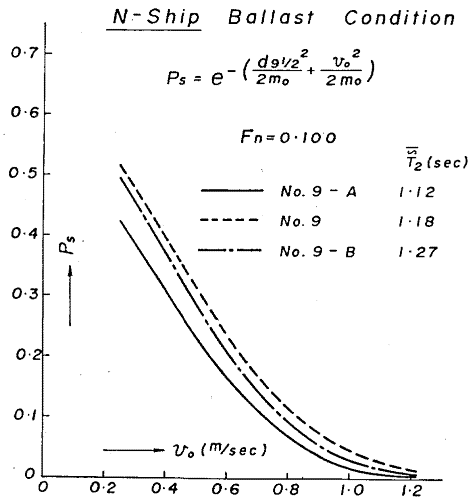

Fig. 74–a Calculated Ps for three kinds of irregular waves

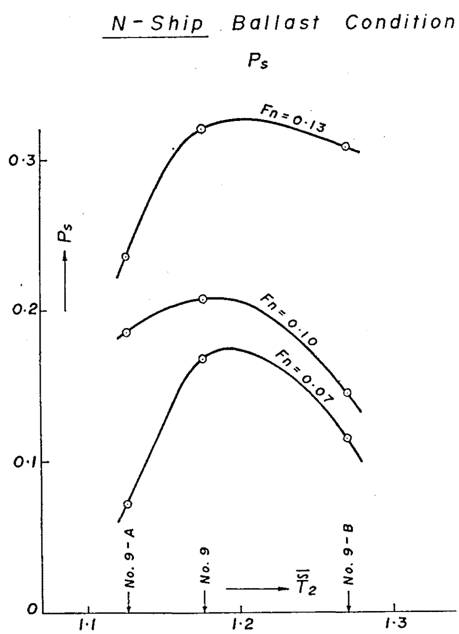

Fig. 74–b Measured values of Ps for three kinds of irregular waves having different mean period

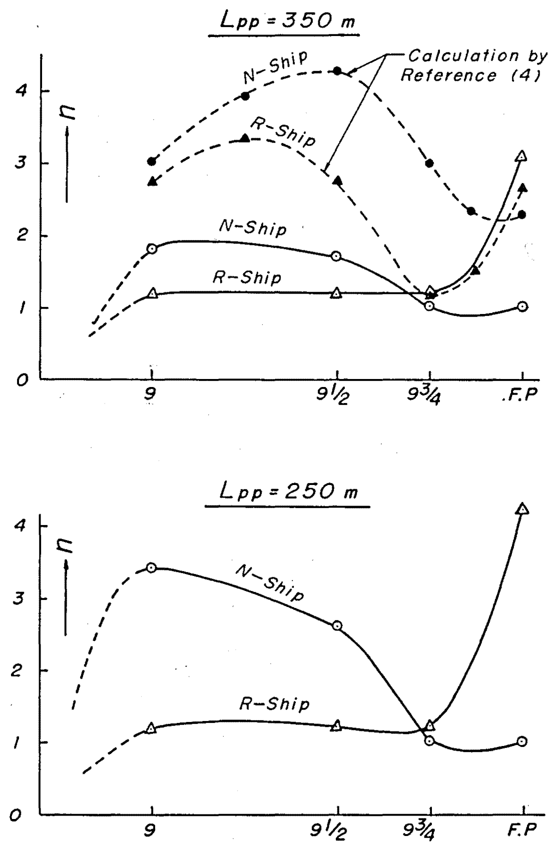

Fig. 75 Maximum impact pressure distribution along ship length described in Table 14

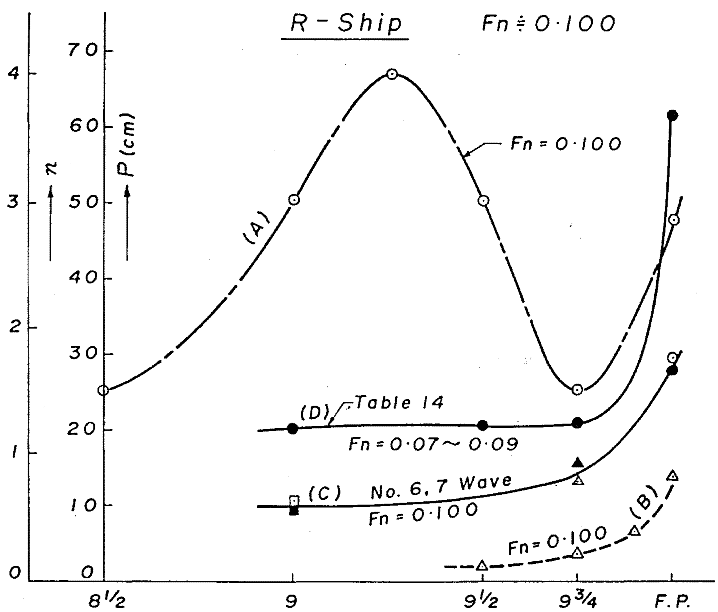

Fig. 76 Distribution of P_{max} along the ship length; (R–ship, Lpp=313 m) (A): calculation by the W. J. method, (B): calculation by the modified W. J. method, (C): measured values in No. 6, 7 waves, (D): estimation from Table 14

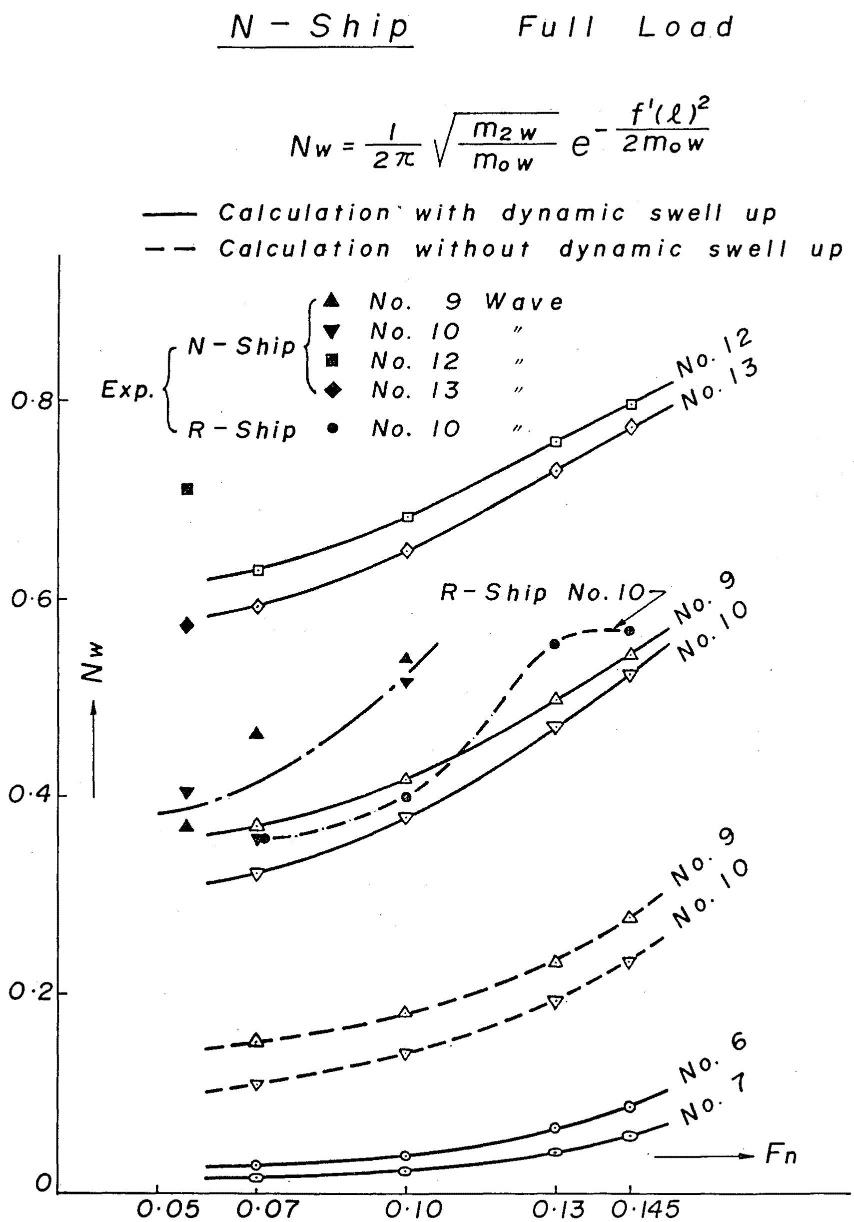

Fig. 77 Comparison of calculated and measured frequency of deck wetness for N-Ship, and comparison of measured deck wetness in No. 10 wave for N-Ship and R-Ship

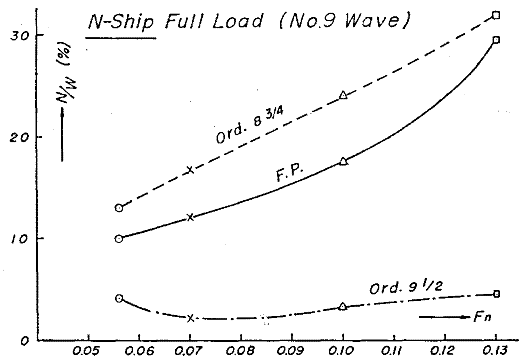

Fig. 78 Measured frequency of occurrence of impact pressure on the deck

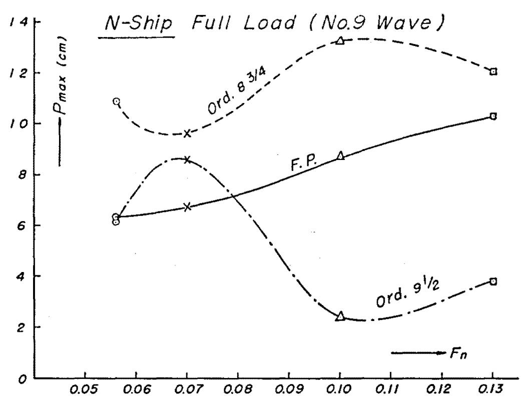

Fig. 79 Variation of maximum impact pressure with ship speed

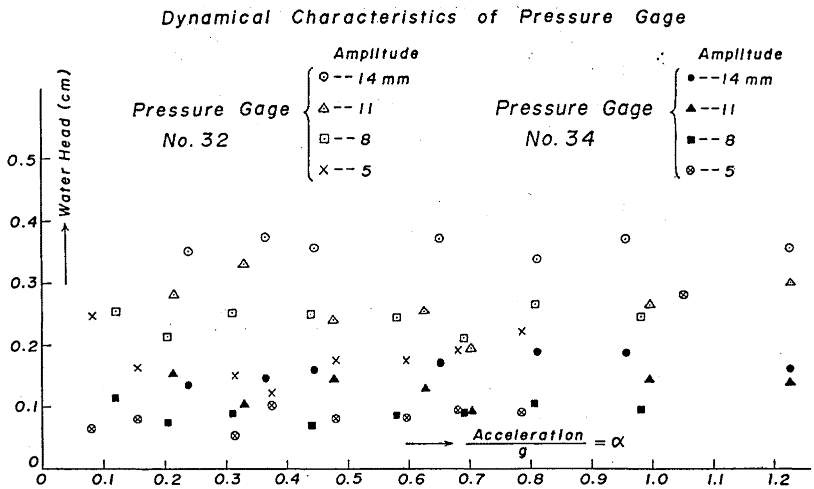

Fig. 80 Dynamic Characteristics of the pressure gage